Tampere University

Sahan Damith Liyanaarachchi

OFDM WAVEFORM OPTIMISATION FOR JOINT COMMUNICATIONS AND SENSING

Master of Science Thesis
Information Technology and Communication Sciences
Examiner: Asst. Prof. Taneli Riihonen
Examiner: Prof. Mikko Valkama
October 2019

ABSTRACT

Sahan Damith Liyanaarachchi: OFDM Waveform Optimisation
for Joint Communications and Sensing
Master of Science Thesis
Tampere University
Master's Degree Programme in Information Technology
October 2019

Radar systems are radios to sense objects in their surrounding environment. These operate at a defined set of frequency ranges. Communication systems are used to transfer information between two points. In the present day, proliferation of mobile devices and the advancement of technology have led to communication systems being ubiquitous. This has made these systems to operate at the frequency bands already used by the radar systems. Thus, the communication signal interferes a radar receiver and vice versa, degrading performance of both systems. Different methods have been proposed to combat this phenomenon. One of the novel topics in this is the RF convergence, where a given bandwidth is used jointly by both systems. A differentiation criterion must be adopted between the two systems so that a receiver is able to separately extract radar and communication signals. The hardware convergence due to the emergence of software-defined radios also motivated a single system be used for both radar and communication.

A joint waveform is adopted for both radar and communication systems, as the transmit signal. As orthogonal frequency-division multiplexing (OFDM) waveform is the most prominent in mobile communications, it is selected as the joint waveform. Considering practical cellular communication systems adopting OFDM, there often exist unused subcarriers within OFDM symbols. These can be filled up with arbitrary data to improve the performance of the radar system. This is the approach used, where the filling up is performed through an optimisation algorithm. The filled subcarriers are termed as radar subcarriers while the rest as communication subcarriers, throughout the thesis.

The optimisation problem minimises the Cramer–Rao lower bounds of the delay and Doppler estimates made by the radar system subject to a set of constraints. It also outputs the indices of the radar and communication subcarriers within an OFDM symbol, which minimise the lower bounds. The first constraint allocates power between radar and communication subcarriers depending on their subcarrier ratio in an OFDM symbol. The second constraint ensures the peak-to-average power ratio (PAPR) of the joint waveform has an acceptable level of PAPR.

The results show that the optimised waveform provides significant improvement in the Cramer–Rao lower bounds compared with the unoptimised waveform. In compensation for this, the power allocated to the communication subcarriers needs to be reduced. Thus, improving the performances of the radar and communication systems are a trade-off. It is also observed that for the minimum lower bounds, radar subcarriers need to be placed at the two edges of an OFDM symbol. Optimisation is also seen to improve the estimation performance of a maximum likelihood estimator, concluding that optimising the subcarriers to minimise a theoretical bound enables to achieve improvement for practical systems.

Keywords: radar, orthogonal frequency-division multiplexing, joint sensing and communication, OFDM, RF convergence, OFDM radar

PREFACE

This Master of Science thesis was written at the Faculty of Information Technology and Communication Sciences, Tampere University. The work was supported by Dr. Riihonen's tenure track starting grant and the RF Convergence project, funded by the Finnish Funding Agency for Innovation.

My sincere appreciation goes to my supervisor, Assistant Professor Taneli Riihonen, for motivating me in selecting the thesis topic and guiding me through the whole research process. The course Radar and Professional Radio Communication Systems taught by him made it easier for me to understand the basic building blocks related to radar, which ultimately allowed me to have a solid foundation in the theoretical aspects of this thesis. My special gratitude goes to Professor Mikko Valkama who provided with me the opportunity to work in the RF Convergence project and gave valuable opinions which moulded my thesis into an academically sound one. These two people shared their precious time to go through my thesis and provided scientific knowledge and constructive criticism while ensuring I had the stimulation to do research, for which I am very grateful.

I would also like to thank my office colleagues Carlos Baquero Barneto and Selahattin Gökceli for their continuous encouragement and making the work place exciting.

I dedicate this thesis to my parents, Carmen and Jayatissa, who always encouraged me to go beyond the distance and achieve more. I must also thank my two loving brothers, Tharuka and Shenal, for being there whenever I needed them. Last but not the least, I would like to mention my best friend Salani, whose unwavering love and support helped me whenever I was in doubt.

Tampere, 28 October 2019

Sahan Damith Liyanaarachchi

CONTENTS

LIST OF FIGURES

LIST OF TABLES

LIST OF SYMBOLS AND ABBREVIATIONS

A	Attenuation constant
A_e	Effective area of antenna
B	Bandwidth
F	Noise factor
F_s	Sampling frequency
G	Directivity gain
K	Number of scatterers
M	Number of OFDM symbols
N	Number of subcarriers
P_{total}	Transmit power
P_{FA}	Probability of false alarm
P_{MD}	Probability of missed detection
R	Range to a target
T	Symbol duration
T_{sw}	Sweep time
β	Radar cross section
γ	Threshold
λ	Wavelength
σ	Noise variance
τ	Delay to a target
f_{D}	Doppler frequency
f_c	Carrier frequency
$p(t)$	Rectangular pulse
t	Time
v	Velocity
$v(t)$	Noise signal
$x(t)$	Transmit signal
$y_r(t)$	Received radar signal
4G	Fourth generation of communication systems

5G	Fifth generation of communication systems
ACF	Autocorrelation Function
AF	Ambiguity Function
AM	Amplitude Modulation
ASK	Amplitude-Shift Keying
BER	Bit Error Rate
BS	Base Station
CCDF	Complementary Cumulative Distribution Function
CDM	Code Division Multiplexing
CE-OFDM	Constant Envelope OFDM
CP	Cyclic Prefix
CRLB	Cramer–Rao Lower Bound
CW	Continuous Wave
DAB	Digital Audio Broadcasting
DL	Downlink
DSA	Dynamic Spectrum Access
DVB	Digital Video Broadcasting
eNB	eNode-B
FDM	Frequency Division Multiplexing
FFT	Fast Fourier Transform
FMCW	Frequency Modulated Continuous Wave
FSPL	Free Space Path Loss
GPS	Global Positioning System
i.i.d	Independent Identically Distributed
I/Q	In-phase and Quadrature
IFFT	Inverse Fast Fourier Transform
ITU	International Telecommunication Union
LFM	Linear Frequency Modulation
LOS	Line Of Sight
LTE	Long Term Evolution
MCPC	Multi Carrier Phase Coded
MF	Matched Filter
MI	Mutual Information
MIMO	Multiple-Input Multiple-Output

MLE	Maximum Likelihood Estimator
MUR	Maximum Unambiguous Range
MUV	Maximum Unambiguous Velocity
NP	Neyman–Pearson
NR	New Radio
OFDM	Orthogonal Frequency Division Multiplexing
PAPR	Peak to Average Power Ratio
PDF	Probability Density Function
PM	Phase Modulation
PMCW	Phase Modulated Continuous Wave
PU	Primary User
QPSK	Quadrature Phase Shift Keying
RAST	Radar As a Subscriber Technology
RCS	Radar Cross Section
RF	Radio Frequency
RMSE	Root Mean Square Error
ROC	Receiver Operating Characteristics
RX	Receiver
SDM	Space Division Multiplexing
SER	Symbol Error Rate
SINR	Signal to Interference plus Noise Ratio
SLL	Sidelobe Level
SNR	Signal to Noise Ratio
SPR	Subcarrier Power Ratio
TD	Time Domain
TDD	Time Division Duplexing
TDM	Time Division Multiplexing
TRX	Transceiver
TX	Transmitter
UWB	Ultra Wideband
WAF	Wideband Ambiguity Function
Wi-Fi	Wireless Fidelity
WiMAX	Worldwide Interoperability for Microwave Access
WLAN	Wireless Local Area Network

1 INTRODUCTION

1.1 Background

From the advent of time, it was seen necessary for mankind that some form of information be transferred from one place to another. In the modern world, this task is handled by radio systems. In addition to communication, other important radio systems are radars that transmit electromagnetic waves towards the environment and using the reflections received at the radar receiver, create a map of the possible objects in the environment. There are different forms of radar systems for different applications in many fields including but not limited to weather forecasting, military applications, medical purposes, aviation and road traffic measurements. Different communication systems prevail for different objectives in different fields, but the most common ones are GSM, 3G UMTS, LTE and 5G New Radio (NR) mobile communication systems.

Radar and communication systems usually function separately from each other. Their independence means that each systems' performance is not dictated or hindered by the other system because each is given a specific frequency range to operate. Development of technology resulted in the proliferation of mobile devices and communication systems became ubiquitous. Due to this reason, communication systems have crowded the frequency spectrum and radar systems cannot anymore operate on specific frequencies but have to share the available spectrum with the communication systems. Due to this co-location of the two systems and operation on the same frequency bands, each system causes interference on the other. The performance of both systems is degraded due to this phenomenon.

Different methods are being developed to address the issues due to this co-existence [15], which can be depicted in four levels as in Figure 1.1. The most basic level is when both systems work independently and nothing is done to mitigate the interference. This is shown as the first level in the figure as isolation. Thus, this degrades the performance of both. In the next level, each system tries to quantify the effect of interference by the other. If at least a portion of the actual interference is quantified correctly, this can be cancelled from the overall interference to gain a small amount of performance improvement. In the next category, the two systems mutually exchange information between themselves so that quantification of interference is better than the earlier level. Therefore, much better performance improvements are observed since the information exchanged is deliberate

and reliable. The final category RF convergence, is the most novel category which is the topology used in this Master's thesis, where a given bandwidth is shared between the two systems. Based on the mechanism by which the separation between the two is done, various solutions have surfaced, which are discussed broadly in Chapter 3.

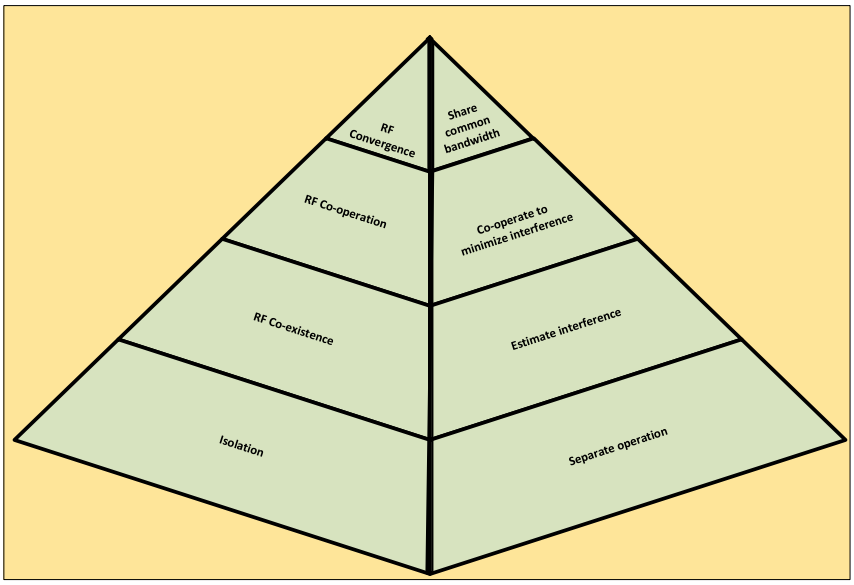

Figure 1.1. *Different levels of joint radar and communication systems*

1.2 Motivation and scope

Different procedures are adopted in practice to separate the operations of radar and communication systems under RF convergence. This thesis narrows the scope of these solutions to multicarrier systems, specifically orthogonal frequency-division multiplexing (OFDM) systems that would separate the joint bandwidth between the two systems. The OFDM waveforms are used in the newest mobile communications systems, LTE and 5G NR. So, employing the same OFDM waveform for radar purposes would essentially mean that the signal processing involved is the same for both systems. Also, the same hardware could be used that would enable to reduce the cost of the devices because two systems do not need to exist, and only one is enough, with software-defined radios being an example.

In mobile communication systems adopting OFDM, there are often unused subcarriers within OFDM symbols. These can be filled up with arbitrary data so that it improves the performance of the radar system. The motivation to use OFDM waveform for both radar and communication systems in this thesis is due to this where the filling up of these subcarriers is performed through an optimisation algorithm, which minimises the variances of the errors made by the radar system in estimating delay and Doppler parameters, while the performance of the communication system is kept at an acceptable level.

1.3 Objectives

For a radar system to estimate the range to a target accurately, it needs to estimate the delay between the transmitted and received signals. Similarly, to estimate the velocity of the target accurately, the Doppler shift between the transmitted and received signals must be estimated. Accuracy in these parameter estimates is the governing factor for the reliability of a radar system. The first objective of this thesis is to mathematically model the radar and communication systems. The second objective is to derive the lower bounds for the variances of the errors made by the radar system in estimating the delay and Doppler of a target. The signal-to-noise ratio (SNR) of the communication system is also derived. Based on these metrics for the radar and the communication systems, performing numerical optimisation to obtain a joint waveform is the next task in hand.

It is the case that minimising the error variances of the radar system has an inverse relationship with improving the SNR of the communication system. It is essential that both systems have an acceptable level of performance, without compromising one system's performance over the other. The penultimate objective is to find the region where both systems can work together with minimal performance degradation. The final objective is to evaluate the performance of optimisation with a practical scenario. For this, maximum likelihood estimation is performed to estimate the delay and Doppler parameters and a comparison of the errors is performed between the optimised and the unoptimised waveforms.

1.4 Results

Based on the mathematical formulation, an optimisation problem is formulated to minimise the error variances of the delay and the Doppler estimates, while also ascertaining the communication system's performance is at an acceptable level. It also outputs the indices for the radar and the communication subcarriers within an OFDM symbol for this minimisation. The formed optimisation problem is evaluated in MATLAB® to find the joint OFDM waveform.

It is observed that the error variances in the estimates of the radar system can be reduced significantly by this optimisation. In compensation for this, the power allocated for the communication subcarriers needs to be reduced. Thus, by having some fixed level of performance for the communication system, it is possible to improve the radar performance. It is also observed that to minimise the error variances, the radar subcarriers should be ideally placed at the edges of an OFDM symbol. Further, the suitability of this optimisation algorithm is evaluated for a practical scenario using a maximum likelihood estimator (MLE). It is seen that the optimised waveform outperforms the unoptimised one, concluding that minimising a theoretical lower bound enables to improve the performance of a practical system as well.

1.5 Organisation

The organisation of the remainder of the thesis is as follows. Chapter 2 is dedicated to the theory behind radio systems. It first narrates the basics about general radios and more specific software-defined radios. Next, it addresses the fundamentals of radar systems, including different signals used and the methodology through which the radar system gains information about the targets in the environment with the help of the detection theory. Radar range equation is also discussed which is used to calculate the power required to detect a target at some distance. Fundamentals of communication systems are discussed next, along with the theory behind OFDM systems. Elements common to both radar and communication systems are addressed next as the final section. Chapter 3 concerns joint systems and discusses the reason for both systems to work together in the future for improvement of performance. Rest of the chapter is solely about the state of the art methodologies to achieve this. It mainly focuses on the RF co-existence, co-operation and convergence topologies used in the literature. Chapter 4 is devoted to deriving the mathematical model for the OFDM waveform to be used as the joint radar and communication waveform. It further discusses the error variances of the delay and Doppler estimates of the radar system. The Cramer–Rao lower bounds for those estimates are derived and an optimisation problem is formed to minimise this. Chapter 5 analyses the results of the thesis. Chapter 6 is about the conclusion and future work pertaining to this thesis.

2 RADIO FUNDAMENTALS

The electromagnetic spectrum encompasses electromagnetic waves from frequencies as low as 3 Hz up to much higher frequencies extending beyond hundreds of YHz. This spectrum is categorised based on the applications that use a collection of frequency range. Each section has its own characteristics depending on their wavelengths and the equipment used to propagate these waves. The frequencies in the range 3Hz-300GHz are categorised as radio waves and used mainly in radio systems [90]. Compared with other frequencies, they reflect, scatter and diffract instead of being dissipated or absorbed by the surrounding objects. Another factor which makes it favourable for use is they are safe for humans, which is not the case for much higher frequencies such as X rays and γ rays [24]. Radio systems have their use in many fields where information needs to be transferred between two points. The source point is usually called a transmitter (TX) and the destination point is the receiver (RX). Block diagram of a general-purpose radio TX and RX is given in Figure 2.1 [34].

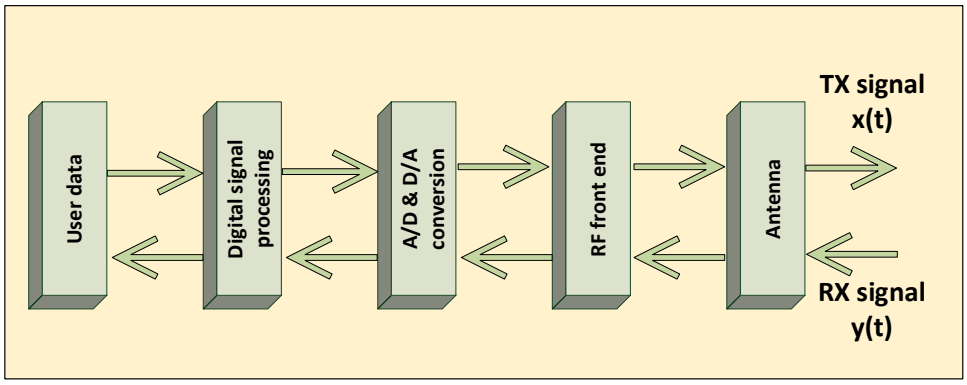

Figure 2.1. *Block diagram of a typical radio system*

Top part of the figure corresponds to the TX while the bottom part is for the RX. The received electromagnetic signal $y(t)$ is usually centred around some radio frequency (RF), termed as the carrier frequency. This is captured by the antenna and transformed into a time-varying electrical signal and fed into the RF front end. The most common components here are filters, an amplifier and a mixer. Usually, the frequency content of the signal captured by the antenna is much larger than the actual signals' bandwidth (BW). Thus, to select only the frequency content corresponding to the signal, it is first filtered, either at once or by a series of filters.

Usually the power of the signal received is quite low and thus it is amplified next. In the RX, a low noise amplifier (LNA) is adopted for this purpose. To make the processing feasible in the following blocks, the signal is down-converted to baseband with the help of the mixer. This operation essentially moves the frequency content which was around the carrier frequency to baseband around zero frequency. This signal is still in continuous-time domain and needs to be converted into digital domain and this is the task of an analog to digital (A/D) converter. The task of the digital signal processor (DSP) is to convert these samples to information that makes sense to the radio user.

Similar operations are performed in the view of a TX. Some user data is fed to the DSP for processing and then it is converted into digital domain and then again to analog domain with the digital to analog (D/A) converter. This continuous-time signal is up-converted to a carrier frequency and amplified with the help of a power amplifier (PA). The amplified signal is then given as an input to the antenna to convert it as an electromagnetic radiation and sent as $x(t)$. These operations regarding TX and RX are discussed broadly later in the chapter.

An important distinction that needs to be made is regarding the baseband and RF signals. An RF signal is simply a real-valued time-varying sinusoidal signal denoted as [94] [1]

$$x(t) = A_{\mathsf{RF}}(t)\cos\left(2\pi f_c t + \phi(t)\right) \tag{2.1}$$

$$= \underbrace{A_{\mathsf{RF}}(t)\cos\left(\phi(t)\right)}_{x_I(t)}\cos\left(2\pi f_c t\right) - \underbrace{A_{\mathsf{RF}}(t)\sin\left(\phi(t)\right)}_{x_Q(t)}\sin\left(2\pi f_c t\right), \tag{2.2}$$

where $A_{\mathsf{RF}}(t)$ is the time varying amplitude of the sinusoid, f_c is the carrier frequency and $\phi(t)$ is a time-dependent phase. The signals $x_I(t)$ and $x_Q(t)$ are called the in-phase (I) and quadrature (Q) components. These can be combined to denote the complex baseband signal $x_{\mathsf{BB}}(t)$ as

$$x_{\mathsf{BB}}(t) = x_I(t) + jx_Q(t). \tag{2.3}$$

Therefore, the relation between the baseband and RF signals can be given as

$$x(t) = \Re\left(x_{\mathsf{BB}}(t)e^{j2\pi f_c t}\right), \tag{2.4}$$

where the RF signal is simply the real part of the frequency-shifted baseband signal.

This thesis is concerned with two applications of radio systems, namely radar and communication systems. There are different parameters that define signals intended for a particular system. When all those parameters are fixed and defined, they are also called waveforms. As such, the latter sections discuss different waveforms in this regard.

[1] The following content on RF signals was adopted from the lecture notes of Mikko Valkama, Jukka Talvitie and Markku Renfors in the course *Communication Theory*, Tampere University of Technology.

2.1 Software-defined radio transceivers

In the past, most radio systems have been designed to perform one single task. This was done so because it is easier to optimise one system when its' intended function is fixed. With the advent of time, it was seen necessary that radio devices be flexible. As a solution to this, first emerged software-controlled radio (SCR) [65], as depicted in Figure 2.2. The difference here is that within the radio some fixed waveforms are defined and the microprocessor has the control to select one of the waveforms depending on the application. An example for this is a mobile device capable of operating between GSM and WCDMA systems.

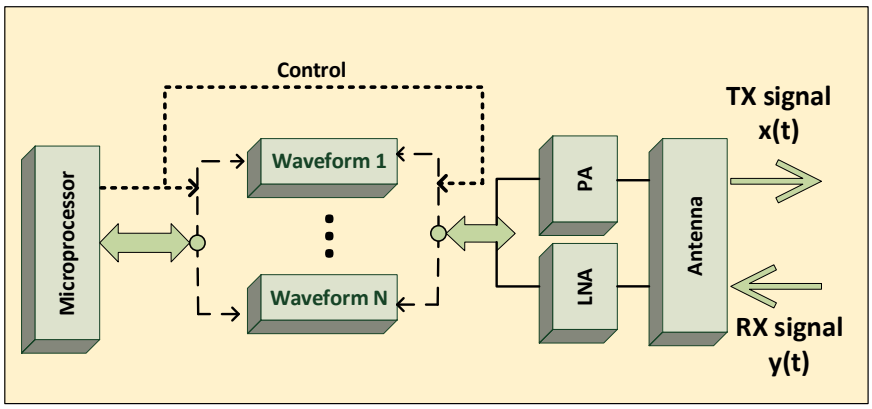

Figure 2.2. *Architecture of an SCR*

The evolution of SCR led to software-defined radio (SDR). An SDR is capable of generating any waveform by changing the processing as required, and is not confined to use fixed waveforms [47]. Figure 2.3 shows the block diagram of an SDR.

SDR TX The architecture of this is depicted in Figure 2.3(a). User data is fed as input to the SDR, to generate an arbitrary waveform. It can be either to generate a communication waveform or a radar waveform. Depending on that, the signal processor produces the I/Q samples. These are in turn supplied to the D/A converter to generate the time-domain I/Q signals after passing them through low-pass filters (LPF), which essentially captures the complex baseband signal defined in (2.3). Each I/Q signal is then multiplied by the carrier RF and added to generate the RF signal as in (2.2). The RF signal is then amplified to the required power level with the help of the PA. It is possible that the PA generates additional frequency components that are not required for transmission, due to the non-idealities. To remove those, a band pass filter (BPF) is used and fed to the the TX antenna to be sent as the TX signal $x(t)$.

SDR RX The received RF signal $y(t)$ is first filtered with a BPF to obtain the frequency content corresponding to the actual signal, as in Figure 2.3(b). It is then amplified with the help of an LNA. This signal is then down-converted either to baseband or to an intermediate frequency (IF). This is some fixed frequency to which the signal is down-converted

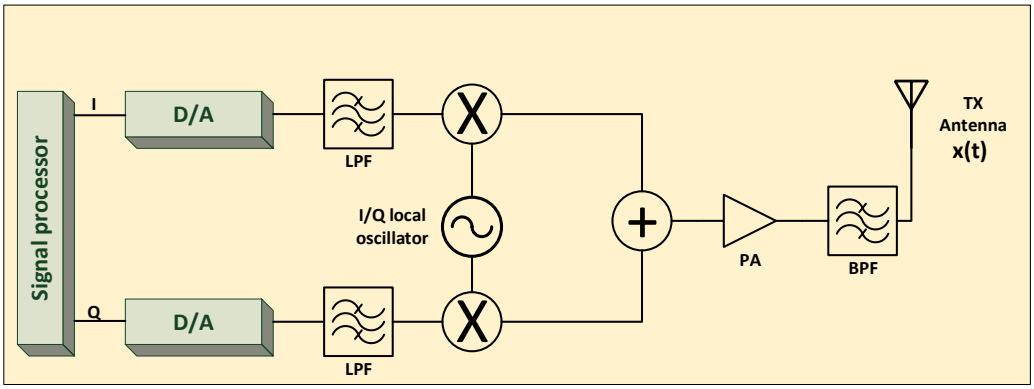

***(a)** SDR TX*

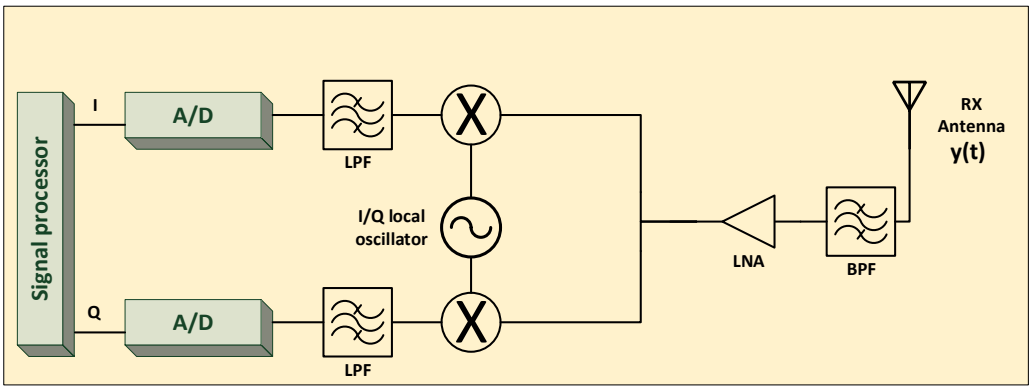

***(b)** SDR RX*

***Figure 2.3.** TX and RX architectures of an SDR*

to. It is possible to have a series of IF where at each down-conversion, the IF is lower than the earlier one. It is then passed through a LPF to obtain the baseband time-domain signal $y_{\text{BB}}(t)$. This signal is then converted into digital domain through a process called sampling and quantisation. The continuous-time signal is sampled at a sampling frequency F_s. This essentially means that the time-domain is discretised and the individual discrete samples are denoted as

$$y_{\text{BB}}[l] = y_{\text{BB}}\left(\frac{t_l}{F_s}\right), \tag{2.5}$$

and $y_{\text{BB}}[l]$ is the discrete sample corresponding to the time instant $t_l = \frac{l}{F_s}, l = 0, ..., L-1$, where L is the total number of samples. Since the amplitude of the time signal is still continuous, it is also discretised with quantising to some discrete levels. These levels are finally mapped to a binary set by denoting each level as a binary number, to obtain the digital I/Q samples. These samples are inputted to the signal processor to extract the required information.

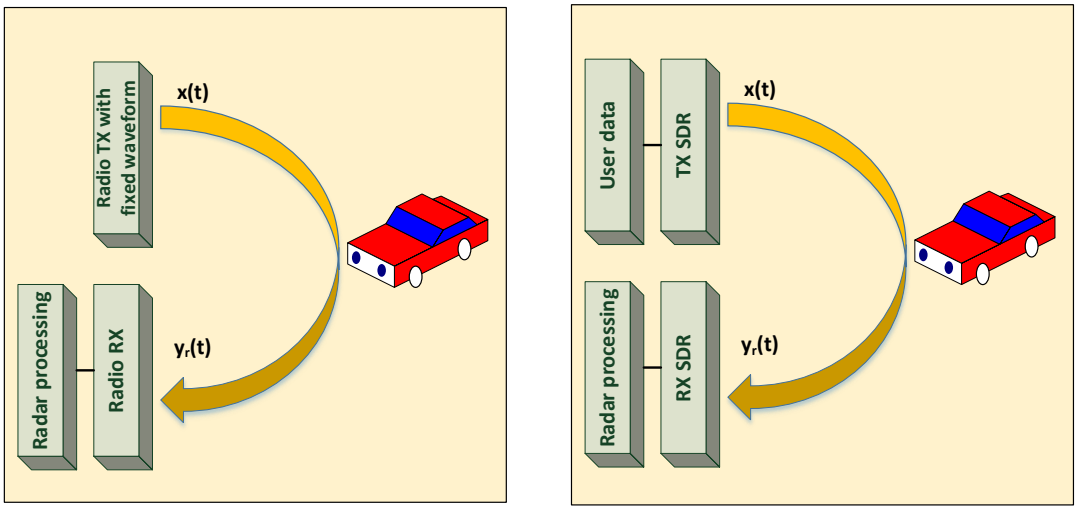

(a) *Conventional radar system* ***(b)*** *Modern radar system with SDR*

Figure 2.4. *Historical and modern radar systems*

2.2 Radar systems

The word radar is a common term that has been there for many decades. The meaning behind this once-acronym is radio detection and ranging. That is, it transmits a signal in the range of radio waves towards the environment. When this signal collides with an object in the environment, it reflects in different directions and is also reflected again towards the radar receiver. A conventional radar system is shown in Figure 2.4(a), where the radar TX and the RX are at the same location. Here, $x(t)$ is the TX signal and $y_r(t)$ is the RX signal at the radar transceiver (TRX). This RX signal is then used for target detection. The reflected signal in real word scenarios is usually attenuated or amplified for different frequencies and time instants and some forms of noise added on top of that with atmospheric noise, solar noise and industrial noise being some examples [33]. Further, interference can happen from different other systems working on the same frequency band. Amidst all these unwanted noise and interference, the radar RX needs to perform target detections. With some additional processing, it is possible to gain information about different details of those targets since the parameters of the reflected signal are different from the transmitted one, depending on the target dynamics. These differences are used to gain information about the said target dynamics which are: target position which entails azimuth angle, elevation angle and the range to the target and also the velocity of the target relative the radar TRX.

Figure 2.4(a) shows historical radar systems where the TX waveform is fixed for a particular application. Figure 2.4(b) shows the same radar system where all the processing is done by an SDR, and is considered a modern radar system. As a result, the TX waveform is not anymore fixed, but able to change it for a wide variety of applications. Here, the user only needs to input the complex samples and the waveform is generated within

the SDR. The flexibility of using an SDR for waveform generation is that the waveform is dependent only upon the complex samples that are supplied as input for the SDR. The reflected signal is captured by the RX SDR and the inverse operations are performed to yield the received complex samples. Since the TX samples are known, a comparison is made with the RX samples to perform radar processing. This is the future direction of radar envisioned by many researchers in the field and is the basis for this thesis.

2.2.1 Signal models

Transmission

Mainly, two types of transmit waveforms are employed by radar systems depending on the application. These are the continuous wave (CW) signals and pulsed waveforms. This thesis uses CW as the signal type, but with OFDM waveform, unlike conventional radar.

Continuous waveforms The most basic continuous waveform in RF is a sinusoidal tone. This waveform cannot be used for target range detection but only for velocity estimation. Thus, it is used for low power and low cost applications. To make CW signals applicable also for range estimation, they are usually frequency modulated or phase modulated, giving rise to frequency modulated continuous wave (FMCW) and phase modulated continuous wave (PMCW) waveforms [70]. An FMCW signal has the following time domain characterisation in baseband:

$$x_{\mathsf{BB}}(t) = \cos\left(\pi \frac{B}{T_{\mathsf{sw}}} t^2\right), 0 \leq t \leq T_{\mathsf{sw}}. \tag{2.6}$$

Signal frequency is changed gradually and linearly across the whole bandwidth B within a time period T_{sw}, which is also called the sweep time of the FMCW signal. This is shown in Figure 2.5(a). The corresponding time-domain waveform is shown in Figure 2.5(b). Before transmission, the baseband signal is modulated to a carrier frequency f_c and the time-domain signal $x(t)$ in RF can be written as

$$x(t) = \cos\left(2\pi f_c t + \pi \frac{B}{T_{\mathsf{sw}}} t^2\right). \tag{2.7}$$

Signal transmission and reception are done simultaneously in CW systems. Due to this, the TX signal couples to the RX signal and it is known as self-interference (SI). Usually the RX signal is weaker when compared with the TX signal, and thus SI completely floods the RX signal. An important concept in radar terminology is the clutter, which refers to the target returns that are not needed for the particular radar application [75]. Usually SI will have the same behaviour as the target clutter. So, in these systems additional processing needs to be performed to remove the TX signal from the RX signal.

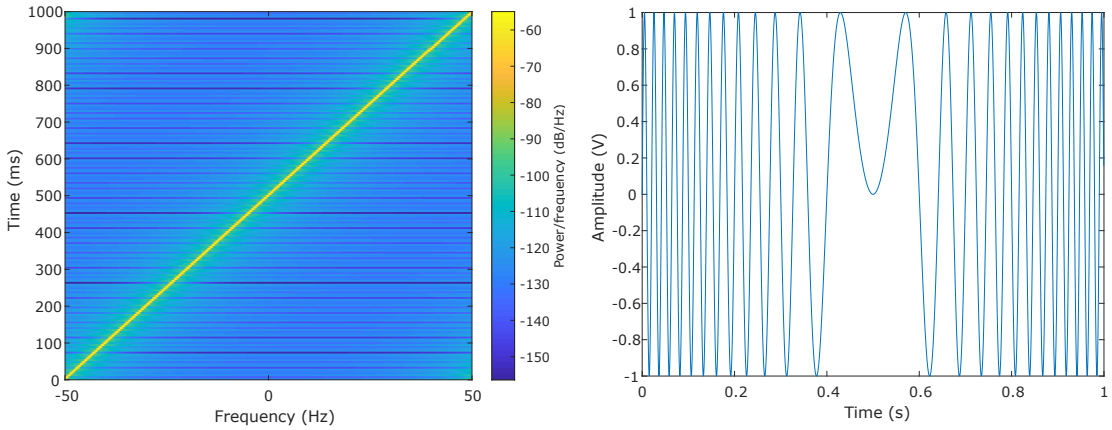

(a) *Spectogram of an FMCW signal* ***(b)*** *FMCW signal in time domain*

Figure 2.5. *Spectogram and time-domain plots of an FMCW signal*

Pulsed waveforms In contrast to CW systems, pulsed waveform systems do not transmit all the time. Instead, they transmit at a particular time period and in the next time period, they do not perform any transmissions but listen for any received signal. During the time period which corresponds to the pulse width, the radar TRX transmits the signal and during the silent period, it listens to any receptions. The time-domain signal expression for the pulsed waveform $x_r(t)$ is

$$x_r(t) = \sum_{m=0}^{M-1} x(t)p(t - mT_{\text{sym}}), \tag{2.8}$$

where $x(t)$ is the transmit signal in RF, M is the number of pulses and T_{sym} is the time duration which is the sum of the pulse width T and the silent period of one pulse and

$$p(t) = \begin{cases} g(t), & 0 \leq t \leq T, \\ 0, & T < t \leq T_{\text{sym}}, \end{cases} \tag{2.9}$$

where $g(t)$ is the pulse shape during the time interval corresponding to the pulse width. In radar systems, usually a train of rectangular pulses is adopted as shown in Figure 2.6. One drawback of pulsed waveforms is that when they are in the transmission phase, it cannot simultaneously perform reception. As such, for the time duration corresponding to the pulse width, the radar system is unable to perform target detection. This creates a blind zone around the radar, which is the minimum distance beyond which the radar is able to detect targets.

Reflection and reception

Despite the type of waveform used for transmission, it undergoes the same effects from the environment. When the transmitted signal hits an object, it gets reflected and travels

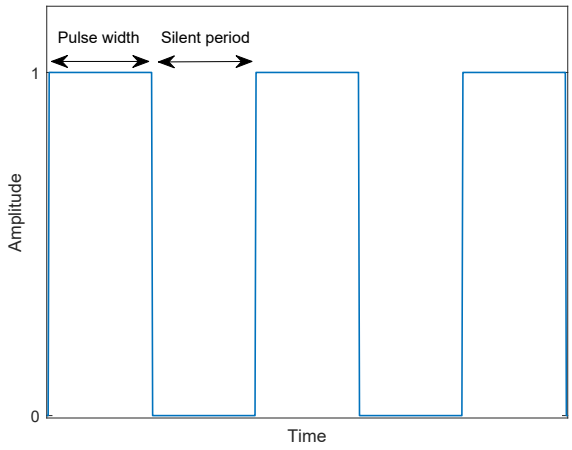

Figure 2.6. *Pulsed waveform*

back and is received by the radar transceiver, after some delay. If the target was also moving, the RX signals' frequency-domain spectrum is shifted compared to that of the TX signal. This shift, also termed as the Doppler effect, is based on the velocity of the target. If the target approaches the radar, it is a positive Doppler shift whereas if it recedes, it is a negative shift. Assuming targets are ideal points, the RX signal is

$$y_r(t) = \sum_{k=1}^{K} A_k x_r(t - \tau_k) e^{j2\pi f_{\mathrm{D},k} t} + v(t), \tag{2.10}$$

where $K, A_k, \tau_k, f_{\mathrm{D},k}$ are the number of targets, respective attenuation, delay and Doppler shift due to each target and $v(t)$ is the noise signal. This can be simplified by substituting from (2.8) as

$$y_r(t) = \sum_{k=1}^{K} A_k e^{j2\pi f_{\mathrm{D},k} t} \sum_{m=0}^{M-1} p(t - \tau_k - mT_{\mathrm{sym}}) + v(t). \tag{2.11}$$

Assuming only one target and one pulse, this can be simplified to observe the effect of reflection from the target as

$$y_r(t) = Ap(t - \tau) e^{j2\pi f_{\mathrm{D}} t} + v(t). \tag{2.12}$$

This shows that the received pulse is delayed by some delay τ and also having some Doppler shift f_D. Figure 2.7(a) depicts the transmitted and received rectangular pulses in time-domain, if the attenuation on (2.12) is neglected. The pulse is reflected and received back after some delay. Since the radar transceiver has knowledge of the transmitted time instant and therefore the time it took for a particular pulse to arrive back, the delay to the target can be estimated, which is shown in the figure. After this delay is known, the range to the target is easily calculated from an equation of linear motion as

$$R = \frac{c\tau}{2}. \tag{2.13}$$

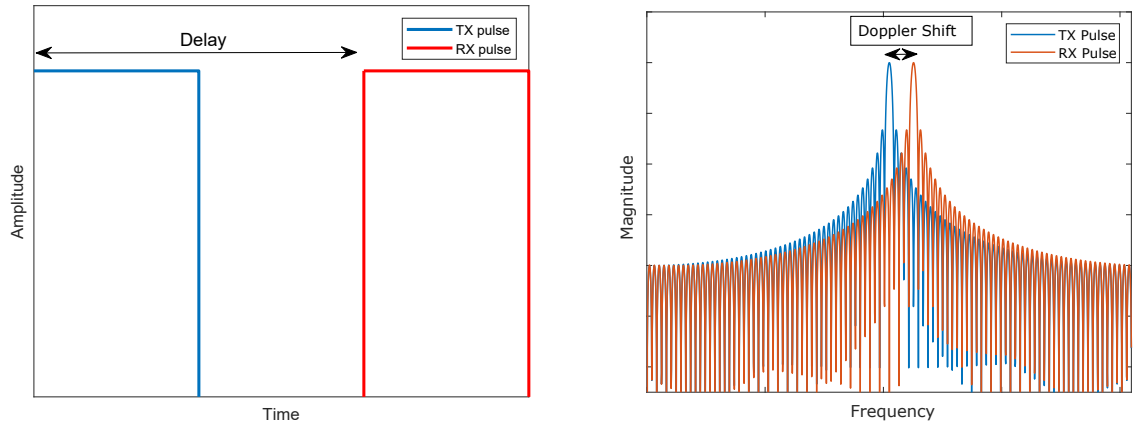

(a) *Transmitted pulse and the received pulse after reflection from a target*

(b) *Spectra of transmitted pulse and received pulse due to Doppler shift*

Figure 2.7. *Transmitted and received pulses in time and frequency domains*

A time-domain rectangular pulse maps to a sinc pulse in frequency domain. Figure 2.7(b) shows the frequency domain plot for TX and RX pulses. Sinc pulse corresponding to the received pulse can be seen to be shifted in frequency with respect to that of the TX pulse. This difference is the Doppler shift and the magnitude of the velocity v is then given by,

$$v = \frac{f_d \lambda}{2}, \tag{2.14}$$

where f_d is the measured Doppler shift and λ is the wavelength corresponding to the carrier frequency.

2.2.2 Radar range equation

For a given application, there is usually a target that needs to be detected at some maximum range. The radar range equation is used to calculate the needed transmit power so that the signal can travel this maximum distance. Considering the noise level, signal-to-noise ratio (SNR) at the radar transceiver can also be calculated. For a pulsed radar system employing M pulses and assuming coherent addition of those, the radar range equation is given below as [75]

$$\text{SNR}(M) = \frac{P_{\text{total}} G^2 \beta \lambda^2 M}{(4\pi)^3 R^4 k T_0 F B}. \tag{2.15}$$

The derivation of this is a three-step process: transmission, reflection and reception. When a TX transmits some signal at power P_T, received power at a distance R is

$$P_{\text{RX,target}} = \frac{P_{\text{total}} G_T \beta}{4\pi R^2}, \tag{2.16}$$

where the directivity gain of the radar TX is G_T. Since the targets can have different shapes, sizes and also different materials they are made of, a common term to quantize the effective area of such targets is the radar cross section (RCS), which is denoted by β. Power captured by the radar RX after the target reflection at the direction of the radar TRX can then be written as

$$P_{\text{RX,TRX}} = \frac{P_{\text{RX,target}} A_e}{4\pi R^2}, \tag{2.17}$$

where radar receiver effective area is A_e. In antenna theory, the relation between the antenna effective area and the gain of the antenna can be formally written as [44]

$$G_R = \frac{4\pi A_e}{\lambda^2}, \tag{2.18}$$

where the directivity gain of the radar RX is G_R. In this thesis, since the radar transmitter and the receiver are both considered to be the same device, the transmitter and receiver gains are assumed to be the same with $G_T = G_R = G$. For uniformly distributed and white Gaussian noise, the noise power at the RX is

$$P_{\text{noise}} = kT_0FB, \tag{2.19}$$

where k, T_0, F, B are the Boltzmann constant, temperature, noise factor and the receiver bandwidth [6]. Using M pulses give a processing gain to yield the equation (2.15). Here, the parameters corresponding to the antennas and the noise are usually known and the only parameters unknown are the range and the SNR. Therefore, by selecting the maximum range the SNR can be deduced, which allows the radar system to evaluate the performance. This can also be done the other way such that the for a fixed SNR, the maximum distance allowed by the radar system can be calculated.

2.2.3 Detection of targets

Detection of targets in the environment given the existence of many non-idealities is the task of a radar system. A statistical methodology termed detection theory is used in this regard. If a target is present in the environment, the reflected pulse is a delayed copy of the transmitted pulse, with some attenuation. The radar system needs to accurately determine this received pulse amidst noise and other interference. That is, it needs to detect the received pulse. This is also termed as hypothesis testing because in order to do this, two hypotheses need to be made, which are [45]

$$H_0 : y_r[n] = v[n], \tag{2.20}$$

$$H_1 : y_r[n] = s[n] + v[n], \tag{2.21}$$

where H_0, H_1 are the null and alternate hypotheses, $y_r[n], v[n], s[n]$ denote the samples corresponding to the received signal, noise signal and received pulse, based on (2.11). The null hypothesis represents the case when the received samples are only due to noise

whereas alternate hypothesis is the case when the received samples are a concatenation of the received pulse and noise. Assuming the noise to be normally distributed, the probability density functions (PDF) for the two hypotheses are

$$p(y_r[n]; H_0) = \frac{1}{(2\pi\sigma^2)^{N/2}} \exp\left(\sum_{n=0}^{N-1} \frac{-|y_r[n]|^2}{2\sigma^2}\right), \tag{2.22}$$

$$p(y_r[n]; H_1) = \frac{1}{(2\pi\sigma^2)^{N/2}} \exp\left(\sum_{n=0}^{N-1} \frac{-|y_r[n] - s[n]|^2}{2\sigma^2}\right), \tag{2.23}$$

where the number of samples is N and the variance of noise samples is σ.

Existence of a target is dependent upon the Neyman–Pearson criterion which is given below as [45]

$$\frac{p(y_r[n]; H_1)}{p(y_r[n]; H_0)} > \gamma, \tag{2.24}$$

where γ is some threshold. In a simple sense, this means that each sample is checked against this threshold and if the sample value is higher than it, it is classified as a target. If it is lower, it is classified as just noise. It is then intuitive that the threshold is the deciding factor. Selecting a reasonable threshold value is dependent on the errors that can be made as shown in Figure 2.8. The darker area denotes the errors that are made when H_0 is true, but H_1 is selected anyway. In radar systems, this means that a target is detected due to the noise, even though a target is not present in reality. These are false alarms for the radar systems and the darker area is the probability of false alarm P_{FA}. Conversely, the lighter area denotes the case where H_1 is true, but H_0 is selected. This would mean that the radar system cannot detect the targets that are present in reality. These are termed as missed detections and the corresponding area is the probability of missed detection P_{MD}. From the figure, it can be seen clearly that increasing γ causes less false alarms but it increases the number of missed detections. On the other hand, decreasing γ decreases the number of missed detections while increasing the number of false alarms. In radar systems, the complementary of P_{MD} is used mostly, termed as the probability of detection P_{D}.

Since γ is the deciding factor for the performance of the radar system, it is determined based on the application and the required P_{FA} and P_{D}. These probabilities are given as

$$P_{\mathsf{FA}} = \int_{\gamma}^{\infty} p(y_r[n]; H_0)\, dy_r, \tag{2.25}$$

$$P_{\mathsf{D}} = \int_{\gamma}^{\infty} p(y_r[n]; H_1)\, dy_r. \tag{2.26}$$

Since these depend on the threshold, another metric used by radar systems is the receiver operating characteristics (ROC), which shows the variation of P_{D} and P_{FA} for different SNR values. This allows for better evaluation of the system performance because it is defined for all thresholds. An example for a ROC curve is given in Figure 2.9.

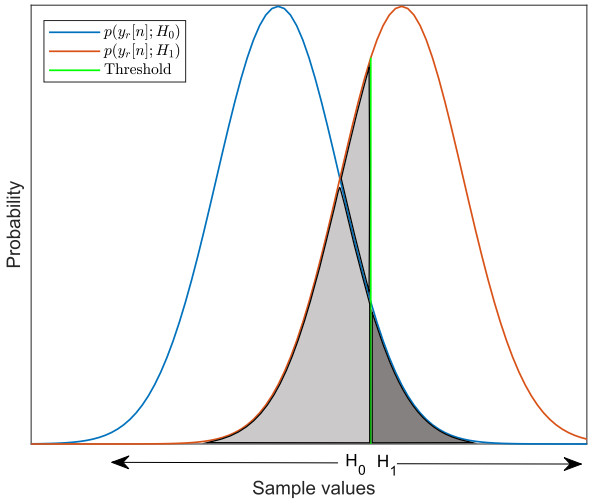

Figure 2.8. *Null and alternate hypotheses for the radar detection*

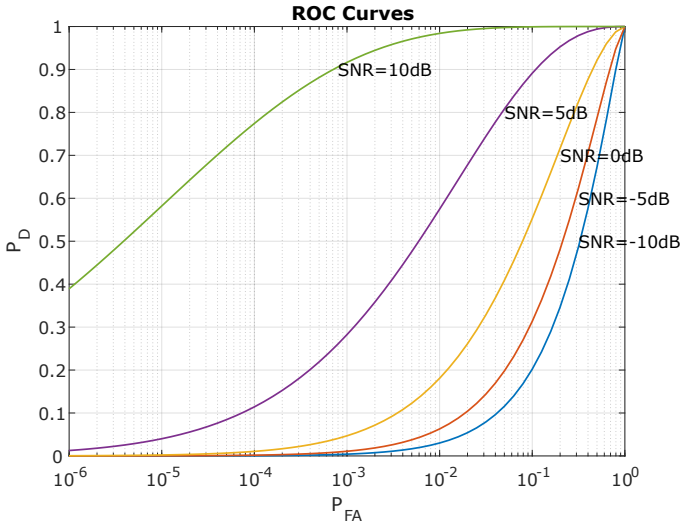

Figure 2.9. *ROC curves for different values of SNR*

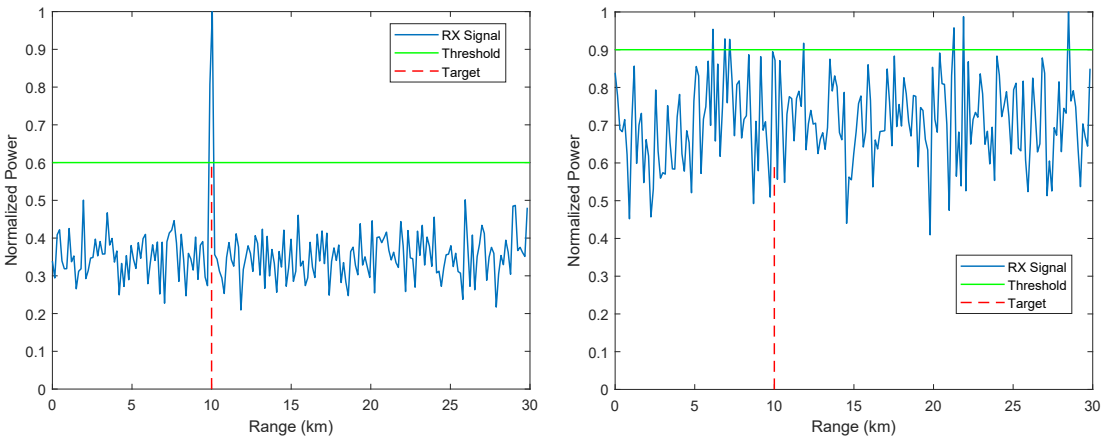

(a) *RX power from a single target* ***(b)*** *RX power from a single target with low SNR*

Figure 2.10. *RX power from a single target amidst low noise and high noise*

Each of the received samples is then mapped to a distance with the help of (2.13). These distance values are also called the range gates. In simple terms, this can be thought of as that each sample corresponds to a distance between the radar transceiver and a hypothetical target. For each of these samples, detection theory is applied for the existence of a target. After the mapping, the power of the samples can be plotted against the range gates. Figure 2.10(a) shows the received power from a single reflection at 10km from the radar. RX power for the range gate related to the target location is the maximum. The threshold is high enough to classify this as a target and also to prevent any false alarms. In contrast to this, Figure 2.10(b) shows a situation where the noise had a substantial effect on the received samples. In this case, the threshold needs to be a bit higher than the earlier case for the detection purpose. But due to the noise, this results in a missed detection. Also, it has caused a few false alarms due to the high noise values.

2.2.4 Processing and metrics of performance

Targets are detected in radar systems based on the comparison between the signals of transmission and reception, searching for some similarity. The idea is to maximise the SNR of the received signal so that the target can be detected at a reasonable precision [75]. Towards this end, the received signal which is attenuated and corrupted with noise, is sent through a matched filter (MF) and the output of this helps in detecting the targets by improving the SNR. It is termed such because MF sequence $h[n]$ is given as

$$h[n] = x^*[-n], \tag{2.27}$$

where $x[n]$ is the sampled sequence for the transmitted radar signal and $*$ denotes the conjugate operation. This is to say that the MF is a mirrored and conjugated version of the transmitted radar signal. The output of the MF $y_{\mathsf{MF}}[n]$ is then given by the convolution between $h[n]$ and $x[n]$ as

$$y_{\mathsf{MF}}[n] = \sum_{b=-\infty}^{\infty} h[b]x[n-b], \tag{2.28}$$

$$= \sum_{b=-\infty}^{\infty} x[b]x^*[b-n]. \tag{2.29}$$

Function which compares the similarity between two signals is the cross correlation function γ, defined as

$$\gamma[c] = \sum_{a=-\infty}^{\infty} x[a]y^*[a-c], \tag{2.30}$$

where $x[a], y[a]$ are the samples corresponding to the two signals and c is the index which corresponds to the lag or the index for which the similarity is considered. Usually, c runs from $(-\frac{N}{2})$ to $(\frac{N}{2}-1)$, where N is the number of samples of the signal. Comparing (2.29) with (2.30), it is evident that MF output checks the similarity between the transmit signal

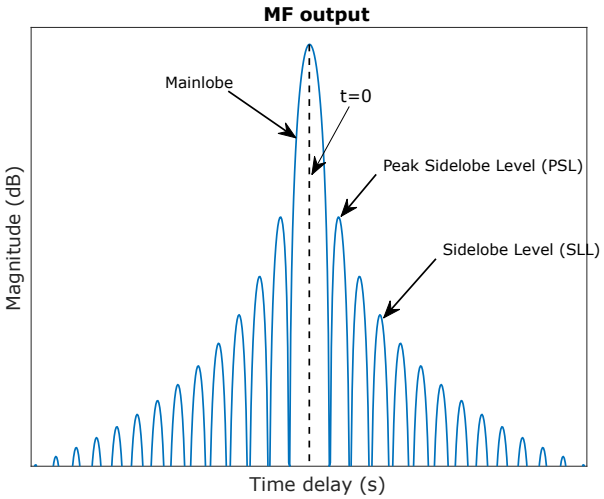

Figure 2.11. *ACF of an FMCW signal*

and the conjugated and delayed transmit signal. This is defined as the autocorrelation function (ACF) of the transmit signal. Therefore, the output of the MF is simply the ACF of the TX signal. Figure 2.11 shows the ACF of an FMCW signal. The width of the mainlobe is proportional to the range resolution, explained a bit later in this section. Having a high peak sidelobe level (PSL) would give the indication there there exists targets at different time instants, which would in turn increase the number of false alarms. So to make accurate time delay estimations, the ideal ACF of the transmitted waveform should be an impulse at $t = 0$, which also means there exists no sidelobes.

The above formation of ACF neglects the existence of a Doppler shift due to the relative velocity of the target with respect to the TX. Similar to delay estimation, a function can be defined similar to ACF in frequency domain. The ideal waveform for Doppler estimation should have an impulse at frequency domain at $f = 0$. Considering both domains, a function can be defined as the ambiguity function (AF), which is given as [54]

$$X(t, f) = \int_{-\infty}^{\infty} \mu(t)\mu^*(t + \tau)\text{exp}\,(j2\pi ft)\,dt, \tag{2.31}$$

where $\mu(t)$ is the transmitted time-domain signal, τ is the delay and $X(t, f)$ is the two-dimensional AF. This is a good indicator to evaluate the resolutions in time and frequency domains, for arbitrary waveforms. An ideal AF would have an impulse at the origin which is called the thumbtack shape. This corresponds to having impulses at $t = 0$ for time delay estimation and $f = 0$ for Doppler shift estimation.

Some metrics of performance are used to quantity radar systems. Range resolution Δr means the minimum distance between two targets in the environment so that the radar RX can process the received pulses and correctly differentiate those two distinctively as two targets. If the distance difference is below than this range resolution, the received pulses can overlap with each other which leads to incorrectly detecting only one target. A similar metric is defined as velocity resolution Δv, which is the minimum velocity dif-

ference between two targets so that the radar RX is able to accurately differentiate the two velocities. In radar systems, there is a maximum distance and velocity which can be estimated unambiguously and are termed as maximum unambiguous range (MUR) and maximum unambiguous velocity (MUV), respectively. For a pulse train modulated with a carrier frequency, expressions for these are given in Table 2.1 [1],

Parameter	Expression
Range resolution	$\Delta r = \frac{c\tau}{2}$
MUR	$\text{MUR} = \frac{c}{2*\text{PRF}}$
Velocity resolution	$\Delta v = \frac{\lambda}{2MT_{\text{sym}}}$
MUV	$\text{MUV} = \frac{\lambda*\text{PRF}}{4}$

Table 2.1. *Performance metrics for a radar system*

where c is the speed of light, τ is the pulse width, PRF is the pulse repetition frequency, λ is the wavelength corresponding to the carrier frequency, M is the number of pulses sent and T is the time duration of one pulse including the silent period.

Pulse compression To have a better range resolution, the pulse width should be decreased which in an ideal case leads to an impulse. However, decreasing the pulse width would have a detrimental effect on the SNR of the received pulse, thus making the detection process harder. Pulse compression separates this relation between the range resolution and the SNR [89]. The basic idea is to modulate the transmitted pulse in frequency or phase. As a result, the pulse can have a longer pulse width which essentially increases the average power and thus the SNR. At the same time, it allows for a better range resolution as if the pulse is having a small pulse width. Some example techniques for pulse compression are: linear frequency modulation (LFM), binary phase codes, Barker codes, poly-phase codes and Frank codes.

2.3 Communication systems

In the most basic sense, communication systems are employed to carry information from one point to another. There is a communication transmitter which sends out information and a communication receiver which gets the information sent. This information is sent through some form of medium. A single carrier is employed in traditional communication systems to which all the information is modulated. In contrast, a new system has emerged which employs a set of carriers. These are known as multicarrier systems. This thesis is concerned about a part of these systems, specifically orthogonal frequency-division multiplexing (OFDM) systems. These multicarrier systems provide the user a number of advantages when compared with the traditional ones, some of which are: efficient channel equalisation strategy for frequency selective channels, ability to change different

parameters corresponding to transmission easily and multiplexing users easily on different frequencies. Coupling the OFDM system with the concept of SDR, architecture of a communication system is as in Figure 2.12. Before continuing on with the description of this block diagram, basics of a communication system [73][2] are discussed first with respect to OFDM .

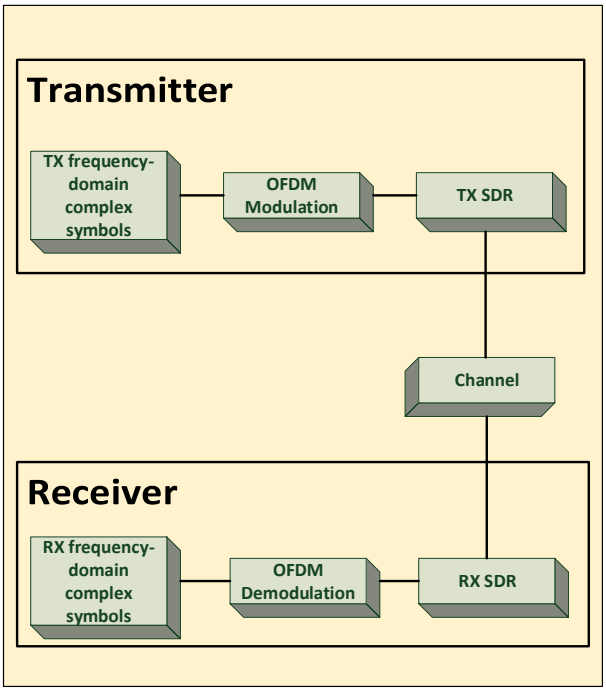

Figure 2.12. *Architecture of an OFDM system using SDR*

Digital Information An important factor about modern communication systems is that all the information considered is in digital form. If an analog signal such as speech is considered, this is converted into digital domain through sampling and quantization. Thus, digital information simply refers to a sequence of 1's and 0's, more commonly known as bits. Moreover in digital communication it is usual practice to concatenate a set of bits to form a symbol. This concatenation is done for a set of bits which are a power of two.

Modulation and demodulation All channels that are considered in digital communication are analog in nature. Thus, information from the transmitter first needs to be converted into analog domain. This is usually done by converting the symbols to continuous wave format with the help of a D/A converter to generate the baseband signal

$$x_{\mathrm{BB}}(t) = A(t)e^{j(2\pi f(t)+\phi(t))}, \tag{2.32}$$

[2]The following content on basics of a communication system was adopted from the lecture notes of Mikko Valkama, Markku Renfors in the course *Digital Communication*, Tampere University of Technology.

where $A(t), \phi(t), f(t)$ are the time-varying amplitude, phase and frequency components defined according to the symbol formation method. Changing these in discrete steps is termed amplitude-shift keying (ASK), phase-shift keying (PSK) and frequency-shift keying (FSK), respectively. There is also a further modulation scheme which combines ASK and PSK, which is to change both the amplitude and phase in discrete steps, known as quadrature amplitude modulation (QAM). The generated baseband signal is not sent directly from the antenna. Instead, it is first modulated/up-converted to a carrier frequency f_c to generate the RF signal

$$x_c(t) = x_{\mathsf{BB}}(t)e^{j2\pi f_c t}. \tag{2.33}$$

Therefore, the information content is centred around this frequency. After the signal is received at the RX, it is then demodulated or down-converted to baseband for processing.

Channel Any information that needs to be conveyed from one point to the other needs to travel through some form of a channel. When an electromagnetic wave travels through a channel, it is received from different directions due to reflections from the targets of the environment. So the same TX signal is received at the RX, from different directions, at different time instants with different amplification/attenuation. This is termed as a multipath channel whose impulse response is given by

$$h(t) = \sum_{l=1}^{L} A_l e^{j\phi_l}\delta(t-\tau_l), \tag{2.34}$$

where total number of reflectors is L, A_l denotes the attenuation per each path, ϕ_l is the phase shift due to the reflection and τ_l is the delay of each path and where

$$\delta(t) = \begin{cases} \infty, & t = 0, \\ 0, & t \neq 0, \end{cases} \tag{2.35}$$

is the Dirac delta function. Taking the Fourier transform of the impulse response $h(t)$, one can obtain the transfer function of the multipath channel as

$$H(f) = \sum_{l=1}^{L} A_l e^{j\phi_l} e^{-j2\pi f\tau_l}. \tag{2.36}$$

As a result, the channel varies for different time instants and also for different frequencies, which are termed time selectivity and frequency selectivity. The transmitted information is then received at different times and frequencies with different amplification/attenuation. This distorts the TX signal and is given by the convolution between $x(t)$ and $h(t)$ as

$$y_c(t) = x(t) * h(t), \tag{2.37}$$

$$y_c(t) = \sum_{l=1}^{L} A_l e^{j\phi_l} A_c(t-\tau_l) e^{(j2\pi f(t-\tau_l)+\phi(t-\tau_l))} e^{j2\pi f_c(t-\tau_l)}. \tag{2.38}$$

Apart from the communication system, different other systems usually work on the same frequency band. These can be other communication systems, man-made systems and professional radio networks. As a result, recovering the TX information becomes difficult since all of the information from these systems merges on top of each other at the RX. Such a phenomenon is called interference. There are different forms of noise added on top of the received signal, which degrade the performance of the communication system even further. It is the task of the RX to obtain the transmitted information accurately which was subjected to these issues.

2.3.1 OFDM link

Figure 2.13 illustrates the steps that are adopted in the transmission and reception of an OFDM signal, where Figure 2.13(a) shows the transmission steps while Figure 2.13(b) shows the reception steps. An overview of these steps is given in this section [74][3].

Whole bandwidth is divided into small portions termed as subcarriers and information is modulated to each of these subcarriers and transmitted at the same time. Information on each subcarrier is then subjected to tight rectangular pulse shaping. As a result, on frequency domain, each subcarrier corresponds to a sinc pulse. Each subcarrier is placed evenly on the frequency axis such that their spacing is $\Delta f = \frac{1}{T}$ where the useful time duration of an OFDM symbol is T. In doing so, each subcarrier becomes orthogonal to each other and as a result, at each sampling instant of the analog signal, each subcarrier does not interfere with the other subcarriers and information could be easily recovered. This is what the orthogonality in OFDM means.

When an OFDM signal encounters a frequency-selective channel, each subcarrier observes only a part of that channel at a given time and it can be considered flat for that particular subcarrier. This makes the channel equalisation straightforward since just one tap is necessary to equalise one subcarrier. Both these are depicted in Figure 2.14. This shows the frequency-domain response of five subcarriers. It is seen clearly that each subcarrier observes only a part of the channel and for that part, the channel observed is flat. Transmitted baseband signal can be written as

$$x_c(t) = \sum_{n=\frac{-N}{2}}^{n=\frac{N}{2}-1} X_n e^{j2\pi n \Delta f t}, \tag{2.39}$$

where N is the number of subcarriers, X_n is the data symbol on each subcarrier and Δf is the spacing between each subcarrier.

[3]The following content on OFDM was adopted from the lecture notes of Mikko Valkama, Markku Renfors in the course *Multicarrier and Multiantenna Techniques*, Tampere University of Technology.

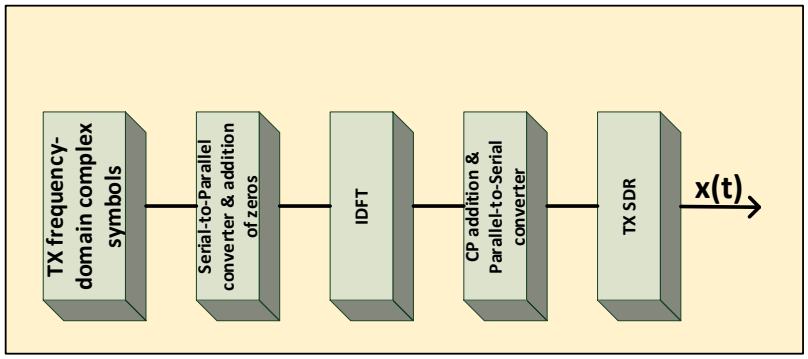

(a) *OFDM transmission*

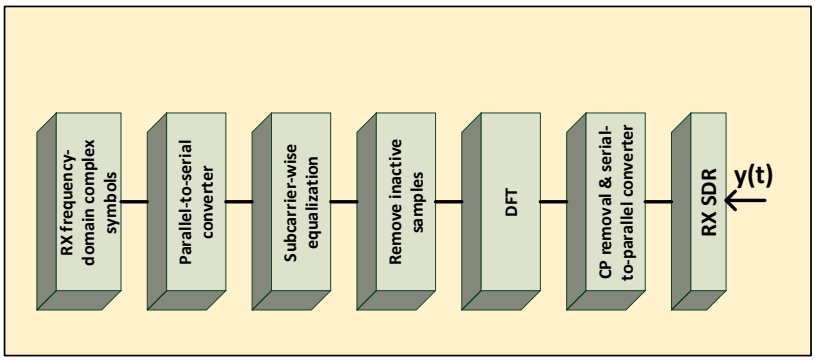

(b) *OFDM reception*

Figure 2.13. *OFDM transmission and reception*

Transmission In OFDM systems, one can quite freely select different modulation and modulation orders for each subcarrier. The incoming frequency-domain complex communication data symbols transmitted on each subcarrier are a serial stream and they are converted into a parallel stream to be sent at the same time. Since many subcarriers are used in OFDM, an efficient processing structure is needed for the whole transmission and reception processes. This is done with the help of the discrete Fourier transform (DFT) and inverse discrete Fourier transform (IDFT). Fast Fourier transform (FFT) and inverse fast Fourier transform (IFFT) operations are the computationally feasible methods to perform the same operations. An IDFT operation for N samples is denoted by

$$x_g = \frac{1}{N} \sum_{n=\frac{-N}{2}}^{n=\frac{N}{2}-1} X_n e^{\frac{j2\pi ng}{N}}, \tag{2.40}$$

where $g = (0, 1, ..., N-1)$ correspond to the time-domain samples. If the IDFT operation size is L and the number of subcarriers is less than that, zeros are padded to the parallel stream to make the IFFT process efficient. Frequency-domain TX symbols are converted to time-domain samples using IDFT.

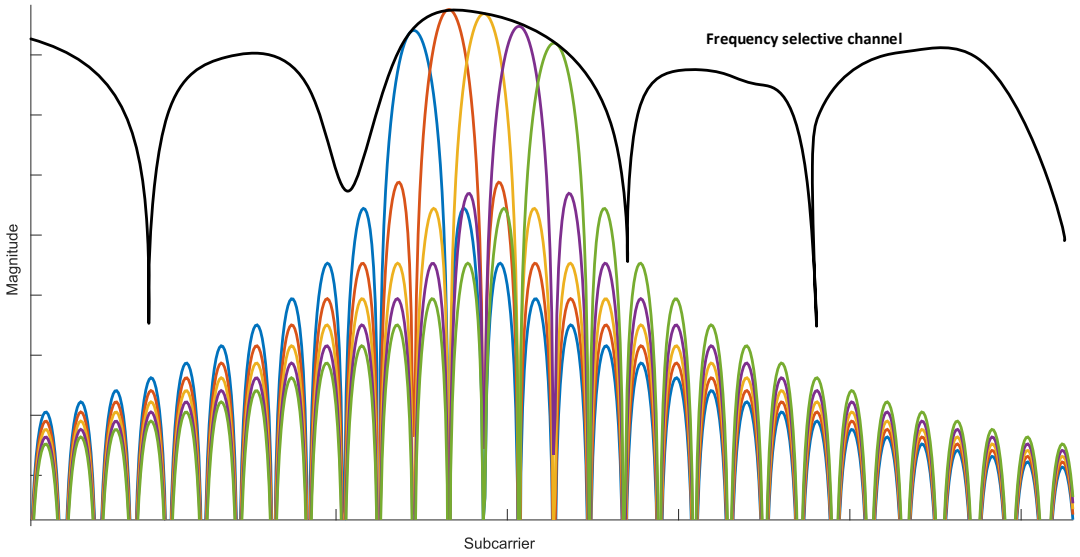

Figure 2.14. *Five subcarriers in OFDM with the channel response*

One additional step is used specifically in OFDM systems to combat multipath propagation. Multipath propagation introduces inter-symbol interference (ISI) and this additionally introduces inter-carrier interference (ICI). Due to this, the orthogonality of the subcarriers is lost. This makes the RX tasks quite difficult and it increases the bit error rate (BER) of the system. In order to prevent this, a guard period is added between OFDM symbols which is termed as the cyclic prefix (CP). This preserves the orthogonality of the subcarriers. Part of the time-domain OFDM symbol at the end is replicated at the start of that particular symbol, to yield the CP for that OFDM symbol. This thesis does not go into much details about the reasons this is performed, but an interested reader can look [69] for more information. The total time T_{sym} taken to transmit one OFDM symbol is

$$T_{\text{sym}} = T + T_{\text{CP}}, \tag{2.41}$$

where T_{CP} is the guard period time. To prepare them for transmission, parallel data is converted to a serial stream. The time-domain samples are fed to the SDR for transmission. $x(t)$ is the OFDM time-domain signal being sent.

Reception The RX simply performs the inverse operations that were done during transmission. The received time-domain signal after going through the channel and added noise is denoted by $y(t)$. This is processed by the RX SDR and it outputs the time-domain samples of the corresponding signal. The samples corresponding to CP are removed next. In order to process all the symbols, they are converted to a parallel stream. Using the inverse operation of IDFT, which was used in transmission, the DFT operation makes the time-domain samples converted into frequency domain, given by

$$X_n = \sum_{g=0}^{N-1} x_g e^{\frac{-j2\pi ng}{N}}, \tag{2.42}$$

where $n = (\frac{-N}{2}, ..., \frac{N}{2} - 1)$. In transmission, zeros were added before the IFFT operation to make the processing easier. These samples are removed here since they do not carry any information in the perspective of the communication link. To compensate for the channel imperfections due to multipath propagation, subcarrier-wise equalisation is adopted usually. This is simply multiplying each subcarrier with a complex number, where the equalisation coefficients are usually found with the help of pilot symbols. Received data symbols on frequency domain are obtained by converting the serial stream to parallel.

Channel equalisation One way to combat against multipath propagation is channel equalisation, where an inverse operation is done to negate the effect of the multipath channel. The multipath channel has some coefficients to represent itself. The idea in equalisation is to estimate these coefficients reliably so their effect can be minimised. To achieve this, the transmitter sends some known symbols to the receiver, more commonly known as pilot symbols, within the information bearing symbols. When these symbols get sent through the channel, they get attenuated and phase-shifted. Since the receiver knows these symbols beforehand, it can reliably estimate the effect of the channel by the comparison between TX and RX pilot symbols. In doing so, the receiver estimates the channel coefficients.

Zero-forcing (ZF) equalisation is used in this thesis. The received frequency-domain symbol at each subcarrier can be written as

$$Y_n = H_n X_n + N_n, \tag{2.43}$$

where Y_n, H_n, X_n, N_n are the received frequency-domain symbol, channel coefficient, transmitted frequency-domain symbol and the noise component on each subcarrier, respectively.

In equalisation, each received symbol is multiplied by a complex symbol C_n such that

$$Y'_n = C_n H_n X_n + C_n N_n. \tag{2.44}$$

This complex number C_n on each subcarrier is found with the help of pilot symbols. In ZF equalisation specifically, $C_n = \frac{1}{H_n}$. That is, equaliser coefficient is the inverse of the channel coefficient for that particular subcarrier, which yields

$$Y'_n = X_n + \frac{N_n}{H_n}. \tag{2.45}$$

The drawback here is that when the magnitude of the the channel coefficient H_n is low, it amplifies the noise component. So, in the case where the channel experiences a deep fade, the noise is amplified. But, it is usually employed due to its simplicity and ease of implementation.

Metrics for performance analysis Some metrics are used to evaluate the performance of any communication system. Typical metrics used are the bit error rate (BER)/symbol error rate (SER), bit rate and the SNR. The BER is the probability of incorrectly detecting a transmitted bit, on average. A synonymous metric is the SER, but instead of bits, symbols from a fixed constellation are considered. The relation between BER and SER can be given as

$$\text{BER} \approx \frac{\text{SER}}{\log_2 Z}, \tag{2.46}$$

where Z corresponds to the level of the modulation symbol. Bit rate of the system denotes the frequency of the bits transferred from TX to RX. For an OFDM symbol, it can be denoted as

$$R_{\text{bit}} = \frac{N \log_2 Z}{T + T_{\text{CP}}}. \tag{2.47}$$

The SNR is a metric to quantize the effect of noise on the signal. It is defined as the ratio between the signal power and the corresponding noise power. For an OFDM subcarrier, this can be denoted in the form, based on (2.45) as

$$\text{SNR}_n = \frac{|H_n|^2 \mathbf{E}\{|X_n|^2\}}{\mathbf{E}\{|N_n|^2\}}, \tag{2.48}$$

where **E** denotes the expectation operation.

If some other system operates on the same frequency band as the communication system, it causes interference and the SNR metric is modified to also include this interference, termed signal-to-interference-plus-noise ratio (SINR), defined as

$$\text{SINR}_n = \frac{|H_n|^2 \mathbf{E}\{|X_n|^2\}}{I_n + \mathbf{E}\{|N_n|^2\}}, \tag{2.49}$$

where I_n denotes the interference power on that particular subcarrier.

In addition to these, some important concepts from the information theory, needed for the latter part of the thesis are discussed here [73]. The transmitted communication signal is assumed as a random variable Q, which can take L discrete values $\{Q_1, \ ..., \ Q_L\}$. Information gained by observing a particular observation Q_k out of these discrete samples is given as

$$h(Q_k) = -\log_2 \left(p(Q_k)\right), \tag{2.50}$$

where operator p denotes probability. Performing this for all the samples and taking the average gives rise to the concept of entropy which is defined as

$$H(Q) = -\sum_{k=1}^{L} p(Q_k) \log_2 \left(p(Q_k)\right). \tag{2.51}$$

This determines the uncertainty regarding Q before observing the samples. If the entropy at the TX is $H(Q)$ and that of at the RX is $H(Q')$, a term is defined as the conditional entropy denoted by $H(Q/Q')$, which is to mean the uncertainty of Q even after Q' has been

observed. Therefore, the amount of information transferred by the channel is defined as the mutual information (MI)

$$I(Q, Q') = H(Q) - H(Q/Q'). \tag{2.52}$$

2.3.2 Commonalities with radar systems

For a communication system, usually the transmitted signal is unknown whereas the channel is known or estimated earlier with the help of pilot symbols. Ability to correctly estimate this transmitted signal and extract the information is important while the channel is of no use in itself. Conversely, in a radar system, the transmitted signal is known whereas the channel needs to be estimated [15]. Therefore the two systems are inherently different in their operation. However, they have similar features on some level.

For all practical systems used in radio communication, a bandwidth of some range within the radio wave spectrum is used. Ideally, it is needed that particular frequencies used by one system do not interfere with any other system so that the information at the receiver can be processed interference-free. This is the same for radar and communication systems. Different radar and communication systems operate at different frequency bands as shown in Figure 2.15 [22, 59, 98]. It is evident that both systems have applications that use the same band allocation and differentiation between the two must be made for both to accomplish their own functionalities.

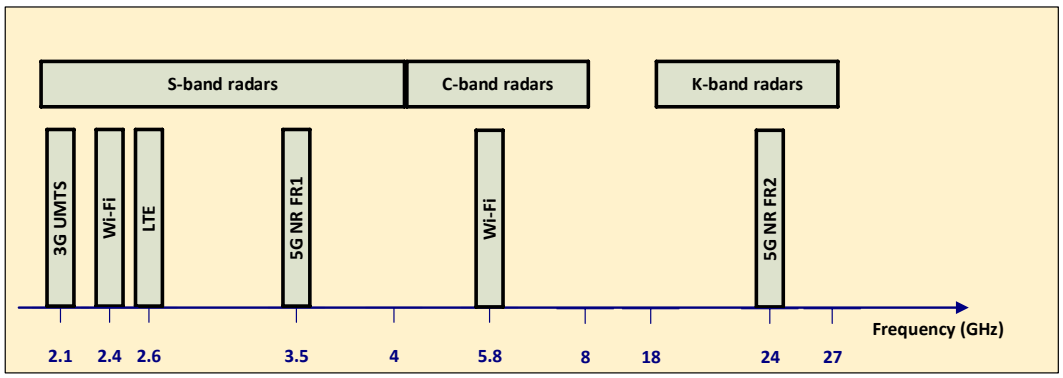

Figure 2.15. *Frequencies of operations for some radar and communication systems*

Referring to Figures 2.4(b) and 2.12, some form of similarity between the two systems is observed in terms of the hardware. In the communication system, the complex data symbols are first OFDM modulated and supplied to the TX SDR. In the radar system to achieve a waveform that is adaptive to the application necessary and the user input, complex samples are also supplied to the TX SDR. The inverse operations are done at the receiver chain for both. As such, the hardware implementation of both are quite similar and these can be combined together to perform both tasks.

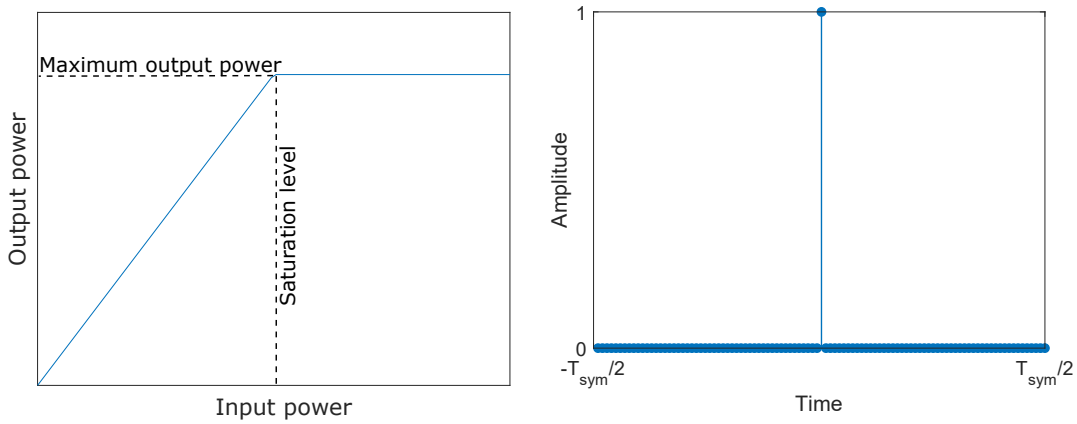

(a) *Characteristic of an ideal PA*

(b) *Ideal signal for a radar pulse*

Figure 2.16. *PA characteristics and an ideal impulse signal for radar*

Usually all radio systems use a PA to amplify the transmit signal. A PA usually has a limited range at which it is working linearly, as shown in Figure 2.16(a). Beyond a certain point, this linearity is destroyed and the PA gets saturated. Therefore, increasing the input power to the PA does not anymore yield a linear power output.

To quantize the effect of the power of a signal, an important parameter necessary in radio transmissions is the peak-to-average-power ratio (PAPR). High PAPR values push the PA to work outside the linear range. For this reason, it is required that the PAPR of the system is kept at a minimum and is an important consideration in designing radio systems. For a general signal in time-domain $x(t)$, PAPR is defined as

$$\text{PAPR} = \frac{\max_{0 \leq t \leq T}\{|x(t)^2|\}}{\text{E}\{|x(t)^2|\}}, \tag{2.53}$$

where T is the time duration for which the signal is observed. Simply put, this is the ratio between the maximum and the average of the squared absolute value of the time-domain signal in baseband. Usually, this ratio is expressed in Decibels. Typical OFDM systems have a high number of subcarriers, thus a high PAPR is evident because there is quite a reasonable probability that the information on each subcarrier can add up constructively in time domain. In the perspective of a radar system, to correctly estimate the delay to the target, the best waveform for this is an impulse signal in time domain as shown in Figure 2.16(b). Having such a signal allows the radar RX to accurately asses the difference in time between the transmitted and the received impulses. However, having an impulsive signal in time domain means that the PAPR of that signal is very high. As such, such a signal is not the best in terms of the transmission.

3 JOINT RADAR AND COMMUNICATION SYSTEMS

State-of-the-art methodologies for joint communications and sensing are discussed under this chapter. It investigates the reasons for the communication and radar systems to work together and discusses the methods that are developed to make this feasible. Section 2.3.2 listed some bands of frequencies the radar systems are allowed to operate. Since they have existed for many years, the operation bands or functionalities have not changed. Conversely, more and more communication devices and technologies come into being and the bands on which they can operate are the bands already used by the radar systems. The way to move forward with this is to combine these together so that each does not cause complications to the other.

Simultaneous operation of two systems in the same frequency band causes obvious interference to both, degrading their performance. This problem is graphically shown in Figure 3.1 where the two systems are shown to operate in the same locality. Due to the scarcity of spectrum, these can also work in the same frequency bands. The transmitted radar and communication or 'RadCom' signals are denoted by $x(t)$ and $x_{\mathsf{c}}(t)$, while $y_{\mathsf{r}}(t), y_{\mathsf{c}}(t)$ denote the received RadCom signals at the radar receiver (RX) and communication RX and $y_{\mathsf{rc}}(t), y_{\mathsf{cr}}(t)$ denote the leaked communication signal at the radar RX and the leaked radar signal at the communication RX. The tasks in hand of the radar and communication RXs are complicated due to these extra leaked signals. Figure 3.1 is a simplified scenario because realistically multiple systems work simultaneously at a given location. This problem is worsened when further sources of interference operate in the vicinity.

To observe the performance degradation a communication system has on a radar system, one metric is the signal-to-interference-plus-noise ratio (SINR) at the radar RX. When there is interference from the communication system, the SINR deteriorates, degrading the detection performance of the radar. Targets at a faraway distance are also difficult to detect since the received power from them is quite low, thus pushing them towards the low-SINR regime [48]. Another metric for radar performance is the ROC curve, which also degrades due to this interference [7, 21].

For the communication system, the SINR can also be used to quantify the interference from the radar system. It is obvious that this interference decreases the SINR at the communication RX, thus degrading its performance [32]. Another metric for the communication system is the bit error rate (BER), which is simply the average probability of incorrectly detecting a transmitted bit. The effect of the interfering radar system is to in-

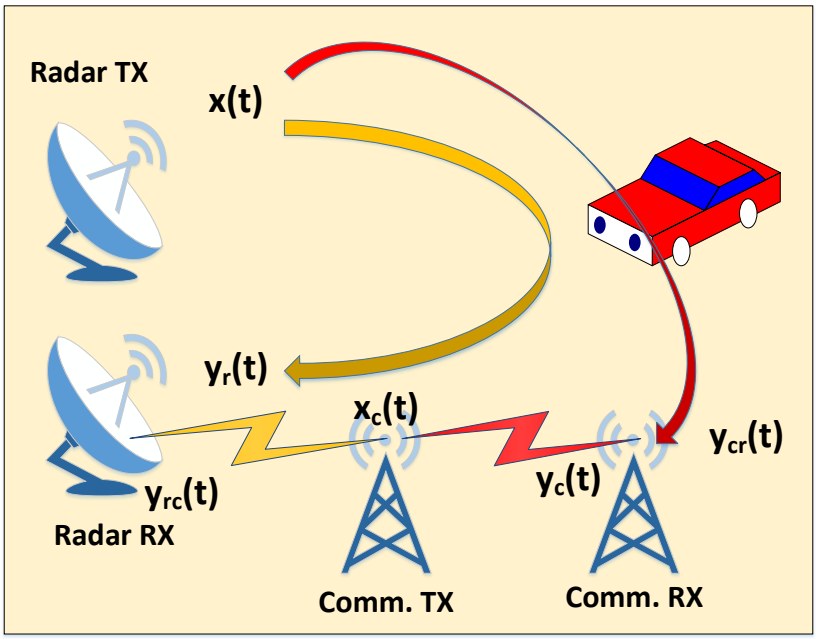

Figure 3.1. *Interference between RadCom systems*

crease the BER, again downgrading the performance [38]. Another methodology in the literature is to use a transponder as a joint system. This is a device which when received some signal, emits a different signal. Usually, when the transponder receives some radar signal, it embeds some communication information, therefore employing the same radar signal also as a communication signal. The main drawback here is that the data rate is quite low and also the same hardware cannot be used for both systems [14].

Above cases conclude that isolated operation of the two systems results in performance degradation for both. Also, it is difficult to achieve good performance if some form of management is not adopted between the two systems. In order for the systems to work in the present or the future without any issues, it is evident that a joint system must be devised to deter degrading the performance of both systems. As such, the following sections discuss the solutions that can be adopted. These can be broadly categorised into three sections, which are [15]

RF co-existence Here, each system recognises that the other system is interfering and tries to mitigate that interference. This is a step up from the legacy systems where both operate in perfect isolation, avoiding the others' interference. Mitigation is done by estimating the other systems' interference. One point to note here is that the interfering system does not willingly provide the information required to estimate this interference, but it is the task of the interfered system.

RF co-operation As the name implies, the speciality here is that both systems co-operate with each other to minimise the interference. Each system does not recognise

the other to be interfering anymore yet information of some level is exchanged between them to improve both systems' performance. This is the fundamental difference between this and RF co-existence.

RF convergence This is the newest trend in joint RadCom systems. Both systems use the same bandwidth jointly since the RF spectrum is scarce. Management between the two systems must be performed and as a result, RF convergent systems are usually built from scratch and in the design phase, resource allocation methods are used to divide the available spectrum for the two systems efficiently.

The subsequent sections go through these and thoroughly discuss the state-of-the-art research in these domains. One point to note here is that RF co-operation is considered as the first step towards RF convergence and thus the Section 3.2 is a combination of both these topics since it is difficult to categorise them specifically.

3.1 Co-existence

In the past, different applications and services were given a fixed bandwidth so that each system would not interfere with the other. One drawback of this fixed allocation is that even though there might not be actual users using that spectrum, others cannot use that because it is not intended for them. This highly inefficient allocation is the actual reason for the spectrum scarcity problem [104]. The concept of sharing the spectrum dynamically has risen as a solution to this problem. The idea behind this approach is that there is a set of users termed primary users (PU) who are allotted a part of the bandwidth. They have the highest priority to use that part but the major difference is that they do not have the full autonomy. Instead, there is also a set of users as the secondary users (SU) who can use the same bandwidth when the other set is inactive or as long as it does not hinder the performance of the PUs. As such, this is an efficient manner to use the available spectrum. In order for this to be successful, existence of PUs should be sensed by the SUs. This is termed as being cognitive in the literature and sharing common bandwidth and management between the systems becomes important as a result [56].

Sharing the spectrum dynamically involves two main tasks, which are, being aware of the surrounding users to know who has access to the RF spectrum at a given time and after this has been performed, accessing the spectrum dynamically, which is termed as dynamic spectrum access (DSA) [51]. There are different methods for the former task, energy detection which compares received energy with a threshold, matched filtering which observes the correlation between TX and RX signals and many more [57]. Thus, depending on which system is considered as the sensing user between RadCom systems, there exists three divisions of cognitive systems [42], cognitive radar where different parameters corresponding to the radar system are changed in an intelligent manner so as not to reduce the performance of the communication system, cognitive communication system

where the direct opposite is performed and the last section being joint cognition, where both systems work together to minimise the performance degradation of both systems, discussed under RF convergence.

Cognitive radar There are three requirements for a cognitive radar. Processing the echoes in an intelligent manner, feedback from TX to RX as the source of intelligence and finally keeping track of the earlier received echoes to develop a map of the environment [41]. The block diagram of a cognitive radar is given in Figure 3.2. The radar TX first sends the waveform as usual. The RX signal is processed by two blocks, the scene analyser which detects the targets from the corresponding received echoes whereas the other block, target tracker, continuously tracks the possible list of targets based on the previous returns. The processed intelligence is then fed back to the TX and it in turn intelligently controls the illumination or changes the transmitted waveform. The feedback mechanism is also made much easier on a monostatic radar system since the TX and RX are co-located.

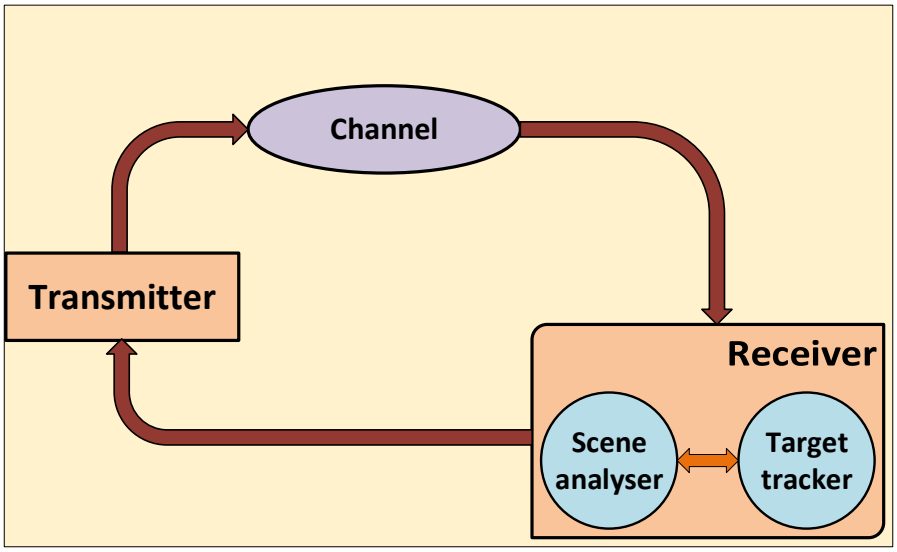

Figure 3.2. *Simplified block diagram of a cognitive radar*

An adaptive mechanism thus can be employed in designing the waveform since cognitive radars are able to change their TX waveform based on feedback. A practical example of a cognitive radar is in electronic warfare. During wartime it might be necessary for a radar system to work in harmony with a friendly communication system operating at the same frequencies. As such, it is necessary for the radar system to not interfere the communication system. The adaptive waveform design is usually centred around maximising the SNR at the RX or maximising the mutual information (MI) [10, 87].

Cognitive communication system Here, the communication users act as SUs and change their transmission parameters so as not to interfere on the radar system. A typical methodology adopted for this is to detect if a radar system is working in the neighbour-

hood and if it is the case, deter communication transmissions from interfering the radar system, using energy detection. The drawback here is that multipath fading causes a deep fade in the PU signal when compared with that of the SU. Thus, it might lead to incorrectly sensing the spectrum. As a solution, co-operative spectrum sensing is used. The idea behind co-operative sensing is that instead of a single node, multiple nodes are considered and the ensemble of realisations from these are used to arrive at the spectrum sensing [101].

Depending on the operation and detection of the radar system, the concept of co-existence space can be divided into four regions. The first region is where a radar system is detected but a communication system cannot interfere. The second region is where a radar system is not detected and interference cannot happen. The third region is where a radar system is detected and interference is possible. Since the radar system is detected, communication system transmissions can be stopped. These regions can be considered safe because interference has no effect or can be controlled. The final region is where a radar system is not detected and interference can happen. This is the challenging area that needs to be managed [62].

A practical example where a cognitive communication system is used can be the co-existence of a wireless local area network (WLAN) with a meteorological radar system. Since the communication system is cognitive, the set of WLAN devices are the SUs while the radar system can be the PU. It is possible that some WLAN devices are not aware of the other WLAN devices thus specifying individual interference levels to those do not make sense. As such, the sum interference by all of the SUs on the PU should be considered [95]. The probability density function (PDF) of the sum interference is derived and its effect is analysed for different propagation environments in this study, concluding that the interference is much more evident in bucolic areas than in metropolitan areas.

In a joint system, received radar signal is usually with low power compared with that of the received communication signal, due to the two-way path loss. If the radar RX has good knowledge about the communication systems' parameters of performance, it can easily re-create the received communication signal due to its high power. Radar RX can first decode the communication signal received into the data symbols and subsequently, converting it into a signal that can be transmitted as the communication signal. This would mean that the radar RX has successfully estimated the interfering communication signal, apart from some amplitude and phase difference. Thus, the RX signal at a given time can be written as

$$y(t) = y_{\text{radar}}(t) + \alpha e^{j\phi} y_{\text{comm}}(t) + n(t), \tag{3.1}$$

where $y_{\text{radar}}(t)$ is the RX radar signal, $y_{\text{comm}}(t)$ is the re-created communication signal, $n(t)$ is the noise signal and α, ϕ are complex coefficients to model amplitude and phase of the re-created signal. If these complex coefficients are estimated perfectly, the radar signal can be easily differentiated by subtracting the re-created signal. Otherwise, the subtraction operation yields a residual term that degrades radar performance. Therefore, the performance is dependent on the accuracy of the parameter estimation process [60].

Co-existence of legacy communication systems with a radar system is another important scenario that needs to be considered. Since the communication systems cannot change their parameters, only the radar waveform can be modified such that it minimises the effect on the communication systems. The received signal $y(t)$ at the radar RX can be written as

$$y(t) = x_{\text{radar}}(t) * h_{\text{radar}}(t) + y_{\text{comm}}(t) + n(t), \tag{3.2}$$

where $x_{\text{radar}}(t), h_{\text{radar}}(t)$ are the TX radar signal and the channel response corresponding the environment, $n(t)$ is the noise signal and $y_{\text{comm}}(t)$ is the signal received by the legacy communication systems. The radar waveform can be devised through an optimisation algorithm to result in better detection for the radar system amidst communication systems' interference. Further, SER of the communication systems can also be improved. The optimisation can be performed through maximisation of SINR at the radar RX under a total power constraint [78]. Further constraints can also be used to ascertain the radar waveform behaves well as a radar signal, which include resolutions in time and frequency, modulus of the signal and peak side-lobe level (PSL) [2].

Considering a pulsed radar system and a communication system using quadrature phase-shift keying (QPSK) modulation, it can be noted that for the duration of the pulse, radar signal interferes the communication signal. It can also be assumed that the phase of the radar signal ϕ_{radar} remains constant between pulses. The received signal in discrete time can then be written as

$$y[k] = x_{\text{radar}}[k] + x_{\text{comm}}[k] + n[k], \tag{3.3}$$

where k is the time index and $x_{\text{radar}}[k], x_{\text{comm.}}[k], n[k]$ denote the samples corresponding to radar, communication and noise signals, respectively. Radar and communications samples are modelled as

$$x_{\text{radar}}[k] = A_{\text{radar}} e^{j\phi_{\text{radar},k}}, \tag{3.4}$$

$$x_{\text{comm}}[k] = A_{\text{comm}} e^{j\phi_{\text{comm},k}}, \tag{3.5}$$

where $A_{\text{radar}}, A_{\text{comm}}, \phi_{\text{radar},k}, \phi_{\text{comm},k}$ are the amplitudes and phases for the corresponding samples, respectively.

Since the communication samples are taken from a QPSK constellation, their phases can take some discrete values given by

$$\phi_{\text{comm},k} \in \left[\frac{\pi}{4}, \frac{3\pi}{4}, \frac{5\pi}{4}, \frac{7\pi}{4}\right]. \tag{3.6}$$

If the radar signal is not removed from the communication RX, it causes errors in the estimation of the communication symbols. As such, by estimating the amplitude and phase of the radar signal, it can be re-created and deducted from the overall signal to obtain the communication signal. This can then be fed to a set of maximum likelihood estimate (MLE) detectors for the four communication symbols. The SER of the communication system decreases with the increased estimation performance [61].

Cognitive approach can also be used for modern communication systems, with an example where the PU is an S-band radar system while the SU is an indoor LTE system. Two types of scenarios can be considered, a small LTE cell indoors and a much larger LTE cell, which correspond to low-power and high-power LTE systems. International telecommunication union (ITU) has defined maximum allowed interference levels for the SU, which operate nearby a radar system adopting same frequencies. Different propagation scenarios exist with small cell just outside the streets, on top of a building, and an outdoor larger cell. Two radar systems are considered with surveillance and meteorological radars. Due to these contrasting radar systems and scenarios, different path loss models and interference requirements are adopted [72].

Figure 3.3 shows the applicability of all the above scenarios. In the prohibition zone, secondary devices cannot work in the same frequency channel or a nearby channel. The protection zone helps the radar system to protect itself against intentional and unintentional violations of the regulations. The SU thus can reside outside these zones as in the figure. For the different scenarios given, feasible distances can be found through analysing the link budgets. A link budget is simply a list of all the possible gains and losses that can happen between a TX and a RX. Thus it is possible for the two systems to co-exist in the case when the small cell is just outside the streets. However, sufficient attention should be given when deploying these small cells on top of buildings. This is because when the BS is on top of a building, it has more probability of interfering the radar system than on the streets, due to the path loss experienced. When an electromagnetic signal travels from one place to the other, the power of the signal declines due to the distance and termed as path loss. Signals from streets attenuate quickly because they have to travel through buildings, humans, vehicles and other objects. However when the BS is on top of buildings, it usually has much more LOS propagation towards the radar RX. For high power cells, the distances are much higher than small cells and this is rather challenging for the SU.

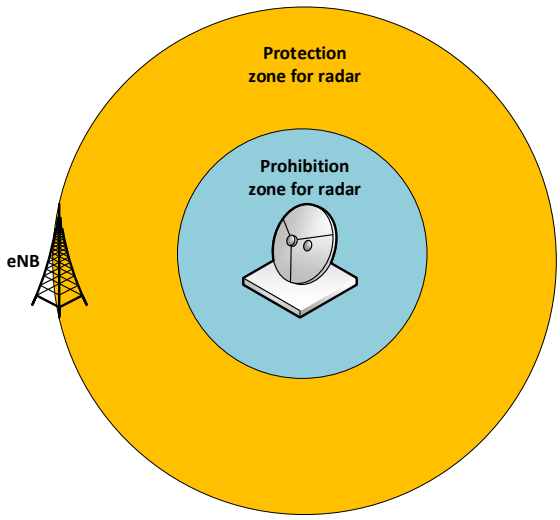

Figure 3.3. *Different zones between radar and LTE systems for co-existence*

3.2 Co-operation and convergence

Different methods have been proposed towards co-operation and convergence as shown in Figure 3.4 [15]. This section is dedicated to these different methods adopted in these categories and gives a comprehensive and complete overview. An important note is that it is strictly difficult to divide all the solutions under separate categories and some form of overlap is observed.

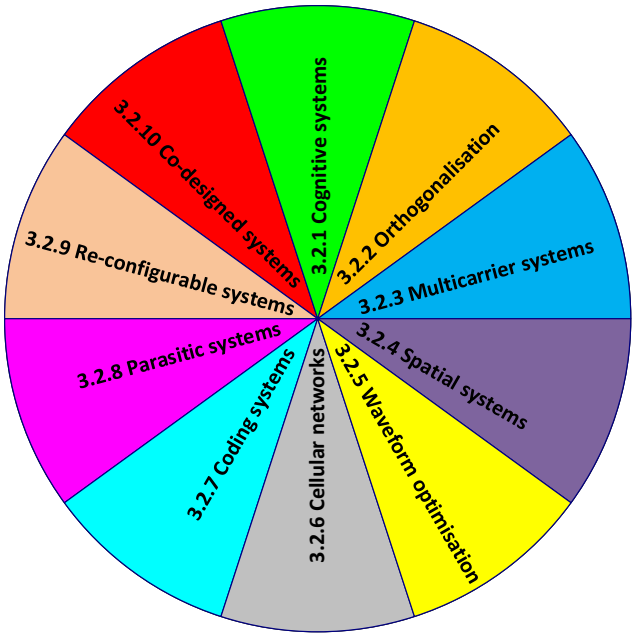

Figure 3.4. *State-of-the-art research categories on RF convergence*

3.2.1 Cognitive systems

In joint cognition systems, both radar and the communication systems are cognitive and can change their parameters to minimise the interference on each other. Cognitive radio typically does the spectrum sensing, termed as spectrum hole detection. Cognitive radar obtains the location information about the targets in the environment. This information is then passed to be processed by the cognitive radio and allows it to have an idea about the users in the environment with their distances. Since the knowledge about the users in the vicinity is known, it can more intelligently allocate spectrum among the users so as to minimise the level of interference. Combining information from both, cognitive radio can provide the cognitive radar the locations about the radio users performing communications. As a result, cognitive radar is able to change its transmitted waveform to not to hinder the performance of those users [64]. In this study, an entropy based method is used for detection of PUs. Entropy of a signal is the maximum when it is Gaussian distributed and the existence of users is identified by the comparison of the entropy of

the RX signal against a threshold and is shown to work better than the conventional energy detection. Simulations show that the interference is decreased while simultaneously increasing the throughput of the communication system.

A cognitive radar can be used in a highly dynamic environment where a communication system is also operating in the vicinity. The cognitive radar can obtain information about different communication users through the cognitive radio and adapt its waveform. An optimisation problem can be formulated where the SINR is taken as an indicator to evaluate the performance, by also constraining the interference the radar can cause for the communication users. Some more constraints to control the radar waveform to yield better resolutions in time and frequency and the amplitude of the signal, can also be applied, resulting in a radar waveform with less power in the interfering sidelobes [3].

3.2.2 Orthogonalisation

Most solutions here use the same transmit waveform for both systems. However, the two signals are made orthogonal in some domain. Inner product of the two signals are defined as

$$< f_{\text{radar}}, f_{\text{comm.}} >= \int_{-\infty}^{\infty} f_{\text{radar}}(x) f_{\text{comm.}}(x) dx, \tag{3.7}$$

where $f_{\text{radar}}(x)$ and $f_{\text{comm.}}(x)$ are the radar and communication signals. For orthogonal signals, the inner product becomes zero [84]. One complication from using orthogonal signals is that the RX has to separate the two signals and then perform the radar processing and communication demodulation. This is the price that needs to be paid in integrating the two signals [20]. Using two orthogonal codes at the TX for the radar and communication signals, RX can easily differentiate the two received signals [86].

Orthogonality in frequency domain can also be used for separating the two signals. A linear frequency-modulated (LFM) waveform, similar to the FMCW signal in Section 2.2 can be used. Here, the orthogonality is maintained by having the two signals as up-chirp and down-chirp. An up-chirp corresponds to a gradual increase in frequency over time whereas in down-chirp, the frequency decreases over time. The communication data are first modulated and up-converted to a carrier frequency and then supplied as input to a chirp filter which creates the up-chirp signal. The radar pulse is also supplied to a chirp filter which formulates the down-chirp signal. These two signals are then summed up and sent. At the RX, the received signal is first sent through a matched filter and given separately for the two systems. In the perspective of the communication system, the output is given to the demodulator to retrieve the communication data while it is fed to a threshold detector to detect the radar targets [77, 102].

Orthogonalisation in time-domain can be observed in a scenario where the communication system is Wi-Fi and the radar system operates on the same bands but sporadic in temporal domain. Thus, even though on frequency domain it coincides with the Wi-Fi system, they can be separated easily in time-domain. The PU is the radar system while the

SU is the communication system. As illustrated in Figure 3.3, the exclusion regions denote the areas where the SU is not allowed to transmit, to prevent interference. In places where the radar systems are placed near the regions with a large population, these exclusion regions can span for several kilometres and thus deem impractical because the communication systems also reside in the vicinity. These regions can be compressed by detecting the presence of the PU and switching to a different channel, due to time-domain orthogonality [80].

In Wi-Fi systems, there exist idle time periods at which transmissions are not performed. These idle times occur quite frequently and it is possible to detect the radar signals during these times. The parameters corresponding to the Wi-Fi system, specifically busy and idle times, can be changed for the betterment of the throughput of the Wi-Fi system and also to improve the detection of the radar signal, making it possible for both systems to work in the same neighbourhood with minimal performance degradation [43]. A similar scenario can be observed where the communication system is a WiMAX system, employing time-division duplexing (TDD), where the transmission and reception are differentiated by having different time slots for each. A pulsed radar system can interfere when a radar pulse is received along with a WiMAX frame and its parameters can be optimised for better performance [103].

3.2.3 Multicarrier systems

Multicarrier signals have also gained interest in the radar community. So-called P3 and P4 codes are digitally phase-coded signals, similar to the analog FMCW signals and these are used in pulse compression. They have ACF with low PSL, similar to Barker codes, and also better Doppler resilience [19]. As such, they are also used as a radar signal [53]. An important remark here is that the codes should be different to each other to achieve good ACF and therefore, complementary sets are used for this purpose. Shifting the code cyclically of a code with ideal autocorrelation properties yields a complementary set and using them result in a waveform with ideal AF in the shape of a thumbtack shape [68]. Multicarrier phase-coded (MCPC) signals can also be used for this purpose since they have high range resolution [63].

The prevalent modern waveform in mobile communications is OFDM. This revolutionised mobile communications since it allowed higher bit rates and easier structures for processing. It is the reason for this to be used in LTE and 5G New Radio systems. One of the ideas for joint communications and sensing has been to use this OFDM signal, stemming from the flexibility of using multicarrier signals in radar. Using OFDM as the joint waveform shows that the amount of pulse compression achieved is proportional to the number of subcarriers and the Doppler resolution is not affected. Thus, having higher number of subcarriers would allow better range resolution. This is an important juncture since conventional LFM waveforms used in radar have a coupling between range and Doppler estimation, which complicates the processing. Conversely, one of the important prop-

erties of using an OFDM waveform for radar is that it decouples the range and Doppler parameters. This allows both of these parameters to be processed independently [27].

A short pulse is necessary for radar systems to have good range resolution. However, this results in a pulse with less energy. One solution to this is pulse compression. Barker codes are a method adopted in this which are a sequence of {-1,1} of N_{Barker} elements such that the ACF has a mainlobe which is N_{Barker} times that of its side-lobes [82]. Due to this property, it is used frequently in radar systems. Drawbacks of this are the difficulty in implementing the system and having a low bandwidth efficiency. Instead, OFDM is a waveform which is able to achieve better resolutions in both range and Doppler domains. Complex symbols for the OFDM pulse of M symbols and N subcarriers can be found such that it generates an AF which resembles the ideal thumbtack shape. Since this ideal shape is difficult to be generated for a practical waveform, an AF with narrow mainlobe and low side-lobe levels can be formulated, to generate a waveform with the range resolution ΔR and Doppler resolution Δf_D given by [83]

$$\Delta R = \frac{t_b}{N}, \tag{3.8}$$

$$\Delta f_D = \frac{1}{M t_b}, \tag{3.9}$$

where t_b is the duration of one OFDM symbol. Reducing the PAPR of the signal is also an important consideration in OFDM, since they generally have high PAPR values. Optimising only the AF does not address this issue. One approach to this is to use a constant envelope (CE-OFDM) signal, where the modulus of the signal in time-domain is constant and does not have arbitrary amplitude [96]. However, this decreases the bandwidth utilisation and decreases the efficiency of the system.

Conventional definition of AF cannot be directly applied to signals with high bandwidth, including OFDM signals because different targets scatter differently at different frequencies and the AF does not capture these. Wideband AF (WAF) is used to address the expansion and compression of time due to the movement of targets, since it cannot be just a shift in the frequency as defined in the AF. The WAF is defined as [79]

$$X(t,f) = \exp\left(j2\pi f_c \gamma \tau\right) \left[\sqrt{\gamma} \int_{-\infty}^{\infty} \mu(t)\mu^*(\gamma(t-\tau))\exp\left(-j2\pi f t\right)\right] dt, \tag{3.10}$$

where γ acknowledges the expansion and compression of time in the received signal, $\mu(t)$ is the complex envelope of the transmitted signal and the other variables have usual meaning. An optimisation criteria can be used to develop an adaptive OFDM waveform such that the output resembles the desired WAF. Since in an ideal WAF, similar to the usual AF, the volume under the function is one, data symbols on each subcarrier can be found to ascertain the volume under the WAF of the adaptive waveform is the same such that the error is minimised. This can produce an ACF much better than the fixed waveform. Since it has lower side-lobes, better range accuracy can be observed [85]. This idea can be extended further for an OFDM waveform with M symbols to be constituting one

radar pulse, each with N subcarriers [52]. Random phase coding is used which makes each OFDM symbol different from one another and the WAF of the waveform is improved. For AF, zero delay corresponds to the Doppler cut while zero Doppler corresponds to the delay cut. Using this approach, the delay and Doppler cuts are improved.

However, using OFDM waveform in conjunction with conventional correlation mechanisms has its drawbacks [15]. Figure 3.5 illustrates the ACF of a typical OFDM signal. It can be noted that the side-lobes are comparative with the peak at the middle. Another issue is that this could result in different ACF for different information of the subcarriers. Therefore, it could provide false targets at different distances for each transmission. Another issue is the fluctuation of the PAPR with the data transmitted each time, which could harm the electronics of the system. Thus, using the OFDM waveform directly for radar purposes is not straightforward and different methods are required to circumvent the mentioned issues.

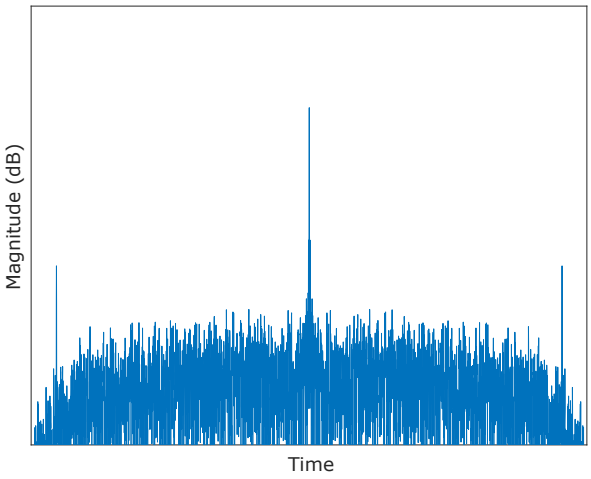

Figure 3.5. *ACF of an OFDM symbol with 1200 subcarriers*

One of the novel ideas to combat against this is called radar processing-based on modulation symbols [92]. Instead of correlating the transmitted and received time-domain signals, information required to process the channel can be inferred from the transmitted and received complex data symbols before equalisation. The impulse response of the channel can be written as

$$h(k) = \frac{1}{N} \sum_{n=0}^{N-1} \frac{g_{\mathsf{RX}}(n)}{g_{\mathsf{TX}}(n)} \exp\left(\frac{j2\pi nk}{N}\right), \tag{3.11}$$

where k corresponds to the index of the channel, number of subcarriers is denoted as N, $g_{\mathsf{RX}}(n), g_{\mathsf{TX}}(n)$ are the received and transmitted data symbols on each subcarrier. This corresponds to the range profile of the radar. The drawbacks discussed earlier are not present here. The dependency of the transmitted information is mitigated since each received complex data symbol is compared with the corresponding transmitted one, which ascertain the performance of the system is independent and does not depend anymore

on the transmitted data. The communication symbols are directly used for the radar purpose and since it can be received by the communication users too, no extra burden is needed. Since the transmitted signal is anyway received back due to the reflections, the same downlink signal can be used to produce the radar image. This idea can be extended to perform not only range estimation, but also for velocity [18]. There are also a few limitations in this method, mainly corresponding to the channel in which the sensing and communication are done. These are shown in Table 3.1 including the typical radar parameters corresponding to the range and velocity [88].

Limitation/parameters	Expression
Doppler tolerance	$\Delta f > 10 f_{\text{D,max}}$
Maximum delay difference	$\Delta t = \frac{T_{\text{CP}}}{2}$
Maximum unambiguous range	$\text{MUR} = \frac{c}{2\Delta f}$
Range resolution	$\Delta r = \frac{c}{2N\Delta f}$
Maximum unambiguous velocity	$\text{MUV} = \frac{\lambda}{2T_{\text{sym}}}$
Velocity resolution	$\Delta v = \frac{\lambda}{2MT_{\text{sym}}}$

Table 3.1. *Common limitations and radar parameters of OFDM radar*

Orthogonality of the subcarriers is crucial for the operation of an OFDM system. Towards this end, the subcarrier spacing Δf must be higher than the maximum Doppler shift $f_{\text{D,max}}$, with ten times usually being more than enough [58]. Since the propagation is considered to be multi-path, the second limitation arises from the maximum difference of time between multipath components Δt. With regards to communication, it is assumed that this is equal to T_{CP}. For radar purposes, since the signal has to travel back, the target should be at a distance corresponding to half of T_{CP}, if FFT based RX processing is performed. Depending on the application, there is usually a maximum range that needs to be detected. As such, the length of CP should be decided based on this. The other two are the typical parameters corresponding to the radar performance. Maximum unambiguous range (MUR) is thus dependent on Δf whereas increasing the number of subcarriers N improves the range resolution. Similarly, maximum unambiguous velocity (MUV) depends on the OFDM symbol duration whereas the velocity resolution is inversely proportional to the number of OFDM symbols. One point to note here is that the concept of MUR/MUV is not available with data transmission since the OFDM symbols are different from one another.

In using the modulation symbols based approach, delay to the target introduces a phase which changes linearly among the subcarriers and is used to estimate the target range whereas the Doppler shift introduces a phase per each OFDM symbol, which is used in velocity estimation of the target. Instead of using a continuous-wave signal as above, a pulsed waveform can also be used for target detection, with one pulse corresponding to one OFDM symbol with N subcarriers [97]. Flexibility of OFDM waveforms for joint sensing and communications purposes led this thesis to use it as the transmit waveform.

The pulse width determines the range resolution as shown in Table 2.1. Since the pulse width and bandwidth are inversely proportional, range resolution also has an inverse relation with the bandwidth. Different radar applications have different needs for this range resolution. More crucial applications like vehicular radar would need better resolution than an air traffic control radar. A multi-modal radar can be used to adaptively change the bandwidth of a radar signal so that the range resolution improves [8, 9]. These articles discuss an LFM waveform with a less bandwidth and threshold detection is performed to detect the targets in the environment. This corresponds to a range profile which is not quite accurate. However, this would give an indication about the locations of potential targets in the environment, resulting in some range gates with potential targets. In the next step, the bandwidth of the waveform is doubled with threshold detection only performed at those range gates that were identified earlier. This would be repeated until the targets are detected up to the required range resolution.

3.2.4 Spatial systems

Another degree of freedom explored for the joint system is the spatial domain. As such, MIMO systems are employed to differentiate RadCom systems. Wireless communication systems use MIMO systems extensively in the present world. Similarly, radar systems employing MIMO are also present nowadays. Thus, much work has been done in using the same MIMO system for both. Before moving on to joint systems, it would be beneficial to first discuss the idea behind MIMO radar. In the previous literature, radar systems usually have one TX and one RX, either monostatic or bi-static. In contrast to this, newer radar systems have developed employing multiple TX and RX antennas. There are usually two types of such antenna systems, phased-array antennas and MIMO antennas. Phased-array systems transmit signals that are correlated from its antennas whereas MIMO systems have the ability to send independent signals which are uncorrelated with each other from its antennas [55].

Figure 3.6 shows the difference between these systems for a multi-static system. In the phased-array radar in Figure 3.6(a), the transmitted signal is the same but multiplied with different scalars. The reflected signal from the targets is a sum of the attenuated versions of the same transmit signal. These types of radar systems are advantageous when the angle at which the target resides is known or when the antennas have already searched through a search volume [28]. Figure 3.6(b) showcases a MIMO radar system where different TX signals from separate antennas are used where U is the number of TX and RX antennas. Therefore, the RX signal is a combination of different signals. The advantage of MIMO is quite evident from here. Since the TX signals are different and have waveform diversity, the received signal provides more information about the environment than the case with phased-array antenna systems.

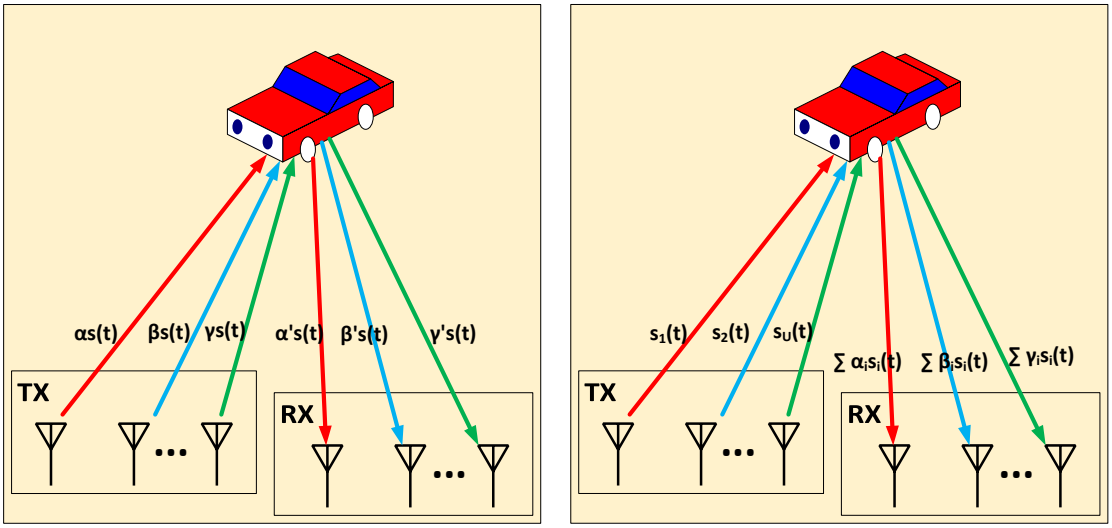

(a) *Phased-array radar system* ***(b)*** *MIMO radar system*

Figure 3.6. *Difference between phased-array and MIMO radar systems*

An advantage of using a MIMO radar is that since it has multiple TX antennas, each antenna can be used to observe a different part of the environment. Thus, it is possible to characterise a larger target, usually called an extended target, with a MIMO radar system [16]. Since multiple transmit signals are used, they can be combined at the RX either constructively or destructively. Due to this, a larger area of an extended target can be covered. Further, a MIMO radar provides better resolution compared to a single-antenna system. Another advantage is the ability to detect slowly moving targets, which would otherwise not be detected [26]. A MIMO radar also possesses many spatial degrees of freedom as given in Table 3.2, where $U_{\text{TX}}, U_{\text{RX}}$ are the number of TX and RX antennas. As such, the received signals can be differentiated easily. Here, distributed system denotes the case where the TX and RX antenna arrays are situated at separate locations.

Type of the system	Maximum degrees of freedom
Single TX antenna, Multiple RX antennas (SIMO)	U_{RX}
Independent TX and RX	$U_{\text{RX}} + U_{\text{TX}}$
MIMO system with monostatic antennas	$\frac{U_{\text{RX}}(U_{\text{TX}}+1)}{2}$
MIMO system with distributed antennas	$U_{\text{RX}} \cdot U_{\text{TX}}$

Table 3.2. *Comparison between different MIMO systems*

Thus, increase in the amount of antennas and hence the independent waveforms transmitted and received, it is possible to assess the objects of the environment quite reliably since the degrees of freedom increase. The MIMO system can also be used to find the angle of arrival, more specifically direction finding (DF). Number of targets that can be detected distinctively is equal to the number of TX antennas, due to the waveform diversity of MIMO [25]. Therefore, using the MIMO radar has many advantages compared to the conventional radar systems and it is only logical that RadCom systems use MIMO.

Combining OFDM and MIMO systems have ignited a spark in joint communications and sensing in the recent past [23]. One subcarrier is transmitted from each antenna at the same time, which are disjoint and they are commuted over time from all antennas, similar to a stepped-frequency response, where the frequency increases with time, similar to Figure 2.5(a). This gives the ability to correctly differentiate the information on each subcarrier at the RX both temporally and spatially. Pulsed radar waveform structure can also be used instead of using a continuous-waveform [58]. As such, one pulse corresponds to M OFDM symbols. The communication information is carried on each subcarrier of these M symbols, to perform joint communication.

3.2.5 Waveform optimisation

Since the idea behind this thesis is to produce OFDM waveforms that are optimal for joint communications and sensing, the following section is about different methods used in literature to achieve this. The main target is to produce a transmit waveform that is better in radar perspective which also gives better performance for the communication system. In the early days, attention was given in optimising only one system whereas the other systems' performance was neglected. So these approaches have been either in improving only the radar characteristics or the communication characteristics [49, 81].

With the emergence of RF convergence, attention was given to maximising both systems' performance. Different methods have been proposed in the optimisation of joint waveforms. Maximisation of the SINR at the radar RX is one method [4]. Another approach would be to maximise the probability of detection P_{D} of the radar system, when the probability of false alarm P_{FA} is fixed and also ascertaining the performance of the communication system is not hindered [11]. Another strategy considered in literature is the maximisation of the mutual information (MI) [10].

Typical radar systems are considered to be active, where parameters are estimated based on the transmitted signals from the radar systems. Both TX and RX antennas are included in the radar system. In contrast to this, passive radar systems use transmitted signals from other systems. As such, they do not have their own TX antennas but only RX antennas. A practical example for this is a radar system using digital audio/video broadcasting (DAB/DVB) systems. In passive radar systems, the radar RX usually receives two signals, the direct signal from the other system and the reflected signal from the targets in the environment. Distances to the targets are estimated with the help of both these signals [100].

Waveform optimisation is also performed in passive radar systems where they use the reflected information from the nearby communication systems [12, 13]. These studies use an optimisation problem to improve the delay estimation parameter which is given as

$$\mathbf{X}_{\text{opt.}} = \text{argmin}_{\mathbf{X}} \text{CRLB}(\hat{\tau}), \tag{3.12}$$

such that

$$\sum_{n=\frac{-N}{2}}^{\frac{N}{2}-1} |X_n|^2 \leq P_{\text{total}}, \tag{3.13}$$

$$|X_n|^2 \leq \delta_1, \tag{3.14}$$

$$|X_n|^2 \leq \frac{\sum_{n=\frac{-N}{2}}^{\frac{N}{2}-1} |X_n|^2 * \text{SPR}_{\text{max}}}{N}, \tag{3.15}$$

where CRLB$(\hat{\tau})$ is the Cramer–Rao lower bound of the delay estimator, $\mathbf{X}_n$ is the frequency-domain transmitted symbol on each subcarrier, N is the total number of subcarriers, $\mathbf{X}_{\text{opt.}}$ is the set of optimal frequency-domain transmitted symbols, P_{total} is the total power constraint, δ_1 is used to control the interference on the communication system and SPR_{max} is the constraint on each subcarrier to maintain the subcarrier power ratio (SPR) of the waveform, which is a similar measure on frequency-domain as PAPR for time-domain and given as

$$\text{SPR} = \frac{\text{max}_n |X_n|^2}{\frac{1}{N}||\mathbf{X}||^2}. \tag{3.16}$$

It is shown that this waveform produces an ACF which reduces the peak side-lobe level (PSL). In terms of radar, this would mean that it produces a waveform with less ambiguity.

When one narrowband signal interferes with another, one common way to mitigate against this is termed as spectrum nulling where if one system knows the frequency range it is interfering on the other system, it can prevent any transmissions in that band. When this is applied to OFDM, it is termed as non-contiguous OFDM (NC-OFDM) where a part of subcarriers is muted or carry no information. However, it is difficult to mute some subcarriers to the required level [37]. For a joint waveform, different requirements need to be met. Some of which are muting interfering subcarriers, narrow mainlobe and low sidelobes in the ACF, which cannot be performed with NC-OFDM. Muting certain subcarriers allows to control the interference by radar system on the communication system and vice versa. Improving the ACF enables better performance in radar range. The study in the reference proposes to use weights for the subcarriers since the characteristics of the waveform depend on them. Subcarrier space is divided into two, subcarriers which need to be muted to a certain level $\boldsymbol{\Omega_1}$ and the subcarriers which carry actual information $\boldsymbol{\Omega_2}$. Each subcarrier X_n is weighted by some complex value W_n. An optimisation problem is formulated to find the set of weights $\mathbf{W}_{\text{opt.}}$ for all subcarriers in a way to

$$\mathbf{W}_{\text{opt.}} = \text{argmax}_{\mathbf{W}} \frac{P_{\mathbf{\Omega_2}}}{P_{\mathbf{\Omega_1}}}, \tag{3.17}$$

such that

$$\frac{|\text{ACF}(\tau_0)|}{\text{ACF}(0)} \leq k_0, \tag{3.18}$$

$$\frac{|\text{ACF}(\tau)|}{\text{ACF}(0)} \leq k, \tau > \tau_0, \tag{3.19}$$

$$\sum_{n=\frac{-N}{2}}^{\frac{N}{2}-1} |W_n X_n|^2 \leq P_{\text{total}}. \tag{3.20}$$

where $P_{\mathbf{\Omega_1}}, P_{\mathbf{\Omega_2}}$ are the power allocated for subcarriers that need to be attenuated for a certain level and power allocated for data subcarriers, $\mathbf{W}_{\text{opt.}}$ is the set of optimum weights and τ_0 is the width of the mainlobe, k_0 is a constant which quantifies the mainlobe width, compared to the peak of the ACF at the origin, N is the total number of subcarriers and k is a constant to control the side-lobe levels of the ACF. The first constraint controls the mainlobe width of the ACF, the second controls the side-lobe levels while the last constraint is a power constraint. So, optimisation problem maximises the power allocated for in-band subcarriers while simultaneously minimising the power for other subcarriers. Using the constraints allow the ACF of the generated waveform to have a narrow mainlobe with lower side-lobe levels.

3.2.6 Cellular networks

Cellular networks are the most significant communication systems in the present world. Due to this, researchers have proposed to use this existing network for radar purposes. Radar as a subscriber technology (RAST) is one method [35]. In this approach, radar users subscribe as communication users to the cellular network and request a given number of subscriptions. Upon getting these, the radar system linearly combines them to produce a waveform with properties suitable for the radar system, through optimisation. Due to this linearity, the communication system sees them as some ordinary cellular users and also it does not interfere the communication system. Assuming the radar subscribes for L subscriptions, the optimisation function is given as

$$\text{argmin}_{\boldsymbol{\zeta}} \text{C} \left(\sum_{a=0}^{L-1} \zeta_a \phi_a \right), \tag{3.21}$$

where

$$\phi_a = [\phi_a(0) \ ... \ \phi_a(D-1)]^T, \tag{3.22}$$

is a sequence of discrete samples of length D from the cellular subscription, $\boldsymbol{\zeta}$ is the vector of coefficients corresponding to the linear combination for L subscriptions and C is some cost function to optimise the radar waveform and it can include variety of measures

with the performance of the side-lobes, tolerance to Doppler, resolutions and the modulus of the waveform.

Using the LTE system for joint communications and sensing is a new approach adopted [5]. An LTE BS continuously transmits OFDM symbols for communication users. Since the TX signal gets reflected and travels back to the BS in the downlink (DL), this signal is used for radar purposes. Since CW is used, SI is dominant here and sufficient isolation between the TX and RX is needed so that the TX signal does not completely flood the RX signal. Range and velocity of the targets are estimated based on this LTE signal. The results are shown for different bandwidths of the LTE signal and also for different time durations. It is seen that as those parameters increase, the estimation performance improves, concluding that efficient target detection and estimation can be performed using an LTE signal used for communication.

A single cellular system can also be used for both purposes due to the advent of 5G NR, thereby adopting a single signal for both systems [71]. This study proposes three types of sensing based on the signals, which are active downlink, where the reflections of the transmit signal are used for sensing, passive downlink, where reflections from other BSs are used for sensing and the last being uplink sensing, where the signals from mobile stations (MS) are used to perform the sensing. Two fundamental challenges exist in sensing, in perspective of the mobile communication signals, where the first one is due to the complicated structure of the mobile signals. Symbols for different users are situated discontinuously at time, frequency and code domains and therefore makes the usual parameter estimation techniques void. The second obstacle comes from complex multipath propagation. Overcoming these issues would allow the already built 5G NR system to perform joint communications and sensing.

Waveform optimisation can also be used for a joint system working in the mm-Wave [50]. The trade-off between the radar and communication system performance due to the use of a joint waveform is analysed in this study. The CRLB is selected for the radar parameters and minimum mean square error (MMSE) is used for the communication system. Three optimisation algorithms are proposed to produce the joint waveform. The first algorithm is to minimise the radar CRLB while constraining the communication systems to have a specific MMSE. The second algorithm does the inverse, where the minimisation is done on the communication MMSE while the constraint is the radar CRLB. The final one is to consider the radar and communication system performance as a linear combination and then have some other constraints regarding the waveform. The results are shown to improve the performance of both systems under low SNR and high number of targets and are better than the conventional waveforms, concluding that this approach can be used to improve the communication data rate while also providing high resolution for the radar in future mm-Wave equipment.

3.2.7 Coding methods

Another interesting approach in the literature for the joint system is the coding method on a symbol basis. The coding employed can be used either to generate a waveform suitable for communication or radar [91]. This study discusses a radar system considered to be cognitive and the communication system is chosen as the PU. First, the channel coefficients corresponding to the PU are estimated. The considered cognitive radar uses a pulsed waveform and at the start of each pulse, the channel estimates calculated earlier are used to check if the PU is active. If the PU is active, the radar pulse is not transmitted, thus preventing interference. Based on the channel coefficients, the radar calculates the probability that the PU is active, at the start of each pulse. This probability is compared with a threshold and if it's higher, it does not transmit.

Golay codes are a set of complementary codes to construct a phase-coded radar waveform. This has an important property that the ACF of the sum of Golay sequences is ideally an impulse at zero [66]. This would mean that using this code sequence removes the side-lobes of the range profile. These are used in data communications as well, with some examples being pilot symbols for OFDM systems and also in CDMA. Thus, it is evident that they can be used for the joint system. However, one drawback of these is that they are not resilient to arbitrary Doppler shifts. In fact, the ideal ACF is only observed when there is no Doppler shift but when there exists some Doppler shift, it has high side-lobe levels. Thus, this study develops a waveform that has ideal ACF for some comparable Doppler shifts.

Joint operation between an ultra-wideband (UWB) radar system and global positioning system (GPS) as the communication system is an interesting application. This would allow the GPS system to work better because it can supplement its performance with the information outputted by the radar system. One drawback of using a UWB system is that the spectrum available at a given time is fixed. Ability of an OFDM signal to change the information on subcarriers from one symbol to another has made it a good candidate for a UWB system and is used as an alternative [29]. A GPS receiver based on software is integrated along with an OFDM radar. One OFDM symbol is considered as one pulse and the subcarriers corresponding to the frequency range of the GPS signal are nulled, to prevent interference.

3.2.8 Parasitic systems

Parasitic systems use another system for its performance [40]. The radar system is the PU and the total bandwidth and power are allocated specifically for this while some communication symbols are embedded inside this radar signal. Different methods are available to achieve this such as waveform diversity method, amplitude modulation (AM), amplitude-shift keying (ASK) and phase modulation (PM) methods. A collection of differ-

ent waveforms is used in the radar system. For each radar pulse, a different waveform is transmitted and this corresponds to a communication symbol from a fixed dictionary. The AM and ASK methods mostly rely on beamforming, where the transmitted beam is focused in directions depending on the location of the users. Assuming there are communication users in different directions, the side-lobe level (SLL) are shaped such that each side-lobe corresponds to one communication symbol. In this case, the mainbeam direction can be used explicitly for radar users while the SLL in other directions are used for communication. Phase modulation methods can also be used because BER of these are better when compared with the other methodologies. As with all PM based methods, communication symbols are detected by observing the difference in phase between two elements. A total of $P + 1$ waveforms are sent at the same time. One waveform is taken as a reference and different pairs are made with this and all the other waveforms. This enables to have P pairs of communication signals. The difference in phase between the two waveforms of each pair is used to modulate the communication symbol [39].

Conversely, a communication signal can be used to embed radar information passively [67]. The considered radar system is a weather radar while the communication system is Wi-Fi. Dynamic frequency selection, which means that the frequency bands for each system are not fixed but selected dynamically, is an important consideration for joint RadCom systems. The RX for the communication system receives both signals at the same time. In the perspective of this RX, the radar signal behaves as a periodic impulse train. As a result, the packet containing the Wi-Fi produces errors and would increase the BER of the system. Increase of this BER is used to detect the existence of the radar system. However, the errors are not only caused by radar pulses and it can be due to collision with other Wi-Fi users or due to the inherent problem of hidden nodes in Wi-Fi networks, where some nodes cannot detect the other nodes. Towards this end, an approach is taken so as to make sure that the BER increase is only due to the working of the radar system. It is shown by simulations that a larger packet triggers a BER which is constant, indicating the presence of a radar system, but packets with shorter duration need more time to observe the radar system.

Joint working between the two systems becomes important in an emergency situation because the radar system needs to detect the targets and the communication system sends this information to a control headquarters [93]. In this study, the PU is the radar system employing UWB noise signal and the communication system is the SU, employing OFDM. The idea is to optimise the radar waveform and the metrics of performance for the two systems are the BER and the resolutions of the AF, for communication and radar, respectively. Since the same TX waveform is used, it also provides security for the communication data, which is much needed in the emergency situations. When this signal is transmitted, it is received by the possible communication users and perform OFDM demodulation in the intended band for communication. This signal when collided with the targets, gets reflected back and is processed by correlating with the TX signal.

3.2.9 Re-configurable systems

Although different methods discussed minimise the interference on each system, it might be possible that at a given time, either one of the systems is not working or not using the bandwidth. Thus, it is redundant to allocate bandwidth for that system using any of the above methods. Towards this, researchers have also proposed using re-configurable systems, where it is possible to configure the system adaptively for either only radar or communication [31]. An example scenario is considered in the study where a potential target on ground is detected by a radar system on a military aircraft. After constructing the radar image, it is communicated to another aircraft using the same platform used for radar, but now as communication. OFDM is used for the radar purpose and the radar image is constructed, and sent to the other aircraft. This idea can be extended further by employing hardware components to construct a re-configurable system [30]. This study depicts that minor changes are needed in terms of software whereas hardware-wise, nothing needs to be changed.

3.2.10 Co-designed systems

In all of the above literature, both systems were discussed separately. In the recent past, it has been proposed that instead of considering them as two distinct systems, to consider them as one full system [36]. A novel performance metric is derived that is equivalent to the conventional capacity expression for a communication system, but including also the radar system. Thus, only one expression exists here which measures the joint performance. A single MI metric can also be applied for the two systems [99]. A radar system with wide bandwidth is considered whereas the communication system is adopting OFDM. A joint waveform is derived which helps in better target detection with minimum interference effect on the OFDM system and higher throughput for the communication system. The derived joint MI is maximised to find the power at each carrier dedicated for RadCom. Joint metric can also be based on Neyman–Pearson (NP) criterion [76]. It has been used conventionally in radar target detection, where it tries to improve P_{D} with a given P_{FA}. The communication and radar performances are linearly combined to arrive at the joint criterion and given as

$$\gamma_{\text{joint}} = -\left[\underbrace{P_{\mathsf{D}} + \eta(\alpha - P_{\mathsf{FA}})}_{\text{radar}} + \underbrace{\zeta I_{\text{comm}}(x,y)}_{\text{comm.}}\right], \tag{3.23}$$

where α, η, ζ are constants that weigh the objective function to obtain the required performance, $I_{\text{comm}}(x,y)$ represents the MI for the communication system where x, y are the transmitted and received data.

4 SYSTEM MODEL

The system model used in this thesis is discussed in this chapter. The first section discusses the joint radar and communication scenario and the specific structure of the OFDM signal used. The signals used in the radar and communication systems are introduced next. Subsequent section derives the maximum likelihood estimator for target parameter estimation in the radar system while errors made in this estimation process are discussed in the final section, where the Cramer–Rao lower bounds for the parameters are derived.

The joint radar and communication system is depicted in Figure 4.1(a). The transmit signal $x(t)$ is a continuous waveform and it is an OFDM signal with M OFDM symbols, each with N subcarriers as shown in Figure 4.1(b). For a CW radar, since the transmission and reception are done at the same time, SI becomes an issue and needs to be controlled.

Time duration of one OFDM symbol including the CP is

$$T_{\text{sym}} = T + T_{\text{CP}}, \tag{4.1}$$

where T is the useful OFDM duration and T_{CP} is the time duration of the cyclic prefix. Number of samples corresponding to these time durations is N and N_{CP}. The pulse repetition interval (PRI) is the same as the OFDM symbol period and is given as

$$PRI = T_{\text{sym}}, \tag{4.2}$$

where it is dependent upon the maximum unambiguous range and velocity. To maintain orthogonality of the subcarriers, the frequency separation between the subcarriers is

$$\Delta f = \frac{1}{T}, \tag{4.3}$$

and the sampling rate is taken to be

$$F_s = \frac{N_{\text{CP}}}{T_{\text{CP}}} = \frac{N}{T} = N\Delta f. \tag{4.4}$$

The parameters necessary for the formation of the radar pulse can vary from one application to another. This thesis assumes that the parameters M, N, PRI are already defined according to the application required.

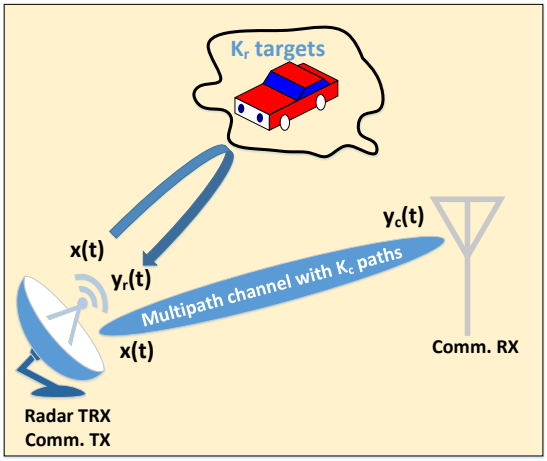

(a) *Joint radar and communication system*

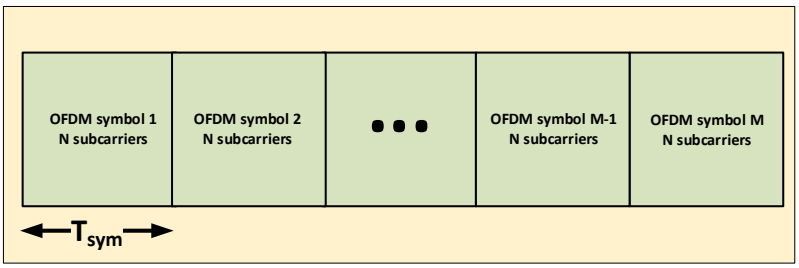

(b) *Signal structure of the TX OFDM signal*

Figure 4.1. *System model and TX signal structure*

4.1 Evaluation scenario and signal structure

When $x(t)$ is transmitted towards the environment, it gets reflected from the targets in the environment and received back at the radar TRX as $y_{\mathrm{r}}(t)$. The signal at the communication RX is $y_{\mathrm{c}}(t)$. Usually in communication systems which employ OFDM as the TX waveform (e.g., LTE, 5G), there exist some subcarriers within each OFDM symbol that are unused and these can be filled up by arbitrary data so that it improves the performance of the radar system. The insertion of data to these subcarriers is done through an optimisation algorithm. These filled subcarriers are hereon known as *radar subcarriers*. For the radar system target detection, both communication and radar subcarriers are used. The indices for communication and radar subcarriers can be arbitrary and non-contiguous for different OFDM symbols.

Radar subcarriers contain some arbitrary complex symbols. As such, both the amplitude and phase of the symbols put in these subcarriers can be freely controlled. The communication symbols are denoted by $D_{n,m}$, where n and m are the indices for the subcarriers and the OFDM symbols. Each communication symbol is weighted by a factor $W_{n,m}$ and the transmitted complex symbol in a communication subcarrier can then be written as

$$X_{\mathrm{c},n,m} = W_{n,m} D_{n,m}. \tag{4.5}$$

Depending on the modulation used in the communication symbols, the weight $W_{n,m}$ can have different forms. If the communication symbols adopt phase-shift keying (PSK), only the amplitude of the weights can be changed. Also, if it is not possible to change the amplitudes of the individual weights due to some constraint on the communication subcarriers, the other option is to scale these amplitudes equally so as not to affect the symbols. If the communication symbols use amplitude-shift keying (ASK), only the phase of the weights can be modified. Further, if the communication symbols are in the form of quadrature amplitude modulation (QAM), the option is to scale all the symbols equally so as not to alter the format of those symbols. These can be denoted as

$$W_{n,m} = \begin{cases} |W_{n,m}|, & \text{PSK}, \\ |W| \text{ for all } n, m, & \text{constrained PSK}, \\ W_{n,m} \text{ such that } |W_{n,m}| = 1, & \text{ASK}, \\ |W| \text{ for all } n, m, & \text{constrained QAM}. \end{cases} \tag{4.6}$$

The total frame which includes both communication and radar subcarriers is used to derive a waveform which is beneficial for both systems. The transmitted complex symbol in a radar subcarrier is denoted by $X_{\mathsf{r},n,m}$. The transmit signal $x(t)$ can then be written based on the continuation of (2.40) for multiple OFDM symbols as

$$x(t) = \frac{1}{N} \sum_{m=0}^{M-1} p(t - mT_{\mathsf{sym}}) \Bigg(\sum_{g \in \mathcal{R}_m} X_{\mathsf{r},m,g} e^{j2\pi g \Delta f (t - mT_{\mathsf{sym}})} + \sum_{g \in \mathcal{C}_m} X_{\mathsf{c},m,g} e^{j2\pi g \Delta f (t - mT_{\mathsf{sym}})} \Bigg), \tag{4.7}$$

where $\mathcal{R}_m$ and $\mathcal{C}_m$ denote the respective indices for radar and communication subcarriers of each OFDM symbol and

$$\mathcal{R}_m \cap \mathcal{C}_m = \varnothing. \tag{4.8}$$

4.2 Radar system

The processing involved in the radar system is discussed in this section. For this, the received signal at the radar receiver is found. The sampling process is explained and the relation between TX and RX symbols on each subcarrier due to the target range and velocity is derived. Based on this, relations between transmitted and received samples are also derived.

4.2.1 Transmission and reception

The radar channel as in Figure 4.1(a) can be denoted with the impulse response

$$h_{\mathsf{r}}(t) = \sum_{k=1}^{K_r} A_k \delta(t - \tau_k) e^{j2\pi f_{\mathsf{D},k} t}, \tag{4.9}$$

where K_r denotes the number of targets. When the TX signal travels through this channel, the received signal is given by

$$y(t) = \sum_{k=1}^{K_r} A_k x(t - \tau_k) e^{j2\pi f_{\mathsf{D},k} t} + v(t), \tag{4.10}$$

where the noisy RX signal is a delayed and attenuated version of the TX signal, also with a phase change corresponding to the relative speed between the target and the transmitter as given in (2.10). In particular, A_k is the two-way attenuation constant for the path between the radar TRX and each target while $f_{\mathsf{D},k}$ and τ_k are the Doppler shift and delay attributed to each target, respectively. The additive noise term $v(t)$ is assumed to be white and Gaussian. Substituting (4.7) in (4.10) and simplifying yields

$$y(t) = \frac{1}{N} \sum_{k=1}^{K_r} \sum_{m=0}^{M-1} \sum_{g=0}^{N-1} A_k X_{m,g} e^{-j2\pi g \Delta f (\tau_k + m T_{\mathsf{sym}})} e^{j2\pi f_{\mathsf{D},k} t} p(t - \tau_k - m T_{\mathsf{sym}}) e^{j2\pi g \Delta f t} + v(t), \tag{4.11}$$

where $X_{n,m}$ is the transmitted frequency-domain symbol and the distinction between communication and radar subcarriers is not used since all the subcarriers are used for target detection.

4.2.2 Sampling

Sampling this signal at F_{s} corresponds to time instants $\frac{l}{F_{\mathsf{s}}}$ where $l = 0, 1, ..., M(N + N_{\mathsf{CP}}) - 1$. The sampled sequence is then given by

$$y[l] = \frac{1}{N} \sum_{k=1}^{K_r} \sum_{m=0}^{M-1} \sum_{g=0}^{N-1} \left[A_k X_{m,g} e^{-j2\pi g \Delta f (\tau_k + m T_{\mathsf{sym}})} e^{j2\pi f_{\mathsf{D},k} \frac{l}{F_{\mathsf{s}}}} p(\frac{l}{F_{\mathsf{s}}} - \tau_k - m T_{\mathsf{sym}}) \right] e^{j2\pi g \Delta f \frac{l}{F_{\mathsf{s}}}} + v[l], \tag{4.12}$$

where $y[l] = y(\frac{l}{F_s})$ and $v[l] = v(\frac{l}{F_s})$. After the A/D conversion, the samples corresponding to CP are removed. Since some samples ($i = 0, 1, ..., MN - 1$) are removed, phase change due to Doppler effect must be compensated. This will be insignificant per subcarrier, but needs to taken into account per OFDM symbol. Denoting each of these time-domain samples per OFDM symbol as $y_{m,i}$ with $v_{m,i}$ as noise samples and also noticing

the term outside the bracket can be represented as $e^{j2\pi g\Delta f\frac{i}{F_\mathsf{s}}} = e^{\frac{j2\pi g\Delta f i}{N\Delta f}} = e^{\frac{j2\pi gi}{N}}$

$$y_{i,m} = \frac{1}{N}\sum_{k=1}^{K_r}\sum_{g=0}^{N-1}\left[A_k X_{m,g} e^{-j2\pi g\Delta f(\tau_k + mT_\mathsf{sym})} e^{j2\pi f_{\mathsf{D},k}\frac{i+m(N+N_\mathsf{CP})}{F_\mathsf{s}}}\right] e^{\frac{j2\pi gi}{N}} + v_{m,l}. \quad (4.13)$$

Because $F_\mathsf{s} \gg f_{\mathsf{D},k}$, last phase term can be approximated as

$$e^{j2\pi f_{\mathsf{D},k}\frac{i+m(N+N_\mathsf{CP})}{F_\mathsf{s}}} = e^{j2\pi\left(\frac{f_{\mathsf{D},k}i}{F_\mathsf{s}} + f_{\mathsf{D},k}mT_\mathsf{sym}\right)} \approx e^{j2\pi f_{\mathsf{D},k}mT_\mathsf{sym}}, \quad (4.14)$$

since $\frac{f_{\mathsf{D},k}i}{F_\mathsf{s}} \approx 0$, to yield the time-domain samples

$$y_{i,m} = \frac{1}{N}\sum_{k=1}^{K_r} A_k e^{j2\pi f_{\mathsf{D},k}mT_\mathsf{sym}} \sum_{g=0}^{N-1}\left[X_{m,g} e^{-j2\pi g\Delta f(\tau_k + mT_\mathsf{sym})}\right] e^{\frac{j2\pi gi}{N}} + v_{m,i}. \quad (4.15)$$

Converting the time-domain samples into frequency domain yields

$$Y_{n,m} = \sum_{k=1}^{K_r} A_k e^{j2\pi f_{\mathsf{D},k}mT_\mathsf{sym}} \overbrace{\sum_{i=0}^{N-1}\underbrace{\frac{1}{N}\sum_{g=0}^{N-1}\left[X_{m,g} e^{-j2\pi g\Delta f(\tau_k + mT_\mathsf{sym})}\right] e^{\frac{j2\pi gi}{N}}}_{\text{N-point IDFT}} e^{\frac{-j2\pi ni}{N}}}^{\text{N-point DFT}} + V_{n,m}, \quad (4.16)$$

where the noise samples $V_{n,m}$ are independent and identically distributed (i.i.d.) and complex white Gaussian. Changing the order of summation yields

$$Y_{n,m} = \frac{1}{N}\sum_{k=1}^{K_r} A_k e^{j2\pi f_{\mathsf{D},k}mT_\mathsf{sym}} \sum_{g=0}^{N-1} X_{m,g} e^{-j2\pi g\Delta f(\tau_k + mT_\mathsf{sym})} \sum_{i=0}^{N-1} e^{\frac{j2\pi i(g-n)}{N}} + V_{n,m}, \quad (4.17)$$

where

$$\sum_{i=0}^{N-1} e^{\frac{j2\pi i(g-n)}{N}} = \begin{cases} N, & \text{if } g = n, \\ 0, & \text{if } g \neq n. \end{cases} \quad (4.18)$$

This can be represented as

$$Y_{n,m} = \sum_{k=1}^{K_r} \tilde{A}_k X_{n,m} e^{-j2\pi n\Delta f\tau_k} e^{j2\pi f_{\mathsf{D,k}}mT_\mathsf{sym}} + V_{n,m}, \quad (4.19)$$

where $\tilde{A}_k = A_k e^{-j2\pi nm\Delta fT_\mathsf{sym}}$, since that exponential is known beforehand and it does not contain any of the parameters. When assuming only one target and neglecting the subscripts for simplicity, the effects of delay and Doppler can be depicted as

$$Y_{n,m} = \tilde{A} X_{n,m} e^{-j2\pi n\Delta f\tau} e^{j2\pi f_\mathsf{D}mT_\mathsf{sym}} + V_{n,m}. \quad (4.20)$$

It is seen that the received symbol is a noisy, phase-changed version of the transmitted symbol, due to the delay and the Doppler effect. Moreover, it is attenuated by the two-way attenuation constant.

The received symbols for one pulse can be denoted in matrix notation assuming $\tilde{A} = 1$

$$\mathbf{Y} = \mathbf{DXB} + \mathbf{V}, \tag{4.21}$$

where $\mathbf{Y}$ is the received symbol matrix of size $N \times M$ and $(\mathbf{Y})_{n,m} = Y_{n,m}$, $\mathbf{D} = \text{diag}(\mathbf{d})$ is a diagonal matrix of size $N \times N$ where each element is given by $\mathbf{d}_n = e^{-j2\pi n \Delta f \tau}$ and $n = (-N/2, ..., N/2 - 1)$, $\mathbf{X}$ is the transmitted symbol matrix of size $N \times M$ and $(\mathbf{X})_{n,m} = X_{n,m}$, $\mathbf{B} = \text{diag}(\mathbf{b})$ is a diagonal matrix of size $M \times M$ where each element is given by $\mathbf{b}_m = e^{j2\pi m f_{\mathsf{D}} T_{\mathsf{sym}}}$ and $m = (0, ..., M-1)$ and $\mathbf{V}$ is the noise matrix of size $N \times M$ and $(\mathbf{V})_{n,m} = V_{n,m}$.

It is essential for the subsequent sections that the signal model be vectorised to the form

$$\mathbf{y} = \mathbf{s} + \mathbf{v}, \tag{4.22}$$

where $\mathbf{y} = \text{vec}(\mathbf{Y})$, $\mathbf{s} = \text{vec}(\mathbf{DXB})$ and $\mathbf{v} = \text{vec}(\mathbf{V})$ are all of the size $NM \times 1$. The mean vector and covariance matrix of $\mathbf{y}$ for can be depicted as

$$\mathbf{m}_{\mathbf{y}} = \mathbf{s}, \tag{4.23}$$

$$\mathbf{\Sigma} = E(\mathbf{s}\mathbf{s}^H) + \sigma^2\mathbf{I} = \mathbf{s}\mathbf{s}^H + \sigma^2\mathbf{I}, \tag{4.24}$$

based on (A.4) and (A.6) in Appendix A.1. Mean and covariance matrix of noise samples are given by

$$\mathbf{E}(\mathbf{v}) = \mathbf{0}, \tag{4.25}$$

$$\mathbf{C}_{\mathbf{v}} = \sigma^2\mathbf{I}, \tag{4.26}$$

where σ^2 is the noise variance and $\mathbf{E}$ is the expectation operator.

4.3 Communication system

The communication channel can be denoted with the impulse response

$$h_{\mathsf{c}}(t) = \sum_{k=1}^{K_c} A_{\mathsf{c},k}\,\delta(t - \tau_{\mathsf{c},k}) e^{j2\pi f_{\mathsf{c,D},k} t}, \tag{4.27}$$

where K_c is the total number of multipath components. The signal received at the communication RX can then be denoted as

$$y_{\mathsf{c}}(t) = \sum_{k=1}^{K_c} A_{\mathsf{c},k}\, x(t - \tau_{\mathsf{c},k}) e^{j2\pi f_{\mathsf{c,D},k} t} + v_{\mathsf{c}}(t), \tag{4.28}$$

which can be simplified based on (4.19) as

$$Y_{\mathsf{C},n,m} = \sum_{k=1}^{K_\mathsf{C}} \tilde{A}_{\mathsf{C},k} X_{\mathsf{C},n,m} e^{-j2\pi n \Delta f \tau_{\mathsf{C},k}} e^{j2\pi f_{\mathsf{C,D},k} m T_{\mathsf{sym}}} + V_{\mathsf{C},m,n}. \tag{4.29}$$

For the communication signal, it is plausible to assume that the multipath channel component per subcarrier, based on the Fourier transform of (4.27) is

$$H_{\mathsf{C},n,m} = \sum_{k=1}^{K_\mathsf{C}} \tilde{A}_{\mathsf{C},k} e^{-j2\pi n \Delta f \tau_{\mathsf{C},k}} e^{j2\pi f_{\mathsf{D},k} m T_{\mathsf{sym}}}, \tag{4.30}$$

and this has been estimated based on the pilot symbols and this information has been fed back to the communication TX. This also assumes that the communication RX knows the subcarriers corresponding to communication and symbols on radar subcarriers are discarded accordingly. The SNR per subcarrier can then be calculated for communication as

$$\mathsf{SNR}_{\mathsf{C},n,m} = P_{m,n} \frac{|H_{\mathsf{C},n,m}|^2}{\sigma_\mathsf{C}^2}, \tag{4.31}$$

where σ_C^2 denotes the variance of noise at the communication RX and

$$P_{n,m} = \mathbf{E}\{|X_{n,m}|^2\}. \tag{4.32}$$

The powers allocated for the communication and optimised radar subcarriers are given respectively as

$$P_{\mathsf{comm.}} = \frac{1}{MN} \sum_{m=0}^{M-1} \sum_{n \in \mathcal{C}_m} |X_{\mathsf{C},n,m}|^2, \tag{4.33}$$

$$P_{\mathsf{radar}} = \frac{1}{MN} \sum_{m=0}^{M-1} \sum_{n \in \mathcal{R}_m} |X_{\mathsf{r},n,m}|^2. \tag{4.34}$$

4.4 Maximum likelihood estimation for distance and velocity

The received frequency-domain symbols are used by the radar system to estimate the the delays and Doppler shifts to the different targets, to derive the distance and velocity of the targets. Towards this end, maximum likelihood estimator (MLE) is used and this section discusses the estimation procedure [17]. The parameter vector $\boldsymbol{\theta}$ that needs to be estimated is

$$\boldsymbol{\theta} = [\tau, f_\mathsf{D}]^T. \tag{4.35}$$

Since the noise samples are i.i.d. and Gaussian distributed, the joint density function of the noise samples $V_{n,m}$ based on (4.20) can be written as

$$\mathcal{P}(\mathbf{V}) = \frac{1}{(\pi\sigma^2)^{MN/2}} \prod_{m=0}^{M-1} \prod_{n=0}^{N-1} \frac{e^{-|V_{n,m}|^2}}{\sigma^2}. \tag{4.36}$$

Substituting for the noise samples assuming $\tilde{A} = 1$ yields the likelihood function

$$\mathcal{P}(\mathbf{Y}; \tilde{\boldsymbol{\theta}}) = \frac{1}{(\pi\sigma^2)^{MN/2}} \prod_{m=0}^{M-1} \prod_{n=0}^{N-1} \frac{e^{-|Y_{n,m} - X_{n,m} e^{-j2\pi n \Delta f \tau} e^{j2\pi m f_{\mathsf{D}} T_{\mathsf{sym}}}|^2}}{\sigma^2}. \tag{4.37}$$

Taking the log-likelihood function results in

$$\mathcal{L}(\mathbf{Y}; \tilde{\boldsymbol{\theta}}) = -\frac{MN}{2} \log(\pi\sigma^2) - \frac{1}{\sigma^2} \sum_{m=0}^{M-1} \sum_{n=0}^{N-1} |Y_{n,m} - X_{n,m} e^{-j2\pi n \Delta f \tau} e^{j2\pi m f_{\mathsf{D}} T_{\mathsf{sym}}}|^2. \tag{4.38}$$

In order for the MLE to be derived, the log-likelihood function needs to be differentiated with respect to the parameter vector and thus from the above equations, terms that do not depend on the parameters can be omitted. The squared term can be simplified further as

$$\begin{aligned} |Y_{n,m} - X_{n,m} e^{-j2\pi n \Delta f \tau} e^{j2\pi m f_{\mathsf{D}} T_{\mathsf{sym}}}|^2 = |Y_{n,m}|^2 + |X_{n,m}|^2 - Y^*_{n,m} X_{n,m} e^{-j2\pi n \Delta f \tau} e^{j2\pi m f_{\mathsf{D}} T_{\mathsf{sym}}} \\ - X^*_{n,m} Y_{n,m} e^{j2\pi n \Delta f \tau} e^{-j2\pi m f_{\mathsf{D}} T_{\mathsf{sym}}}. \end{aligned} \tag{4.39}$$

Noting that the last two terms are conjugates of each other result in

$$\begin{aligned} |Y_{n,m} - X_{n,m} e^{-j2\pi n \Delta f \tau} e^{j2\pi m f_{\mathsf{D}} T_{\mathsf{sym}}}|^2 = |Y_{n,m}|^2 + |X_{n,m}|^2 \\ - 2\Re(Y^*_{n,m} X_{n,m} e^{-j2\pi n \Delta f \tau} e^{j2\pi m f_{\mathsf{D}} T_{\mathsf{sym}}}). \end{aligned} \tag{4.40}$$

The simplified log-likelihood function after removing the terms that do not depend of the parameters is

$$\mathcal{L}(\mathbf{Y}; \tilde{\boldsymbol{\theta}}) = \Re \left[\sum_{m=0}^{M-1} \sum_{n=0}^{N-1} Y^*_{n,m} X_{n,m} e^{-j2\pi n \Delta f \tau} e^{j2\pi m f_{\mathsf{D}} T_{\mathsf{sym}}} \right]. \tag{4.41}$$

In order to derive the MLE, this needs to be differentiated with respect to each of the parameters to yield

$$\frac{\partial \mathcal{L}(\mathbf{Y}; \tilde{\boldsymbol{\theta}})}{\partial \tau} = (-j4\pi\Delta f) \Re \left[\sum_{m=0}^{M-1} \sum_{n=0}^{N-1} (n) Y^*_{n,m} X_{n,m} e^{-j2\pi n \Delta f \tau} e^{j2\pi m f_{\mathsf{D}} T_{\mathsf{sym}}} \right], \tag{4.42}$$

$$\frac{\partial \mathcal{L}(\mathbf{Y}; \tilde{\boldsymbol{\theta}})}{\partial f_{\mathsf{D}}} = (j4\pi T_{\mathsf{sym}}) \Re \left[\sum_{m=0}^{M-1} \sum_{n=0}^{N-1} (m) Y^*_{n,m} X_{n,m} e^{-j2\pi n \Delta f \tau} e^{j2\pi m f_{\mathsf{D}} T_{\mathsf{sym}}} \right]. \tag{4.43}$$

To derive the MLE, these need to be equated to zero. This cannot be solved easily and instead, the procedure adopted in [17] is used. Rearranging (4.41) as

$$\mathcal{L}(\mathbf{Y}; \tilde{\boldsymbol{\theta}}) = \Re \left[\sum_{m=0}^{M-1} \left(\sum_{n=0}^{N-1} Z_{n,m} e^{-j2\pi n \Delta f \tau} \right) e^{j2\pi m f_{\mathsf{D}} T_{\mathsf{sym}}} \right], \tag{4.44}$$

where $Z_{n,m} = Y^*_{n,m} X_{n,m}$, it is seen that the inner and outer sums have some similarity with the definitions of DFT and IDFT. Therefore, MLE is found with the help of these by

quantising the delay and Doppler frequency parameters as

$$\tau_{n'} = \frac{n'}{N\Delta f},\ n' = 0, ..., N-1, \tag{4.45}$$

$$f_{D_{m'}} = \frac{m'}{MT_{\mathsf{sym}}},\ m' = 0, ..., M-1. \tag{4.46}$$

Substituting these in (4.44) results in

$$\mathcal{L}(n', m') = \Re\left[\overbrace{\sum_{m=0}^{M-1}\underbrace{\left(\sum_{n=0}^{N-1} Z_{n,m} e^{\frac{-j2\pi nn'}{N}}\right)}_{N\text{-length FFT}} e^{\frac{j2\pi mm'}{M}}}^{M\text{-length IFFT}}\right]. \tag{4.47}$$

To find the parameters which correspond to the MLE, values of m', n' are found as the values that maximise the log-likelihood function and denoted as

$$\left(n_{\mathsf{max}}, m_{\mathsf{max}}\right) = \mathrm{argmax}\left(\mathcal{L}(n', m')\right). \tag{4.48}$$

These are substituted in (4.45) and (4.46) to estimate the parameter value set

$$\hat{\boldsymbol{\theta}} = [\hat{\tau}, \hat{f_{\mathsf{D}}}]^T. \tag{4.49}$$

4.5 Cramer–Rao lower bounds for distance and velocity estimation

It is usually the case for any parameter estimation process that the estimated parameter values deviate from the true values for those parameters, causing some errors. The variances of these errors for the delay and Doppler estimates can be given as

$$\mathbf{var}(\hat{\tau}) = \mathbf{E}\left((\hat{\tau} - \tau)^2\right), \tag{4.50}$$

$$\mathbf{var}(\hat{f_{\mathsf{D}}}) = \mathbf{E}\left((\hat{f_{\mathsf{D}}} - f_{\mathsf{D}})^2\right), \tag{4.51}$$

where **var** is the variance of the estimator. It is essential that these variances be minimised. For a given parameter set, the minimum variance of any estimator is limited by the Cramer–Rao lower bound (CRLB) and can be calculated by the inverse Fisher matrix [46].

For the signal model given by (4.21), CRLB for the estimators are calculated from (A.14) as given in the Appendix A.1 as

$$I(\boldsymbol{\theta})_{i,j} = 2\Re\left[\frac{\partial \mathbf{s}^H}{\partial \boldsymbol{\theta}_i}(\mathbf{s}\mathbf{s}^H + \sigma^2\mathbf{I})^{-1}\frac{\partial \mathbf{s}}{\partial \boldsymbol{\theta}_j}\right], \tag{4.52}$$

where $I(\boldsymbol{\theta})_{i,j}$ corresponds to the element in the i^{th} row and j^{th} column of the Fisher

matrix. Depending on the variable with respect to which the vector **s** is differentiated, this can be simplified as

$$I(\boldsymbol{\theta})_{i,j} = 2\Re\left[\mathbf{s}^H \mathbf{D}_i (\mathbf{s}\mathbf{s}^H + \sigma^2 \mathbf{I})^{-1} \mathbf{D}_j \mathbf{s}\right]. \tag{4.53}$$

If the differentiating variable is τ, $\mathbf{D}_i = \mathbf{D}_\tau = \text{diag}(\mathbf{d}_\tau)$, in which $\mathbf{d}_\tau$ is a vector of size $NM \times 1$ where the first N elements are $(-N/2, ..., N/2-1)$ and these N elements being repeated for M times. Similarly, if the differentiating variable is f_D, $\mathbf{D}_j = \mathbf{D}_{f_\mathsf{D}} = \text{diag}(\mathbf{d}_{f_\mathsf{D}})$, in which $\mathbf{d}_{f_\mathsf{D}}$ is a vector of size $NM \times 1$ where sets of N elements are the same, with the starting and ending indices being zero and $M-1$ respectively. Each element of the Fisher matrix which is now of size 2×2 is derived using (4.53)

$$I(\boldsymbol{\theta})_{1,1} = 2\Re\left[(2\pi\Delta f)^2 \mathbf{s}^H \mathbf{D}_\tau (\mathbf{s}\mathbf{s}^H + \sigma^2 \mathbf{I})^{-1} \mathbf{D}_\tau \mathbf{s}\right], \tag{4.54}$$

$$I(\boldsymbol{\theta})_{1,2} = 2\Re\left[(-4\pi^2\Delta f T_{\mathsf{sym}}) \mathbf{s}^H \mathbf{D}_\tau (\mathbf{s}\mathbf{s}^H + \sigma^2 \mathbf{I})^{-1} \mathbf{D}_{f_\mathsf{D}} \mathbf{s}\right], \tag{4.55}$$

$$I(\boldsymbol{\theta})_{2,1} = 2\Re\left[(-4\pi^2\Delta f T_{\mathsf{sym}}) \mathbf{s}^H \mathbf{D}_{f_\mathsf{D}} (\mathbf{s}\mathbf{s}^H + \sigma^2 \mathbf{I})^{-1} \mathbf{D}_\tau \mathbf{s}\right], \tag{4.56}$$

$$I(\boldsymbol{\theta})_{2,2} = 2\Re\left[(2\pi T_{\mathsf{sym}})^2 \mathbf{s}^H \mathbf{D}_{f_\mathsf{D}} (\mathbf{s}\mathbf{s}^H + \sigma^2 \mathbf{I})^{-1} \mathbf{D}_{f_\mathsf{D}} \mathbf{s}\right]. \tag{4.57}$$

Therefore, the Fisher matrix and its inverse are given by

$$I(\boldsymbol{\theta}) = \begin{bmatrix} I(\boldsymbol{\theta})_{1,1} & I(\boldsymbol{\theta})_{1,2} \\ I(\boldsymbol{\theta})_{2,1} & I(\boldsymbol{\theta})_{2,2} \end{bmatrix}, \tag{4.58}$$

$$I^{-1}(\boldsymbol{\theta}) = \frac{\begin{bmatrix} I(\boldsymbol{\theta})_{2,2} & -I(\boldsymbol{\theta})_{1,2} \\ -I(\boldsymbol{\theta})_{2,1} & I(\boldsymbol{\theta})_{1,1} \end{bmatrix}}{\det I(\boldsymbol{\theta})}. \tag{4.59}$$

The CRLB for the two estimators are given by the diagonal elements of the inverse Fisher matrix, where the first diagonal elements corresponds to CRLB of the delay estimate while the seconds corresponds to that of the Doppler estimate. Thus, these are given as

$$\text{var}(\hat{\tau}) \geq \frac{I(\boldsymbol{\theta})_{2,2}}{\det I(\boldsymbol{\theta})} = \text{CRLB}(\hat{\tau}), \tag{4.60}$$

$$\text{var}(\hat{f}_\mathsf{D}) \geq \frac{I(\boldsymbol{\theta})_{1,1}}{\det I(\boldsymbol{\theta})} = \text{CRLB}(\hat{f}_\mathsf{D}). \tag{4.61}$$

5 RESULTS AND ANALYSIS

The contribution of this thesis is discussed in this chapter. This mainly focuses on the optimisation problem that is used to fill up the radar subcarriers. The performance of both the radar and communication systems are analysed. The effect of the individual constraints on the performance are also evaluated. Maximum likelihood estimation is also performed to evaluate the suitability of the optimisation algorithm for a practical scenario.

5.1 Optimisation problem

The optimisation problem can be given mathematically as

$$\mathrm{argmin}_{\mathbf{X}_c,\mathbf{X}_r,\mathcal{R},\mathcal{C}}\mathsf{CRLB}(\hat{\tau}) \text{ or } \mathrm{argmin}_{\mathbf{X}_c,\mathbf{X}_r,\mathcal{R},\mathcal{C}}\mathsf{CRLB}(\hat{f}_{\mathsf{D}}) \tag{5.1}$$

such that

$$P_{\text{comm.}} + P_{\text{radar}} = P_{\text{total}}, \tag{5.2}$$

$$\mathsf{PAPR}_{x(t)} \leq \mathsf{PAPR}_{\text{max}}, \tag{5.3}$$

$$\mathsf{SNR}_{\text{c},n,m} \geq \mathsf{SNR}_{\text{min}}, \tag{5.4}$$

where $P_{\text{total}}, \mathcal{R}, \mathcal{C}, \mathsf{PAPR}_{\text{max}}, \mathsf{SNR}_{\text{min}}$ are the power constraint for the transmit signal, indices corresponding to radar and communication subcarriers for the whole pulse, PAPR constraint for the transmit signal and the minimum SNR per communication subcarrier.

The optimisation problem minimises the CRLB of the estimators of delay and Doppler shift for the radar system under a set of constraints. The first constraint is the total power constraint, which ensures that the transmit signal has enough power. It is also equipped with a PAPR constraint such that the final signal transmitted is feasible to be used in practice, since OFDM signals usually have very high PAPR values. In order for the communication system to have a good performance, the last constraint is the SNR constraint for the communication subcarriers which ascertains that the communication subcarriers achieve at least a minimum SNR. The general optimisation problem outputs the complex weights for the radar subcarriers $\mathbf{X}_r$ and also the weights for the communication subcarriers $\mathbf{X}_c$, for the whole pulse. It also outputs the optimal indices for the radar and communication subcarriers within each OFDM symbol.

Algorithm 1 Optimisation algorithm

Initialise $\mathbf{X}_c, \mathbf{X}_r$ with random values
Set constant parameter values according to Table (5.1)
Set $P_{\text{total}}, \alpha, \gamma$ constraint values
Set constraint tolerance $\Delta_{\text{con.}}$
Set function tolerance $\Delta_{\text{func.}}$
Compute $\text{CRLB}(\hat{\tau}), \text{CRLB}(\hat{f_{\text{D}}})$ according to (4.60) and (4.61)
Compute $P_{x(t)}, \text{PAPR}_{x(t)}, \text{SNR}_{\text{c},n,m}$
while $(\text{CRLB}(\hat{\tau}), \text{CRLB}(\hat{f_{\text{D}}}) > \Delta_{\text{func.}})$ **and** $(|P_{x(t)} - P_{\text{total}}| > \Delta_{\text{con.}})$ **and** $(\text{PAPR}_{x(t)} - \alpha > \Delta_{\text{con.}})$ **and** $(\text{SNR}_{\text{c},n,m} - \gamma < \Delta_{\text{con.}})$ **do**
    Set $\mathbf{X}_c \leftarrow \mathbf{X}_{c,\text{new}}$
    Set $\mathbf{X}_r \leftarrow \mathbf{X}_{r,\text{new}}$
    Compute $P_{x(t)}, \text{PAPR}_{x(t)}, \text{SNR}_{\text{c},n,m}$
    Compute $\text{CRLB}(\hat{\tau}), \text{CRLB}(\hat{f_{\text{D}}})$
$\text{CRLB}(\hat{\tau})_{\text{min}}, \text{CRLB}(\hat{f_{\text{D}}})_{\text{min}} = \text{CRLB}(\hat{\tau}), \text{CRLB}(\hat{f_{\text{D}}})$
$\text{PAPR}_{x(t),\text{min}} = \text{PAPR}_{x(t)}$
$\text{SNR}_{\text{c},n,m,\text{max}} = \text{SNR}_{\text{c},n,m}$

The optimisation problem can be also broken into different sub-problems. The first and foremost is the effect of optimisation on the performance of the radar and communication systems. The variances of the errors made in parameter estimation need to be analysed for the radar system while the SNR of the communication subcarriers need to be observed for the communication system. The second sub-problem can be thought of as the locations of the radar and the communication subcarriers within an OFDM symbol, for better performance. After the joint waveform is found with the help of optimisation, its effect needs to be observed for a practical estimator. For this, the maximum likelihood estimator (MLE) is considered and is chosen as the third sub-problem.

Algorithm 1 is evaluated numerically in MATLAB®. The essence of the optimisation problem can be thought of as to improve the radar systems' performance by minimising the errors in the estimators while simultaneously maximising the SNR of the communication subcarriers.

To evaluate the optimisation algorithm, a joint system is simulated in MATLAB® and is denoted in Figure 4.1(a). The parameters necessary for the formation of the system are given in Table 5.1. It is assumed that the communication and radar subcarriers in an OFDM symbol are in the locations denoted by Figure 5.1, to simplify the optimisation problem. For the communication channel, a multipath channel is simulated with the power delay profile as shown in Figure 5.2.

The generated spectrum due to optimisation is depicted in Figure 5.3(a). It is seen that the part of the spectrum corresponding to communication is amplified when compared with that of the radar subcarriers. This happens due to the addition of the SNR constraint on the optimisation problem. Increase of the SNR constraint causes this spectrum to be amplified even further. In perspective of transmission, it is necessary that the spectrum of the transmit signal either be flat to some level or the amplification can be controlled.

Parameter	Value
M	3
N	1200
Δf	50kHz
FFT size	2048
f_c	2GHz
SNR(M)	10dB
β	1m^2
B	60MHz
F	10
λ	0.15m
G_{dB}	20dB

Table 5.1. *Parameters for the simulations*

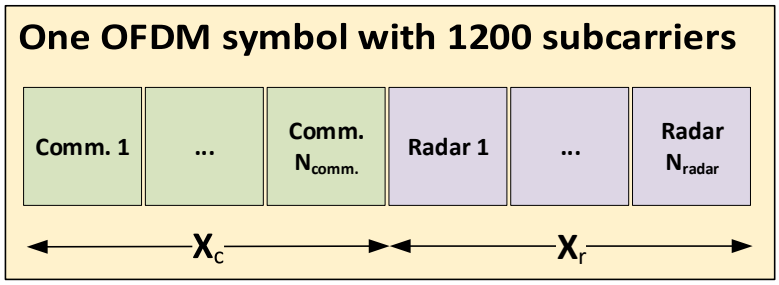

Figure 5.1. *Locations of the communication and radar subcarriers in an OFDM symbol*

However, since the amplification depends on the SNR constraint, this is not desired.

To address this issue, the optimisation problem is modified as

$$\text{argmin}_{\mathbf{X}_r,\mathcal{R},\mathcal{C}}\text{CRLB}(\hat{\tau}) \text{ or } \text{argmin}_{\mathbf{X}_r,\mathcal{R},\mathcal{C}}\text{CRLB}(\hat{f}_{\text{D}}) \tag{5.5}$$

such that

$$P_{\text{radar}} = (1-\delta)P_{\text{total}}, \tag{5.6}$$

$$\text{PAPR}_{x(t)} \leq \text{PAPR}_{\text{max}}, \tag{5.7}$$

and the corresponding algorithm to this is given in Algorithm 2.

The power allocated out of the total power P_{total} for the communication subcarriers is now decided in advance. Since a flat transmit spectrum is desired, the power between

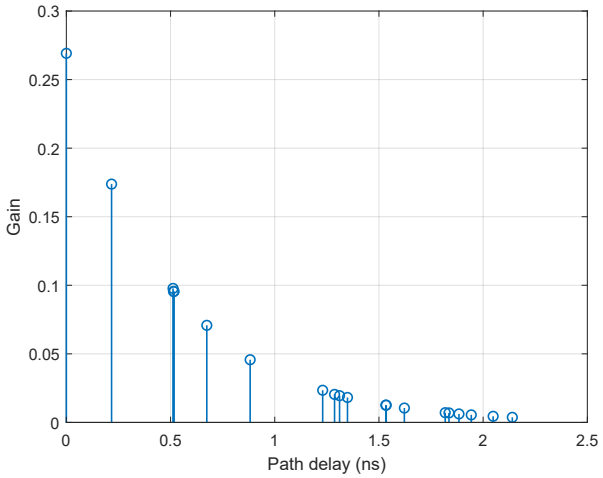

Figure 5.2. *Power delay profile*

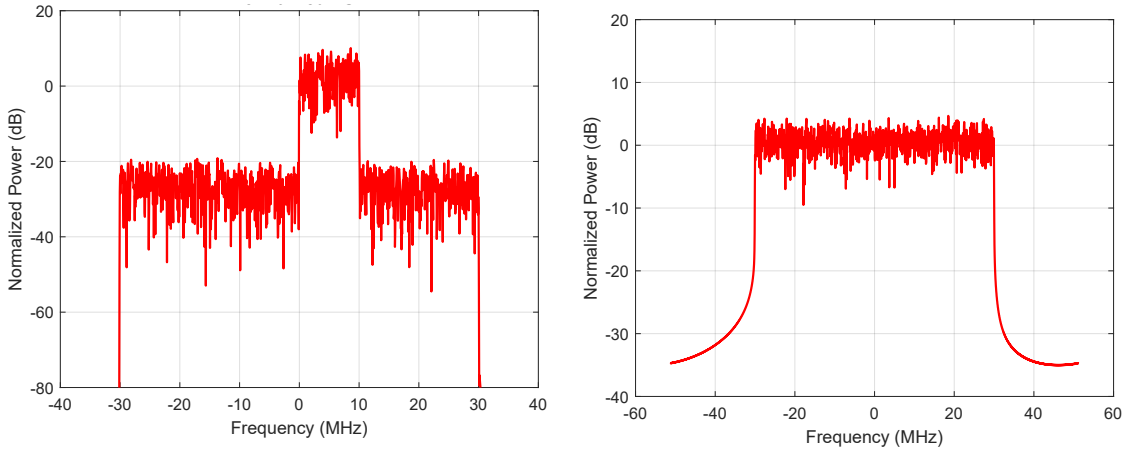

(a) *Spectrum of the waveform generated due to optimisation with SNR constraint =* $10dB$

(b) *Spectrum of the waveform generated due to modified optimisation*

Figure 5.3. *Spectrum of the waveform for initial and modified optimisations with 200 comm. subcarriers and PAPR constraint =* $7dB$

communication and radar subcarriers is decided by their subcarrier ratio. That is

$$\frac{P_{\text{comm.}}}{P_{\text{radar}}} = \frac{N_{\text{comm.}}}{N_{\text{radar}}}, \tag{5.8}$$

$$P_{\text{comm.}} = P_{\text{total}} \frac{N_{\text{comm.}}}{N}, \tag{5.9}$$

where $P_{\text{comm.}}, P_{\text{radar}}$ are the power allocated for communication and radar subcarriers and $N_{\text{comm.}}, N_{\text{radar}}$ are the number of communication and radar subcarriers, respectively. The proportion of power allocated for the communication subcarriers is then $\delta = \frac{N_{\text{comm.}}}{N}$. Each communication subcarrier is weighted by the same value W which is given by

$$W = \sqrt{\frac{P_{\text{total}}}{N}}, \tag{5.10}$$

Algorithm 2 Modified optimisation algorithm

1: Initialise $\mathbf{X}_r$ with random values
2: Set constant parameter values according to Table (5.1)
3: Set $P_{\text{total}}, \alpha, \delta$ constraint values
4: Set constraint tolerance $\Delta_{\text{con.}}$
5: Set function tolerance $\Delta_{\text{func.}}$
6: Compute $\text{CRLB}(\hat{\tau}), \text{CRLB}(\hat{f_{\text{D}}})$ according to (4.60) and (4.61)
7: Compute $P_{\text{radar}}, \text{PAPR}_{x(t)}$
8: **while** $(\text{CRLB}(\hat{\tau}), \text{CRLB}(\hat{f_{\text{D}}}) > \Delta_{\text{func.}})$ **and** $(|P_{\text{radar}} - (1-\delta)P_{\text{total}}| > \Delta_{\text{con.}})$ **and** $(\text{PAPR}_{x(t)} - \alpha > \Delta_{\text{con.}})$ **do**
9: Set $\mathbf{X}_r \leftarrow \mathbf{X}_{r,\text{new}}$
10: Compute $P_{\text{radar}}, \text{PAPR}_{x(t)}$
11: Compute $\text{CRLB}(\hat{\tau}), \text{CRLB}(\hat{f_{\text{D}}})$
12: $\text{CRLB}(\hat{\tau})_{\text{min}}, \text{CRLB}(\hat{f_{\text{D}}})_{\text{min}} = \text{CRLB}(\hat{\tau}), \text{CRLB}(\hat{f_{\text{D}}})$
13: $\text{PAPR}_{x(t),\text{min}} = \text{PAPR}_{x(t)}$
14: $P_{\text{radar}} = (1-\delta)P_{\text{total}}$

such that the transmitted complex symbol on a communication subcarrier is

$$X_{\text{c},n,m} = WD_{n,m}, \tag{5.11}$$

and the total communication power

$$P_{\text{comm.}} = N_{\text{comm.}} * |X_c|^2, \tag{5.12}$$

is equivalent to (5.9).

Figure 5.3(b) shows the spectrum of the waveform due to the modified optimisation problem. It can be seen that the initial drawback of a part of the spectrum being amplified is removed and modified optimisation yields a waveform that is flat. Table 5.2 shows the different parameters values for the figures depicted in Figure 5.3.

Parameter value	Initial optimisation	Modified optimisation
PAPR achieved	7.0 dB	7.0 dB
Standard deviation of distance error	0.00051m	0.00073m
Standard deviation of velocity error	0.08ms^{-1}	0.13ms^{-1}

Table 5.2. *Comparison between two optimisation problems for a fixed scenario*

Figure 5.4 shows the changes in the spectrum with the number of communication subcarriers in an OFDM symbol for Doppler estimate optimisation. For this, the most important factor is the spectrum as shown in the Figure 2.7(b). Thus, having a single tone in the frequency domain allows to accurately estimate the Doppler shift of the received signal. This is the case when all are radar subcarriers in an OFDM symbol, which corresponds to the figure when $\text{N}_{\text{comm.}} = 0$. When the number of communication subcarriers increases, it can be seen that the spectrum still has an impulse.

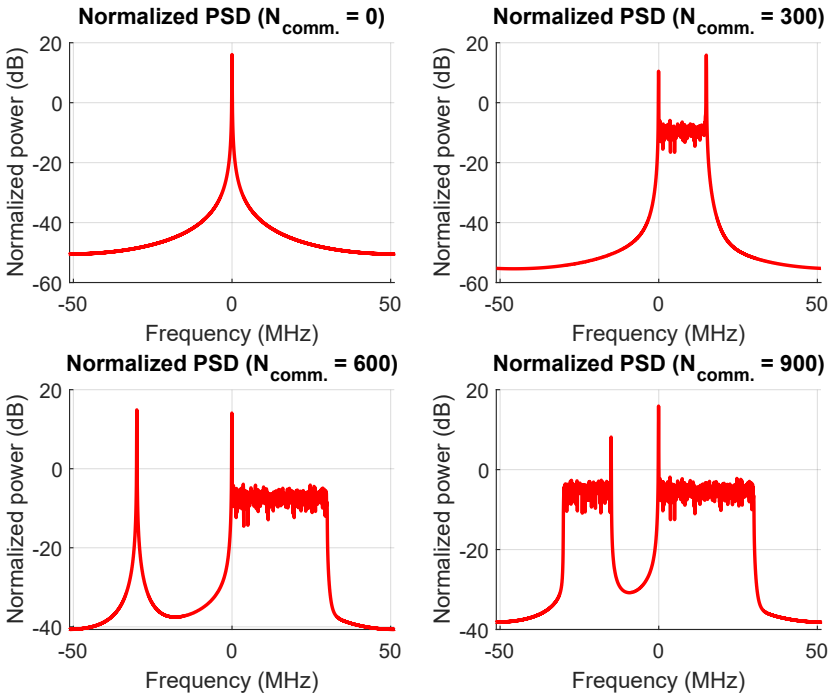

Figure 5.4. *Variation of the spectrum of the optimised waveform for Doppler estimation under modified optimisation*

To observe the effect of optimisation, the standard deviation of the CRLBs of delay and Doppler estimates are converted into a distance error and a velocity error as per (2.13) and (2.14). Figure 5.5 shows the effect of optimisation on these errors. The effect on the distance estimation is analysed first. It is seen that optimisation provides much better performance in distance estimation when compared with the unoptimised case. In the unoptimised case, the radar subcarriers are considered to be empty. As an example, comparing the two curves when the number of communication subcarriers is 600 shows that the distance error is reduced in the optimised case. But, to compensate for the reduced error, the power of the communication subcarriers is reduced by half as per (5.9). Therefore, a 3dB power loss is incurred for the communication subcarriers to improve this distance error. This essentially means that distance error of the radar system can be improved by reducing the power allocated for the communication subcarriers. Also when all the subcarriers are communication, it is seen that it produces the worst distance error and converges to the unoptimised case.

If a part of the subcarriers is dedicated for communication, the number of radar subcarriers decreases and this decreases the flexibility in optimisation since in the radar subcarriers both the phase and the amplitude of the complex symbols can be changed whereas for the communication subcarriers, it is only the amplitude. The convergence is due to this because no radar subcarriers are left for the optimisation. But, if radar subcarriers are left, it is seen that the optimisation problem is able to optimise them to reduce the distance error.

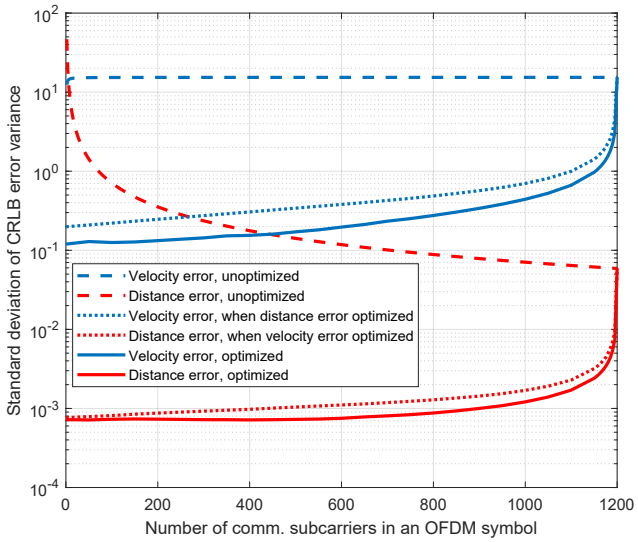

Figure 5.5. *Error variation for the two estimates with the number of communication subcarriers*

Another interesting point to note from the figure is that if the number of radar subcarriers is about 10% of the total number of subcarriers, the theoretical distance error can be reduced by almost a decade. Also, increasing the number of radar subcarriers beyond a certain point does not anymore yield performance improvement for the radar system. This is also in line with a typical communication system, since maximally only about a quarter of the subcarriers is unused in an OFDM symbol. Thus, these can be optimised without any issue since no information is conveyed on those subcarriers for the communication system.

Similar to the distance error variation, it is seen that the velocity error increases with the increase of the number of communication subcarriers in an OFDM symbol, since the optimisation loses the number of variables that can be optimised. Comparing with the unoptimised case, it is clear that the optimisation problem reduces the standard deviation of the velocity error as well.

The optimisation of the distance and the velocity estimates were done separately where the optimisation of one does not depend on the other. This figure also shows the behaviour of the unoptimised variable when the other is optimised. When the distance estimate is optimised, the variation of the error of the velocity variable is also to increase with the number of communication subcarriers. However, this error variation is much higher than the case when the velocity variable is optimised. Same observation can be made for the distance estimate.

5.2 Performance of the communication system

When the OFDM signal is transmitted through the multipath channel with the power delay profile as in Figure 5.2, it is received at the communication receiver after being distorted due to multipaths and also with reduced power due to the free-space path loss (FSPL), which is shown in Figure 5.6. Depending on the SNR at the communication receiver, the received communication signal can be above or below the noise floor. In this figure, it is shown to be above.

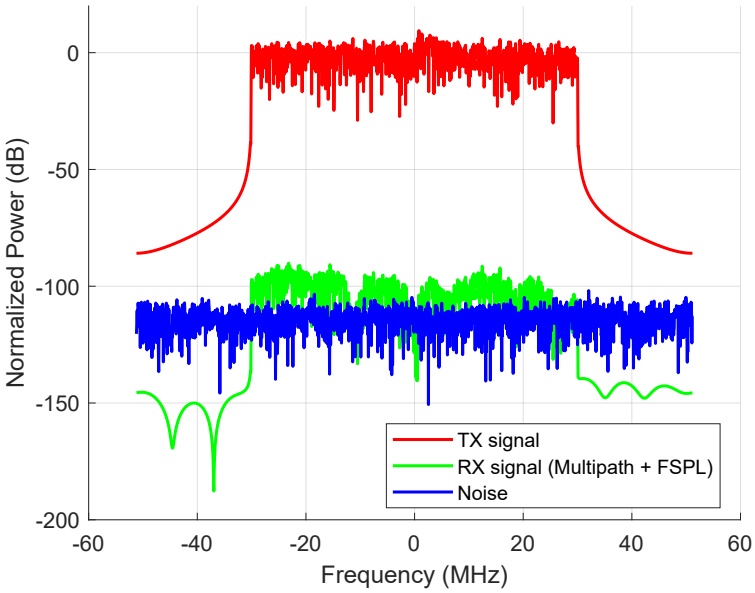

Figure 5.6. *Frequency domain plot*

After applying the SNR constraint for the communication subcarriers together with the power constraint and the PAPR constraint, Figures 5.7(a) and 5.7(b) show the effect of optimisation for communication subcarriers. For both cases, it is observed that optimisation improves the SNR of the communication subcarriers. It is also seen that increasing the SNR constraint improves the SNR of the communication subcarriers even further. Figure 5.7(c) depicts the same variation for the modified optimisation problem.

Table 5.3 shows the change in the average SNR for the two optimisation methods. It is seen that when there is an SNR constraint, the average SNR value is quite higher than without it. Also, when the SNR constraint is made tighter, the average SNR decreases. In comparing the average SNR values of the two optimisation problems without the SNR constraint, it is seen that under the modified optimisation problem, the average SNR is lower than with the original optimisation problem. The reason for this is due to the fact that in the original one, individual weights of the communication subcarriers can be controlled but in the case for the modified one, the weights for them are already fixed. Thus, in the modified approach, the optimisation loses some flexibility to change the weights as intended for the communication subcarriers.

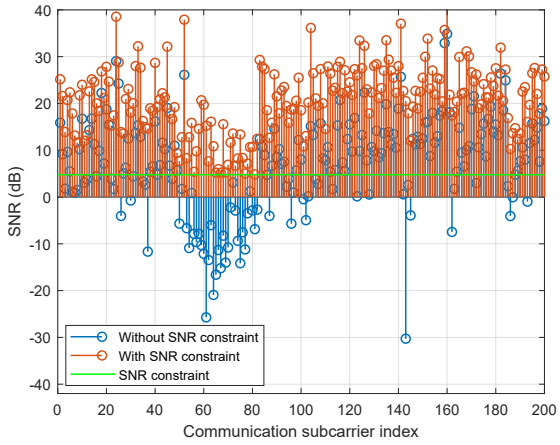

(a) *SNR of the communication subcarriers for SNR constraint* $= 3\ (4.8dB)$

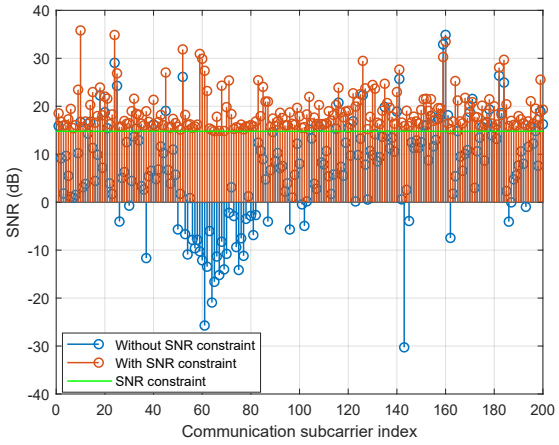

(b) *SNR of the communication subcarriers for SNR constraint* $= 30\ (14.8dB)$

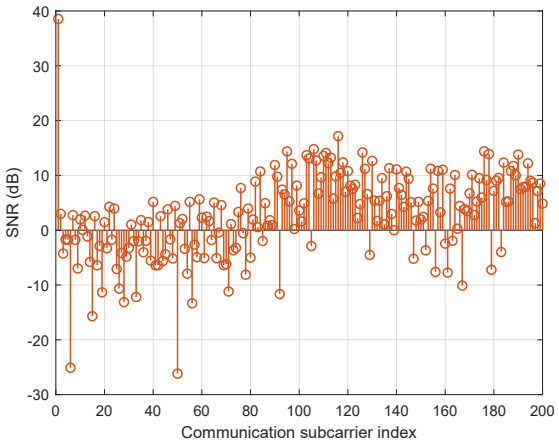

(c) *SNR of the communication subcarriers for the modified optimisation problem*

Figure 5.7. *Comparison of the SNR of the communication subcarriers with and without SNR constraint for two different constraints*

Case	Average SNR
Without SNR constraint	6.88 dB
With SNR constraint 3 (4.8dB)	20.73 dB
With SNR constraint 30 (14.8dB)	19.00 dB
Modified optimisation problem	2.88 dB

Table 5.3. *Comparison between average SNR*

5.3 PAPR of the waveform

For delay and Doppler estimation, time and frequency domains are the important ones, respectively. Thus, the effect of the PAPR constraint is discussed for these domains in this section. Figure 5.8 denotes the effect of the PAPR constraint on the time-domain waveform optimised for delay estimation. Having a lower PAPR constraint causes the

amplitudes of the time-domain samples to be bounded by a lower value than when considered with that of a higher PAPR constraint. Also, it was seen that the PAPR constraint causes the velocity error to be increased than without it. The reason for this can be observed in the Figure 5.9. In particular, Figure 5.9(a) shows the case when 200 subcarriers are unused in an OFDM symbol and can be optimised. The peak in frequency domain thus makes the Doppler estimation much more precise, thereby reducing the error. But, when a PAPR constraint of 7dB is added, that peak is not distinctive as the earlier case whereas the frequency spectrum has gotten flat, as shown in Figure 5.9(b). In this case, the Doppler estimation is not accurate as the earlier one. But, to maintain the practicality of the waveform transmitted, the PAPR constraint is important.

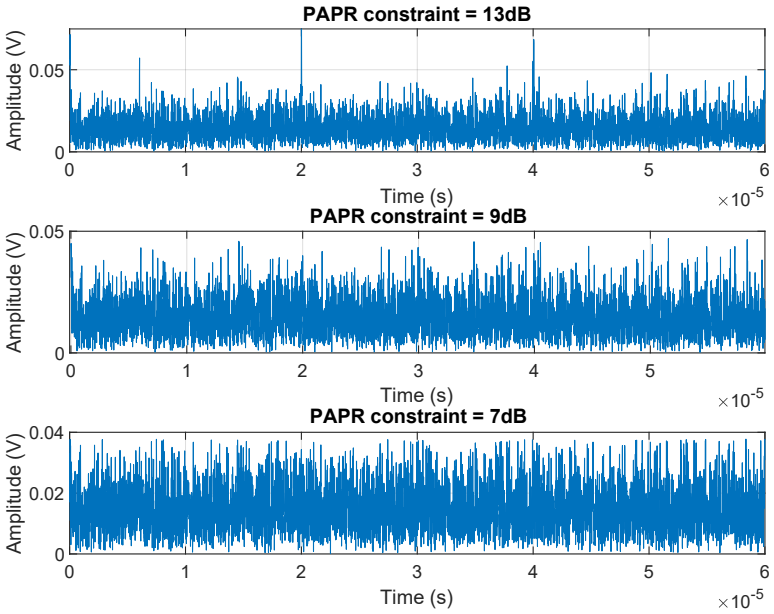

Figure 5.8. *Effect of the PAPR constraint on the time-domain waveform*

Figure 5.10 shows the effect of the PAPR constraint on delay and Doppler optimisation. For delay optimisation without the PAPR constraint, when there are not any communication subcarriers, the PAPR of the waveform is quite high. But, the inclusion of the communication subcarriers is seen to decrease the PAPR of the waveform. In contrast, for Doppler optimisation without PAPR constraint, it is seen that the addition of the communication subcarriers more or less increases the PAPR of the waveform. The PAPR variation for Doppler optimisation showcases that the PAPR for different number of communication subcarriers have quite reasonable values for a practical waveform intended for transmission. The same cannot be said for the PAPR variation for delay optimisation. For both these cases, when a PAPR constraint is applied to the optimisation problem, the PAPR of the waveform is seen to be in line with that, with the only exception being when all the subcarriers are used for communication. In this case, since there exist no radar subcarriers, the optimisation problem cannot optimise the waveform anymore. Thus, the PAPR of the waveform is higher than the PAPR constraint set.

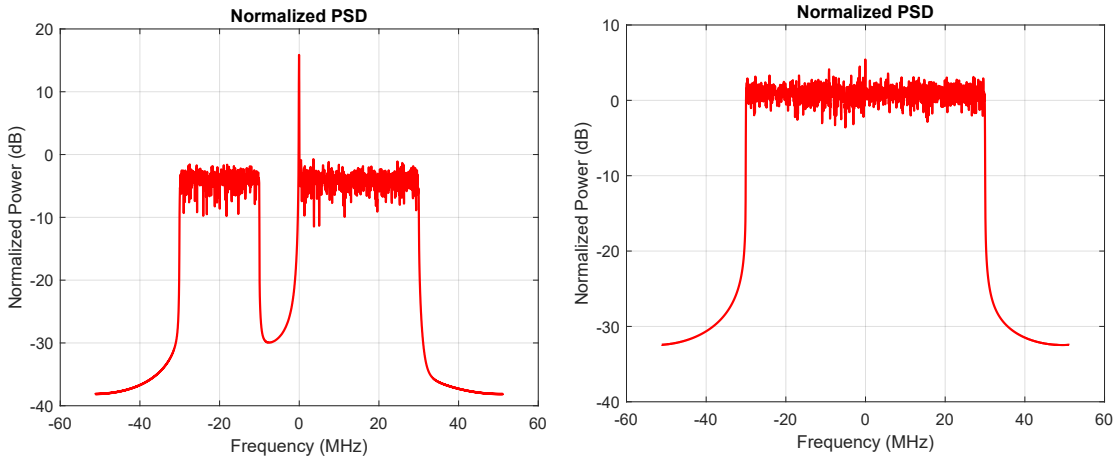

(a) *Spectrum of the waveform without the PAPR constraint, for* $n_{comm.} = 200$

(b) *Spectrum of the waveform with PAPR constraint=7dB, for* $n_{comm.} = 200$

Figure 5.9. *Spectrum of the waveform with and without the PAPR constraint for optimisation under Doppler estimate*

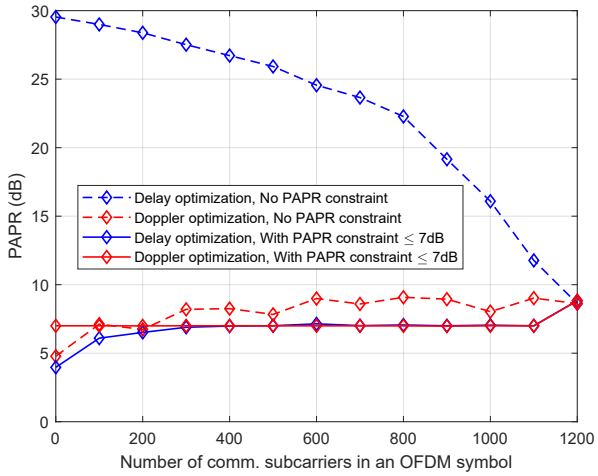

Figure 5.10. *Variation of PAPR of the waveform for delay and Doppler optimisations, with and without PAPR constraints*

It is interesting to observe the effect of the communication subcarriers on the PAPR of the waveform. Figure 5.11(a) shows the complementary cumulative distribution function (CCDF) for the optimisation problem without the PAPR constraint, for delay optimisation, while Figure 5.11(b) is the same for Doppler optimisation. For delay optimisation, when all are radar subcarriers, there are not any communication subcarriers. But when the number of communication subcarriers is increased, it is seen that the PAPR of the waveform decreases. This was also evident in the Figure 5.10. For Doppler optimisation, it is seen that the increase of the number of communication subcarriers also increases the PAPR of the waveform.

Figure 5.11(c) shows the CCDF for different PAPR constraints for delay optimisation. When there is no PAPR constraint, it is seen that the PAPR of the waveform is quite high. When the PAPR constraint is added, it is seen to decrease the PAPR of the waveform

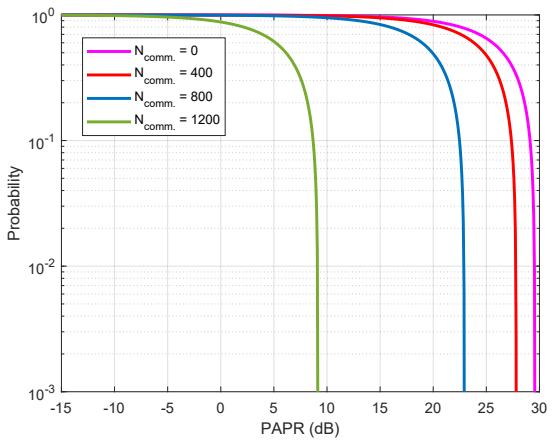

(a) *CCDF for different number of communication subcarriers, for delay optimisation*

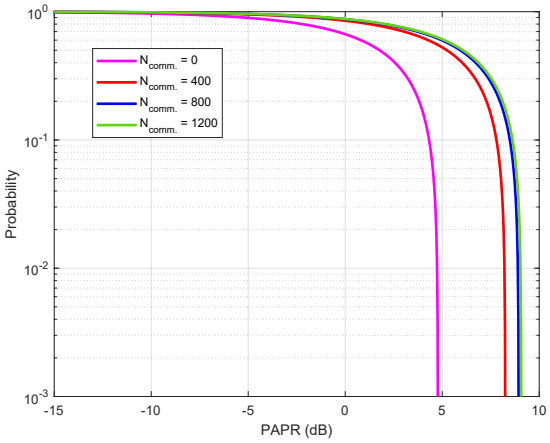

(b) *CCDF for different number of communication subcarriers, for Doppler optimisation*

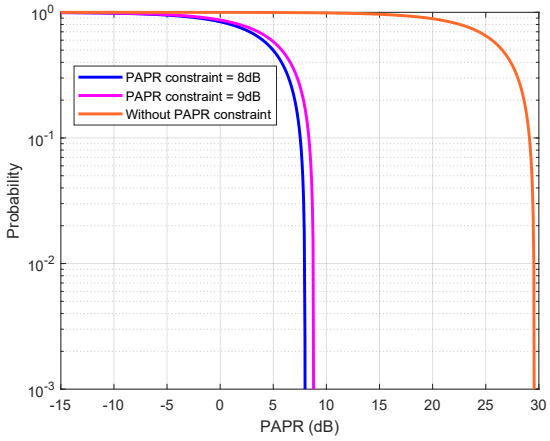

(c) *CCDF for different PAPR constraints when $N_{comm.} = 0$, for delay optimisation*

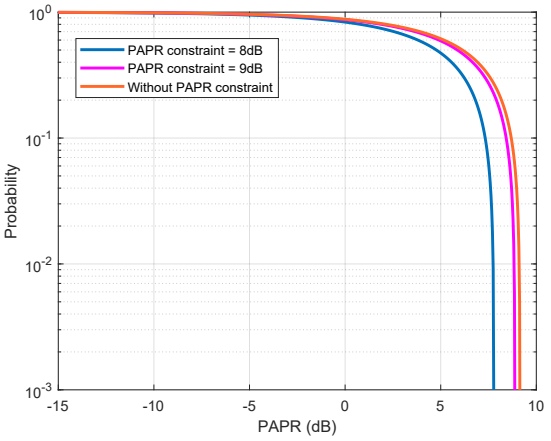

(d) *CCDF for different PAPR constraints when $N_{comm.} = 600$, for Doppler optimisation*

Figure 5.11. *Effect of the number of communication subcarriers and the PAPR constraint for the CCDF of delay and Doppler optimisation*

as required. A similar figure is shown in 5.11(d) for Doppler optimisation. It is seen that tightening the PAPR constraint allows the PAPR of the waveform to be bounded by that.

5.4 Optimal locations of the communication and radar subcarriers

Up to this point, the locations of the communication and radar subcarriers are as in Figure 5.1. As the next part, optimal indices corresponding to communication and radar subcarriers within one OFDM symbol are evaluated. In the first method, the total number of subcarriers is divided into a finite number of blocks. It is then assumed that the communication subcarriers reside in one or more blocks, depending on the number of communication subcarriers within an OFDM symbol with higher the number of communication subcarriers, higher the possible number of blocks. The optimisation problem is then

evaluated at each possible combination of the blocks of communication and the indices of communication subcarriers corresponding to the minimum distance error are taken as the optimal indices. Figure 5.12 depicts the optimal locations of the communication and radar subcarriers within an OFDM symbol. It is seen that when the communication subcarriers are placed at the centre or when the radar subcarriers are located at the edges of an OFDM symbol, distance error is the minimum.

Instead of defining the communication subcarriers block-wise, their locations are also selected in random. The optimisation problem is then evaluated for these random locations. This procedure is done for many iterations and the optimal locations are selected similar to the earlier case. Figure 5.13(a) compares the error variation due to this method and the earlier method. The maximum and minimum error variations for the first case using combinations of blocks are denoted as worst and best combinations in the figure. The other curve depicts the variation of minimum distance error for the random allocation. It is seen that the minimum distance error variation is the lowest in the block-wise approach. As a comparison between the variation of the two cases, this figure also shows the degree of improvement of distance error.

From the figure it can be seen that the block-wise approach yields around 150% of performance improvement for the radar system when the distance error is compared. Also, if the optimal locations of the communication subcarriers are random, it becomes a difficult task for the communication RX to select the communication subcarriers for each and every OFDM symbol. Also, if it were the case, it would put an extra overhead on the communication system since the TX needs to convey the corresponding indices to the RX. But when the block-wise approach is adopted, the RX only needs to know the number of communication subcarriers in an OFDM symbol and since they are located at the centre of the OFDM symbol, it can easily discard the symbols on other set of subcarriers. Therefore, the block-wise approach is optimal in the sense of minimising the distance error and also easier to be implemented in practice.

Figure 5.13(b) denotes the effect on the velocity error for the combinations approach. It is also seen that the velocity error is a bit higher in the worst combination approach than the other one.

5.5 Effect of optimisation on maximum likelihood estimation of parameters

The motivation behind this section is to compare the effect of optimisation on a practical estimator performance. The methodology adopted in Section 4.4 is used. Both range and velocity estimations are performed. Figure 5.14 depicts the 2D range-velocity map for an example situation with parameters as in Table 5.4. To consider a valid target, each sample of the received signal needs to be above the threshold and also within the box defined in the figure. Otherwise, it is considered a false alarm.

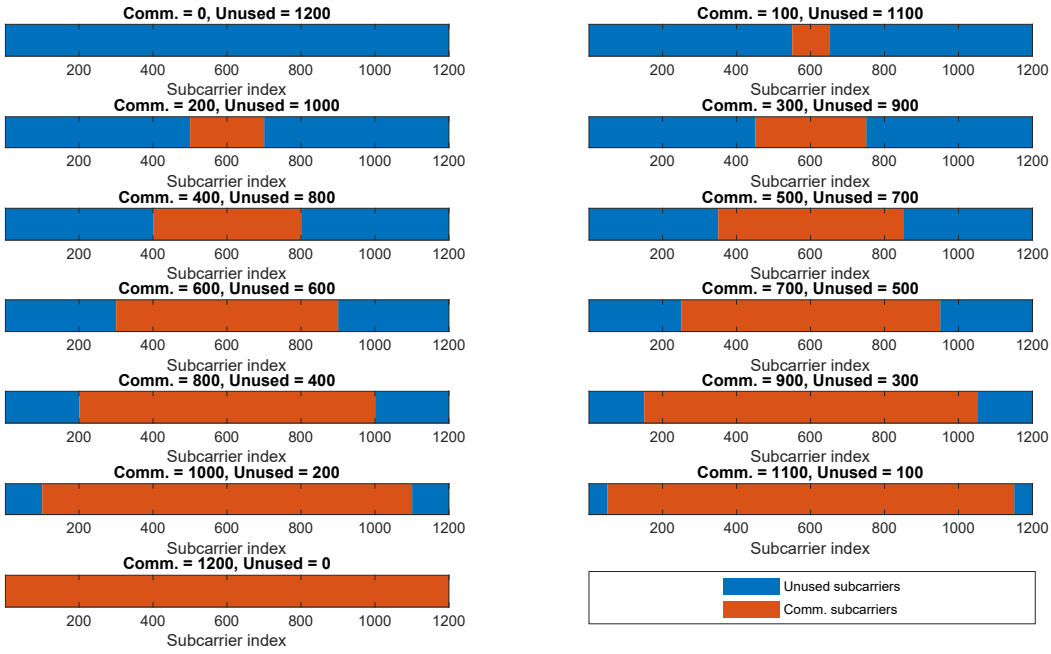

Figure 5.12. *Optimal locations of the communication and radar subcarriers in an OFDM symbol*

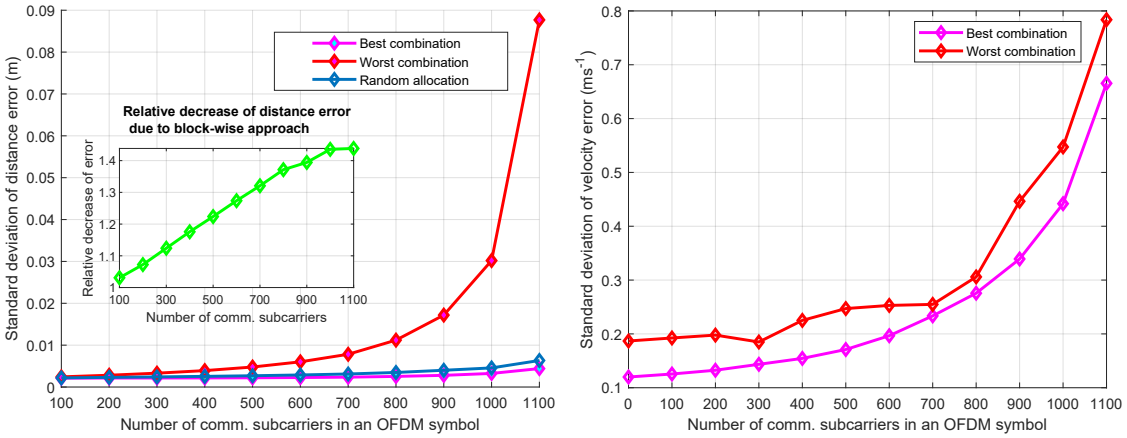

(a) *Comparison of standard deviation of distance error for the two methods*

(b) *Comparison of standard deviation of velocity error for the best and worst combinations*

Figure 5.13. *Variation of standard deviation errors of distance and velocity measurements*

Parameter	Value
Target location	$[0; 0; 1500m]$
Target velocity	$[0; 0; 220ms^{-1}]$
P_{FA}	1%
SNR	-10 dB

Table 5.4. *Parameters for MLE estimation*

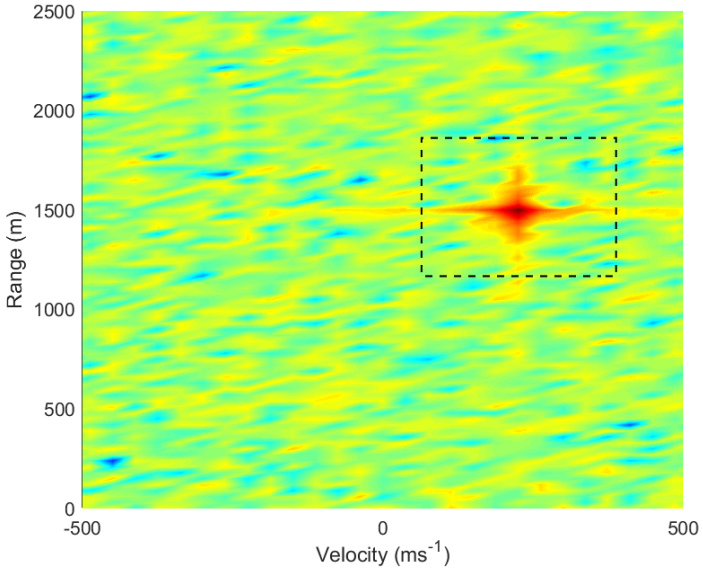

Figure 5.14. *2D range-velocity map for a target*

Amplitude of noise samples is Rayleigh distributed with the PDF function

$$\mathcal{P}_{\text{noise}}(n) = \frac{n}{\sigma^2} \exp\left(\frac{-n^2}{2\sigma^2}\right). \tag{5.13}$$

Using (2.25), the false alarm probability can be calculated as

$$P_{\text{FA}} = \int_{V_T}^{\infty} \frac{n}{\sigma^2} \exp\left(\frac{-n^2}{2\sigma^2}\right) dn = \exp\left(\frac{-V_T^2}{2\sigma^2}\right), \tag{5.14}$$

where V_T is the required threshold value. This can be then used to calculate the threshold value needed to obtain a fixed false alarm probability and is used here as

$$V_T = \sqrt{2\sigma^2 \ln\left(\frac{1}{P_{\text{FA}}}\right)}. \tag{5.15}$$

For a single SNR value, the MLE output is evaluated for many random iterations and the root mean square error (RMSE) of both distance and velocity are measured. The location and velocity of the target are also randomised so that its' location x and velocity v are uniformly distributed random variables at the centre of a bin with intervals $\left[x - \frac{\Delta r}{2}, x + \frac{\Delta r}{2}\right]$ and $\left[v - \frac{\Delta v}{2}, v + \frac{\Delta v}{2}\right]$, where $\Delta r, \Delta v$ are the range resolution and the velocity resolution respectively. This is done for a range of SNR values to compare the effect of optimisation with the unoptimised waveform.

Figure 5.15(a) depicts a situation where the OFDM waveform consists of three OFDM symbols with 1200 active subcarriers. The curves denote that for low SNR values, the RMSE difference between the two cases is higher than in the high SNR regime. Also, for high SNR values, the RMSE approaches an error floor and does not decrease beyond that. This error floor is higher for the unoptimised case.

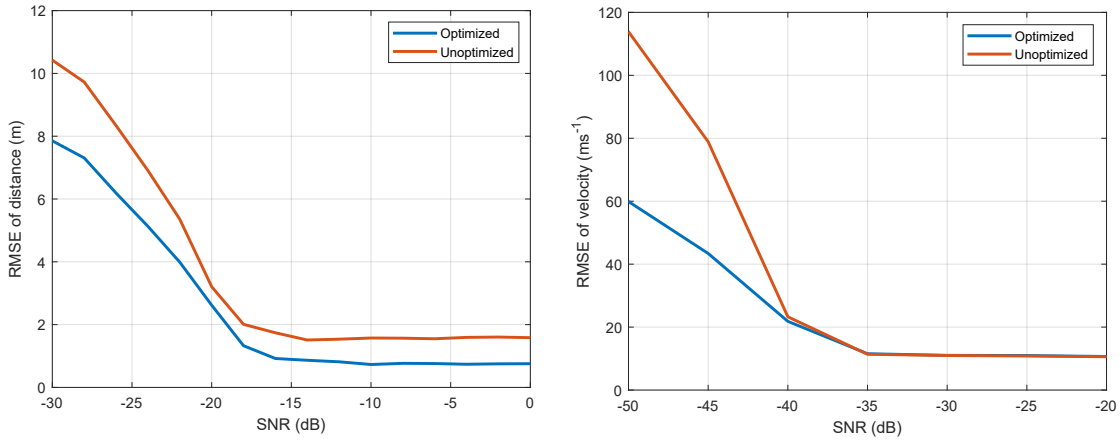

(a) *Distance measurement error* ***(b)*** *Velocity measurement error*

Figure 5.15. *Variation of RMSE of distance and velocity measurements with SNR for the optimised and unoptimised waveforms when* $M = 20$ *and* $N = 1200$

Similarly, Figure 5.15(b) denotes the change in the the RMSE of velocity measurement with SNR for the optimised and the unoptimised waveforms. To have a good resolution in velocity, the number of OFDM symbols is the governing factor. Thus, for this case, 100 OFDM symbols are used but with 40 subcarriers each. The reason for using a low number of active subcarriers is because the whole simulation is quite time-consuming for a large number of active subcarriers and the idea here is to denote the effectiveness of the optimisation also for velocity measurement. The figure shows that for low SNR values, the RMSE of velocity for the optimised waveform is lower than the unoptimised one. However, when a sufficient SNR level is reached, both waveforms achieve the same error floor. These results thereby show that optimising a theoretical bound for the two estimates allows the errors of practical estimators to be reduced as well.

6 CONCLUSION AND FUTURE WORK

This thesis considers a joint radar and communication system with the radar TRX and the communication TX being the same device while its RX is at some distance. The same OFDM waveform is used for both systems for transmission. Unused subcarriers within OFDM symbols are filled up with arbitrary data to improve the performance of the radar system based on an optimisation algorithm. This also ensures the performance of the communication system is kept at an acceptable level.

The optimisation problem minimises the Cramer–Rao lower bounds of the delay and Doppler estimates subject to a set of constraints. The first constraint allocates a proportion of the total transmit power for the radar subcarriers, with this proportion depending on the subcarrier ratio between the radar and communication subcarriers in an OFDM symbol. Thus, this also defines the power allocated for the communication subcarriers, and thereby the performance of the communication system. The second constraint ensures the PAPR of the waveform generated has an acceptable level. The optimisation problem also finds the indices of the communication and radar subcarriers within an OFDM symbol, which minimize the lower bounds.

In comparing the Cramer–Rao lower bounds of the delay and Doppler estimates for the optimised and unoptimised waveforms, it can be observed that significant improvement of error is possible with this optimisation algorithm. In compensation for this, the power allocated for the communication subcarriers needs to be reduced. Thus, improvement of performance for the radar and the communication systems is a trade-off. Another interesting observation is that if about 10% of the subcarriers of an OFDM symbol are used as radar subcarriers, the Cramer–Rao lower bound errors can be reduced by almost a decade. This is also in line with a typical communication system, since most of the subcarriers in an OFDM symbol are used for communication and only a small amount is available for use as radar subcarriers.

It is also observed that the locations of the radar and communication subcarriers within an OFDM symbol have an impact on the Cramer–Rao lower bound errors. For minimum error, the radar subcarriers need to be placed at the edges of an OFDM symbol while the communication subcarriers are centrally located. Further, the locations of the radar and communication subcarriers are also selected in random and it can be observed that the errors made are almost equivalent to placing the radar subcarriers at the edges. Thus, it can be concluded that the first approach does not put extra overhead on the communication RX, since knowing only the number of communication subcarriers within

an OFDM symbol allows it to easily discard the radar subcarriers. If the latter allocation is used, it would put extra overhead on the communication RX since the locations of the radar subcarriers would be random for each OFDM symbol and the communication TX needs to specify the locations of each OFDM symbol to the communication RX.

The Cramer–Rao lower bound optimisation is a theoretical/mathematical bound. The suitability of the optimised waveform for practical needs would need to make sure that it also works if and when a practical estimator is used. One common estimator that is used in practice is the maximum likelihood estimator. As such, the effectiveness of optimisation is compared with the unoptimised one when maximum likelihood estimation is adopted and it is clearly seen that the optimised waveform outperforms the unoptimised one. For delay optimisation, optimised waveform surpasses the unoptimised one when the SNR at the radar TRX is low. When it is high, both waveforms reach separate error floors where the optimised one is lower. For Doppler estimation, a similar trend is observed for lower SNR values while for higher values, they reach the same error floor.

6.1 Future work

The generic OFDM signal generated through this optimisation problem is not directly applicable in LTE or 5G NR systems because the specific signal structure of those was not considered. The next step would be to solve the optimisation problem by considering a predefined signal structure. Due to this, the unused subcarriers will be decided by a scheduler and the designer would not anymore have the freedom to select the locations of the subcarriers. Also, the effect of the pilot symbols and other control symbols need to be considered. After modifying the signal to accommodate modern communication systems, the joint waveform can be implemented as a practical system and its effect be observed.

REFERENCES

[1] C. Alabaster. *Pulse Doppler Radar: Principles, Technology, Applications*. Institution of Engineering and Technology, 2012. ISBN: 978-1891121982.

[2] A. Aubry, V. Carotenuto and A. De Maio. Radar waveform design with multiple spectral compatibility constraints. *IEEE Radar Conference (RadarConf)*. May 2016, 1–6. DOI: 10.1109/RADAR.2016.7485190.

[3] A. Aubry, A. De Maio, M. Piezzo, M. M. Naghsh, M. Soltanalian and P. Stoica. Cognitive radar waveform design for spectral coexistence in signal-dependent interference. *IEEE Radar Conference*. May 2014, 474–478. DOI: 10.1109/RADAR.2014.6875638.

[4] A. Aubry, A. D. Maio, Y. Huang, M. Piezzo and A. Farina. A new radar waveform design algorithm with improved feasibility for spectral coexistence. *IEEE Transactions on Aerospace and Electronic Systems*. Vol. 51. 2. Apr. 2015, 1029–1038. DOI: 10.1109/TAES.2014.140093.

[5] C. B. Barneto, L. Anttila, M. Fleischer and M. Valkama. OFDM Radar with LTE Waveform: Processing and Performance. *IEEE Radio and Wireless Symposium (RWS)*. Jan. 2019, 1–4. DOI: 10.1109/RWS.2019.8714410.

[6] D. Barton. *Radar Equations for Modern Radar*. Artech House radar library. Artech House, 2013. ISBN: 9781608075218.

[7] M. R. Bell, N. Devroye, D. Erricolo, T. Koduri, S. Rao and D. Tuninetti. Results on spectrum sharing between a radar and a communications system. *International Conference on Electromagnetics in Advanced Applications (ICEAA)*. Aug. 2014, 826–829. DOI: 10.1109/ICEAA.2014.6903972.

[8] S. S. Bhat, R. M. Narayanan and M. Rangaswamy. Bandwidth sharing and scheduling for multimodal radar with communications and tracking. *IEEE Sensor Array and Multichannel Signal Processing Workshop (SAM)*. June 2012, 233–236. DOI: 10.1109/SAM.2012.6250476.

[9] S. Bhat, R. Narayanan and M. Rangaswamy. An adaptive multimodal radar system with progressive resolution enhancement. *International Waveform Diversity and Design Conference*. Aug. 2010, 95–99. DOI: 10.1109/WDD.2010.5592382.

[10] M. Bica, K. Huang, V. Koivunen and U. Mitra. Mutual information based radar waveform design for joint radar and cellular communication systems. *IEEE International Conference on Acoustics, Speech and Signal Processing (ICASSP)*. Mar. 2016, 3671–3675. DOI: 10.1109/ICASSP.2016.7472362.

[11] M. Bica, K. Huang, U. Mitra and V. Koivunen. Opportunistic Radar Waveform Design in Joint Radar and Cellular Communication Systems. *IEEE Global Communications Conference (GLOBECOM)*. Dec. 2015, 1–7. DOI: 10.1109/GLOCOM.2015.7417624.

[12] M. Bica and V. Koivunen. Delay estimation method for coexisting radar and wireless communication systems. *IEEE Radar Conference (RadarConf)*. May 2017, 1557–1561. DOI: 10.1109/RADAR.2017.7944455.

[13] M. Bica and V. Koivunen. Radar Waveform Optimization for Target Parameter Estimation in Cooperative Radar-Communications Systems. *IEEE Transactions on Aerospace and Electronic Systems*. 2018, 1–1. DOI: 10.1109/TAES.2018.2884806.

[14] P. Bidigare. The Shannon channel capacity of a radar system. *Asilomar Conference on Signals, Systems and Computers*. Vol. 1. Nov. 2002, 113–117. DOI: 10.1109/ACSSC.2002.1197159.

[15] D. W. Bliss. Cooperative radar and communications signaling: The estimation and information theory odd couple. *IEEE Radar Conference*. May 2014, 50–55. DOI: 10.1109/RADAR.2014.6875553.

[16] D. W. Bliss and K. W. Forsythe. Multiple-input multiple-output (MIMO) radar and imaging: degrees of freedom and resolution. *The Thirty-Seventh Asilomar Conference on Signals, Systems Computers*. Vol. 1. Nov. 2003, 54–59. DOI: 10.1109/ACSSC.2003.1291865.

[17] K. M. Braun. OFDM Radar Algorithms in Mobile Communication Networks. PhD thesis. 2014. DOI: 10.5445/IR/1000038892.

[18] M. Braun, C. Sturm and F. K. Jondral. Maximum likelihood speed and distance estimation for OFDM radar. *IEEE Radar Conference*. May 2010, 256–261. DOI: 10.1109/RADAR.2010.5494616.

[19] C.C. Wang and H.C. Shyu. An extended Frank code and new technique for implementing P3 and P4 codes. *IEEE Transactions on Aerospace and Electronic Systems*. Vol. 25. 4. July 1989, 442–448. DOI: 10.1109/7.32076.

[20] X. Chen, X. Wang, S. Xu and J. Zhang. A novel radar waveform compatible with communication. *International Conference on Computational Problem-Solving (ICCP)*. Oct. 2011, 177–181. DOI: 10.1109/ICCPS.2011.6092272.

[21] B. D. Cordill, S. A. Seguin and L. Cohen. Electromagnetic interference to radar receivers due to in-band OFDM communications systems. *IEEE International Symposium on Electromagnetic Compatibility*. Aug. 2013, 72–75. DOI: 10.1109/ISEMC.2013.6670384.

[22] E. Dahlman, S. Parkvall and J. Skold. *5G NR: The Next Generation Wireless Access Technology*. Elsevier Science, 2018. ISBN: 9780128143230.

[23] B. J. Donnet and I. D. Longstaff. Combining MIMO Radar with OFDM Communications. *European Radar Conference*. Sept. 2006, 37–40. DOI: 10.1109/EURAD.2006.280267.

[24] S. W. Ellingson. *Radio Systems Engineering*. Cambridge University Press, 2016. DOI: 10.1017/CBO9781107705852.

[25] E. Fishler, A. Haimovich, R. Blum, D. Chizhik, L. Cimini and R. Valenzuela. MIMO radar: an idea whose time has come. *IEEE Radar Conference*. Apr. 2004, 71–78. DOI: 10.1109/NRC.2004.1316398.

[26] K. W. Forsythe and D. W. Bliss. Waveform Correlation and Optimization Issues for MIMO Radar. *Thirty-Ninth Asilomar Conference on Signals, Systems and Computers,* Oct. 2005, 1306–1310. DOI: 10.1109/ACSSC.2005.1599974.

[27] G. E. A. Franken, H. Nikookar and P. V. Genderen. Doppler Tolerance of OFDM-coded Radar Signals. *European Radar Conference*. Sept. 2006, 108–111. DOI: 10.1109/EURAD.2006.280285.

[28] D. R. Fuhrmann and G. San Antonio. Transmit beamforming for MIMO radar systems using partial signal correlation. *Thirty-Eighth Asilomar Conference on Signals, Systems and Computers*. Vol. 1. Nov. 2004, 295–299 Vol.1. DOI: 10.1109/ACSSC.2004.1399140.

[29] D. Garmatyuk and Y. J. M. and. On co-existence of in-band UWB-OFDM and GPS signals: Tracking performance analysis. *IEEE/ION Position, Location and Navigation Symposium*. May 2008, 196–202. DOI: 10.1109/PLANS.2008.4570090.

[30] D. Garmatyuk, J. Schuerger, K. Kauffman and S. Spalding. Wideband OFDM system for radar and communications. *IEEE Radar Conference*. May 2009, 1–6. DOI: 10.1109/RADAR.2009.4977024.

[31] D. Garmatyuk, J. Schuerger, Y. T. Morton, K. Binns, M. Durbin and J. Kimani. Feasibility study of a multi-carrier dual-use imaging radar and communication system. *European Radar Conference*. Oct. 2007, 194–197. DOI: 10.1109/EURAD.2007.4404970.

[32] M. Ghorbanzadeh, E. Visotsky, P. Moorut, W. Yang and C. Clancy. Radar inband and out-of-band interference into LTE macro and small cell uplinks in the 3.5 GHz band. *IEEE Wireless Communications and Networking Conference (WCNC)*. Mar. 2015, 1829–1834. DOI: 10.1109/WCNC.2015.7127746.

[33] C. M. Goldie and R. G. E. Pinch. *Communication Theory*. London Mathematical Society Student Texts. Cambridge University Press, 1991. DOI: 10.1017/CBO9781139172448.

[34] E. Grayver. *Implementing Software Defined Radio*. Springer New York, 2012. ISBN: 9781441993328.

[35] J. R. Guerci and R. M. Guerci. RAST: Radar as a subscriber technology for wireless spectrum cohabitation. *IEEE Radar Conference*. May 2014, 1130–1134. DOI: 10.1109/RADAR.2014.6875765.

[36] J. R. Guerci, R. M. Guerci, A. Lackpour and D. Moskowitz. Joint design and operation of shared spectrum access for radar and communications. *IEEE Radar Conference (RadarCon)*. May 2015, 761–766. DOI: 10.1109/RADAR.2015.7131098.

[37] T. Guo and R. Qiu. OFDM waveform design compromising spectral nulling, sidelobe suppression and range resolution. *IEEE Radar Conference*. May 2014, 1424–1429. DOI: 10.1109/RADAR.2014.6875823.

[38] J. Han, B. Wang, W. Wang, Y. Zhang and W. Xia. Analysis for the BER of LTE system with the interference from radar. *IET International Conference on Communication Technology and Application (ICCTA)*. Oct. 2011, 452–456. DOI: 10.1049/cp.2011.0709.

[39] A. Hassanien, M. G. Amin, Y. D. Zhang and F. Ahmad. Dual-Function Radar-Communications: Information Embedding Using Sidelobe Control and Waveform Diversity. *IEEE Transactions on Signal Processing*. Vol. 64. 8. Apr. 2016, 2168–2181. DOI: 10.1109/TSP.2015.2505667.

[40] A. Hassanien, M. G. Amin, Y. D. Zhang, F. Ahmad and B. Himed. Non-coherent PSK-based dual-function radar-communication systems. *IEEE Radar Conference (RadarConf)*. May 2016, 1–6. DOI: 10.1109/RADAR.2016.7485066.

[41] S. Haykin. Cognitive radar: a way of the future. *IEEE Signal Processing Magazine*. Vol. 23. 1. Jan. 2006, 30–40. DOI: 10.1109/MSP.2006.1593335.

[42] H. T. Hayvaci and B. Tavli. Spectrum sharing in radar and wireless communication systems: A review. *International Conference on Electromagnetics in Advanced Applications (ICEAA)*. Aug. 2014, 810–813. DOI: 10.1109/ICEAA.2014.6903969.

[43] IEEE Standard for Information technology—Telecommunications and information exchange between systems Local and metropolitan area networks—Specific requirements - Part 11: Wireless LAN Medium Access Control (MAC) and Physical Layer (PHY) Specifications. *IEEE Std 802.11-2016 (Revision of IEEE Std 802.11-2012)* (Dec. 2016), 1–3534. DOI: 10.1109/IEEESTD.2016.7786995.

[44] R. Johnson and H. Jasik. *Antenna Engineering Handbook*. Electronics Electrical Engineering. McGraw-Hill, 1993. ISBN: 9780070323810.

[45] S. Kay. *Fundamentals of Statistical Signal Processing: Detection theory*. Fundamentals of Statistical Signal Processing. PTR Prentice-Hall, 1993.

[46] S. M. Kay. *Fundamentals of Statistical Signal Processing: Estimation Theory*. Prentice-Hall, Inc., 1993. ISBN: 0-13-345711-7.

[47] P. B. Kenington. *RF and Baseband Techniques for Software Defined Radio.* Mobile Communications Series. Artech House, Inc, 2005. ISBN: 9781580537933.

[48] A. Khawar, A. Abdelhadi and T. C. Clancy. A mathematical analysis of cellular interference on the performance of S-band military radar systems. *Wireless Telecommunications Symposium*. Apr. 2014, 1–8. DOI: 10.1109/WTS.2014.6835028.

[49] S. Kim, J. J. Park and K. Bian. PSUN: An OFDM scheme for coexistence with pulsed radar. *International Conference on Computing, Networking and Communications (ICNC)*. Feb. 2015, 984–988. DOI: 10.1109/ICCNC.2015.7069480.

[50] P. Kumari, S. A. Vorobyov and J. Heath Robert W. Adaptive Virtual Waveform Design for Millimeter-Wave Joint Communication-Radar. *arXiv e-prints*. Apr. 2019.

[51] M. Labib, V. Marojevic, A. F. Martone, J. H. Reed and A. I. Zaghloui. *Coexistence between communications and radar systems: A survey*. Vol. 2017. 362. Sept. 2017, 74–82. DOI: 10.23919/URSIRSB.2017.8267374.

[52] G. Lellouch, A. Mishra and M. Inggs. Processing alternatives in OFDM radar. *International Radar Conference*. Oct. 2014, 1–6. DOI: 10.1109/RADAR.2014.7060450.

[53] N. Levanon. Multifrequency radar signals. *IEEE International Radar Conference*. May 2000, 683–688. DOI: 10.1109/RADAR.2000.851916.

[54] H. J. Li and Y. W. Kiang. Radar and Inverse Scattering. *The Electrical Engineering Handbook*. Academic Press, 2005, 671–690. ISBN: 978-0-12-170960-0. DOI: https://doi.org/10.1016/B978-012170960-0/50047-5.

[55] J. Li and P. Stoica. MIMO Radar with Colocated Antennas. *IEEE Signal Processing Magazine*. Vol. 24. 5. Sept. 2007, 106–114. DOI: 10.1109/MSP.2007.904812.

[56] Y. Liang, K. Chen, G. Y. Li and P. Mahonen. Cognitive radio networking and communications: an overview. *IEEE Transactions on Vehicular Technology*. Vol. 60. 7. Sept. 2011, 3386–3407. DOI: 10.1109/TVT.2011.2158673.

[57] Y. Liang, K. Chen, G. Y. Li and P. Mahonen. Cognitive radio networking and communications: an overview. *IEEE Transactions on Vehicular Technology*. Vol. 60. 7. Sept. 2011, 3386–3407. DOI: 10.1109/TVT.2011.2158673.

[58] Y. Liu, G. Liao, Z. Yang and J. Xu. Design of integrated radar and communication system based on MIMO-OFDM waveform. *Journal of Systems Engineering and Electronics*. Vol. 28. 4. Aug. 2017, 669–680. DOI: 10.21629/JSEE.2017.04.06.

[59] H. B. P. Ltd. *Elisa Finland*. URL: https://halberdbastion.com/intelligence/mobile-networks/elisa-finland.

[60] M. P. Masarik and N. S. Subotic. Cramèr-Rao lower bounds for radar parameter estimation in noise plus structured interference. *IEEE Radar Conference (RadarConf)*. May 2016, 1–4. DOI: 10.1109/RADAR.2016.7485105.

[61] G. Meager, R. A. Romero and Z. Staples. Estimation and cancellation of high powered radar interference for communication signal collection. *IEEE Radar Conference (RadarConf)*. May 2016, 1–4. DOI: 10.1109/RADAR.2016.7485263.

[62] S. M. Mishra, A. Sahai and R. W. Brodersen. Cooperative Sensing among Cognitive Radios. *IEEE International Conference on Communications*. Vol. 4. June 2006, 1658–1663. DOI: 10.1109/ICC.2006.254957.

[63] R. Mohseni, A. Sheikhi and M. A. Masnadi Shirazi. A new approach to compress Multicarrier Phase-Coded signals. *IEEE Radar Conference*. May 2008, 1–6. DOI: 10.1109/RADAR.2008.4720800.

[64] Y. Nijsure, Y. Chen, C. Yuen and Y. H. Chew. Location-aware spectrum and power allocation in joint cognitive communication-radar networks. *International Conference on Cognitive Radio Oriented Wireless Networks and Communications*. June 2011, 171–175. DOI: 10.4108/icst.crowncom.2011.245751.

[65] Ofcom. *An Evaluation of Software Defined Radio – An Overview*. URL: https://www.ofcom.org.uk/__data/assets/pdf_file/0018/40338/evaluation_sdr.pdf.

[66] A. Pezeshki, A. R. Calderbank, W. Moran and S. D. Howard. Doppler Resilient Golay Complementary Waveforms. *IEEE Transactions on Information Theory*. Vol. 54. 9. Sept. 2008, 4254–4266. DOI: 10.1109/TIT.2008.928292.

[67] C. Pisa, A. Garcia-Saavedra and D. J Leith. Investigating Bit Error Patterns for Radar Pulse Detection in IEEE 802.11. *International Conference on Wireless and Mobile Communications*. Aug. 2014.

[68] B. M. Povovic. Complementary sets based on sequences with ideal periodic autocorrelation. *Electronics Letters*. Vol. 26. 18. Aug. 1990, 1428–1430. DOI: 10.1049/el:19900916.

[69] M. O. Pun, M. Morelli and C. C. J. Kuo. *Multi-Carrier Techniques For Broadband Wireless Communications: A Signal Processing Perspectives*. Imperial College Press, 2007. ISBN: 1860949460.

[70] radartutorial.eu. *Continuous Wave Radar*. URL: http://www.radartutorial.eu/02.basics/Continuous%20Wave%20Radar.en.html.

[71] M. L. Rahman, J. A. Zhang, X. Huang, Y. J. Guo and R. W. H. Jr. Framework for a Perceptive Mobile Network using Joint Communication and Radar Sensing. *arXiv e-prints*. Vol. abs/1901.05558. 2019. arXiv: 1901.05558. URL: http://arxiv.org/abs/1901.05558.

[72] M. Rahman and J. S. Karlsson. Feasibility evaluations for secondary LTE usage in 2.7–2.9GHz radar bands. *IEEE International Symposium on Personal, Indoor and Mobile Radio Communications*. Sept. 2011, 525–530. DOI: 10.1109/PIMRC.2011.6140017.

[73] M. Renfors and M. Valkama. *Digital Communication lecture notes, Tampere University of Technology*. 2018.

[74] M. Renfors and M. Valkama. *Multicarrier and Multiantenna Techniques lecture notes, Tampere University of Technology*. 2018.

[75] M. A. Richards, J. Scheer, W. A. Holm and W. L. Melvin. *Principles of modern radar*. Citeseer, 2010.

[76] C. D. Richmond, P. Basu, R. E. Learned, J. Vian, A. Worthen and M. Lockard. Performance bounds on cooperative radar and communication systems operation. *IEEE Radar Conference (RadarConf)*. May 2016, 1–6. DOI: 10.1109/RADAR.2016.7485101.

[77] M. Roberton and E. R. Brown. Integrated radar and communications based on chirped spread-spectrum techniques. *IEEE MTT-S International Microwave Symposium Digest*. Vol. 1. June 2003, 611–614. DOI: 10.1109/MWSYM.2003.1211013.

[78] R. A. Romero and K. D. Shepherd. Friendly Spectrally Shaped Radar Waveform With Legacy Communication Systems for Shared Access and Spectrum Management. *IEEE Access*. Vol. 3. 2015, 1541–1554. DOI: 10.1109/ACCESS.2015.2473169.

[79] M. Ruggiano and P. van Genderen. Radar and communication waveform: Wideband ambiguity function and narrowband approximation. *IET International Conference on Radar Systems*. Oct. 2007, 1–5. DOI: 10.1049/cp:20070528.

[80] H. Safavi-Naeini, S. Roy and S. Ashrafi. Spectrum Sharing of Radar and Wi-Fi Networks: The Sensing/Throughput Tradeoff. *IEEE Transactions on Cognitive Communications and Networking*. Vol. 1. 4. Dec. 2015, 372–382. DOI: 10.1109/TCCN.2016.2557338.

[81] R. Saruthirathanaworakun, J. M. Peha and L. M. Correia. Opportunistic Sharing Between Rotating Radar and Cellular. *IEEE Journal on Selected Areas in Communications*. Vol. 30. 10. Nov. 2012, 1900–1910. DOI: 10.1109/JSAC.2012.121106.

[82] K. U. Schmidt and J. Willms. Barker sequences of odd length. *Designs, Codes and Cryptography*. Vol. 80. 2. Aug. 2016, 409–414. DOI: 10.1007/s10623-015-0104-4.

[83] M. A. Sebt, A. Sheikhi and M. M. Nayebi. Orthogonal frequency-division multiplexing radar signal design with optimised ambiguity function and low peak-to-average power ratio. *IET Radar, Sonar Navigation*. Vol. 3. 2. Apr. 2009, 122–132. DOI: 10.1049/iet-rsn:20080106.

[84] J. Semmlow. Chapter 2 - Basic Concepts in Signal Processing. *Signals and Systems for Bioengineers (Second Edition)*. Second Edition. Biomedical Engineering. Boston: Academic Press, 2012, 35–80. ISBN: 978-0-12-384982-3. DOI: https://doi.org/10.1016/B978-0-12-384982-3.00002-X.

[85] S. Sen and A. Nehorai. Adaptive Design of OFDM Radar Signal With Improved Wideband Ambiguity Function. *IEEE Transactions on Signal Processing*. Vol. 58. 2. Feb. 2010, 928–933. DOI: 10.1109/TSP.2009.2032456.

[86] X. Shaojian, C. Bing and Z. Ping. Radar-Communication Integration Based on DSSS Techniques. *8th international Conference on Signal Processing*. Vol. 4. Nov. 2006. DOI: 10.1109/ICOSP.2006.346041.

[87] K. D. Shepherd and R. A. Romero. Radar waveform design in active communications channel. *Asilomar Conference on Signals, Systems and Computers*. Nov. 2013, 1515–1519. DOI: 10.1109/ACSSC.2013.6810549.

[88] Y. L. Sit, C. Sturm and T. Zwick. Doppler estimation in an OFDM joint radar and communication system. *German Microwave Conference*. Mar. 2011, 1–4.

[89] M. Skolnik. *Radar Handbook, Third Edition*. McGraw-Hill Education, 2008. ISBN: 9780071485470.

[90] T. Stimac. *Definition of frequency bands*. URL: http://www.vlf.it/frequency/bands.html.

[91] P. Stinco, M. Greco, F. Gini and B. Himed. Channel parameters estimation for cognitive radar systems. *4th International Workshop on Cognitive Information Processing (CIP)*. May 2014, 1–6. DOI: 10.1109/CIP.2014.6844514.

[92] C. Sturm, T. Zwick and W. Wiesbeck. An OFDM System Concept for Joint Radar and Communications Operations. *IEEE 69th Vehicular Technology Conference (VTC)*. Apr. 2009, 1–5. DOI: 10.1109/VETECS.2009.5073387.

[93] S. C. Surender, R. M. Narayanan and C. R. Das. Performance Analysis of Communications amp; Radar Coexistence in a Covert UWB OSA System. *IEEE Global Telecommunications Conference (GLOBECOM)*. Dec. 2010, 1–5. DOI: 10.1109/GLOCOM.2010.5683837.

[94] J. Talvitie, M. Renfors and M. Valkama. *Communication Theory lecture notes, Tampere University of Technology*. 2017.

[95] M. Tercero, K. W. Sung and J. Zander. Impact of aggregate interference on meteorological radar from secondary users. *IEEE Wireless Communications and Networking Conference*. Mar. 2011, 2167–2172. DOI: 10.1109/WCNC.2011.5779468.

[96] S. C. Thompson and J. P. Stralka. Constant envelope OFDM for power-efficient radar and data communications. *International Waveform Diversity and Design Conference*. Feb. 2009, 291–295. DOI: 10.1109/WDDC.2009.4800363.

[97] X. Tian, T. Zhang, Q. Zhang, H. Xu and Z. Song. Range and velocity estimation for OFDM-based radar-radio systems. *9th International Conference on Wireless Communications and Signal Processing (WCSP)*. Oct. 2017, 1–6. DOI: 10.1109/WCSP.2017.8170917.

[98] T. F. Transport and C. Agency. *Frequency Division Table*. URL: http://pilvi.viestintavirasto.fi/attachments/maaraykset/Taajuusjakotaulukko_suomi_3.1.2018.pdf.

[99] A. Turlapaty and Y. Jin. A joint design of transmit waveforms for radar and communications systems in coexistence. *IEEE Radar Conference*. May 2014, 315–319. DOI: 10.1109/RADAR.2014.6875606.

[100] L. Ulander. *Passive Radar, an overview*. URL: https://www.fmv.se/Global/Dokument/Nyheter%20och%20Press/2016/Sensorsymposium%202016/6_Ullander_FOI_SensorSymposium.pdf.

[101] L. Wang, J. Mcgeehan, C. Williams and A. Doufexi. Application of cooperative sensing in radar-communications coexistence. *IET Communications*. Vol. 2. Aug. 2008, 856–868. DOI: 10.1049/iet-com:20070403.

[102] Y. Xie, R. Tao and T. Wang. Method of Waveform Design for Radar and Communication Integrated System Based on CSS. *First International Conference on Instrumentation, Measurement, Computer, Communication and Control*. Oct. 2011, 737–739. DOI: 10.1109/IMCCC.2011.187.

[103] B. W. Zarikoff and D. Weldon. Detection of Pulsed Radar in a Time Division Duplexed System. *IEEE 73rd Vehicular Technology Conference (VTC)*. May 2011, 1–5. DOI: 10.1109/VETECS.2011.5956166.

[104] Q. Zhao. A survey of dynamic spectrum access: signal processing, networking, and regulatory policy. *IEEE Signal Processing Magazine*. 2007, 79–89.

APPENDIX

A.1 Derivation of the Fisher matrix for the parameter set

For a system model of the vector form

$$\mathbf{y} = \mathbf{s} + \mathbf{v}, \tag{A.1}$$

where $\mathbf{y}, \mathbf{s}, \mathbf{v}$ are the vectors of size $P \times 1$ corresponding to the output, input and noise samples, respectively. The idea is to estimate the set of parameters given by

$$\boldsymbol{\theta} = [\tau, f_{\mathrm{D}}]^T, \tag{A.2}$$

which is of size 2×1. Assuming the noise is a zero mean complex Gaussian random vector with i.i.d. samples, the covariance matrix of noise samples $\mathbf{v}$ can be written as

$$\mathbf{C_v} = \sigma^2 \mathbf{I}. \tag{A.3}$$

With $\mathbf{E}(\mathbf{v}) = \boldsymbol{\mu} = \mathbf{0}$, the multivariate PDF of noise is then given by $\mathbf{v} \sim \mathcal{CN}(\mathbf{0}, \sigma^2\mathbf{I})$. Calculating the mean vector and the covariance matrix of $\mathbf{y}$

$$\mathbf{m_y} = \mathbf{E}(\mathbf{y}) = \mathbf{E}(\mathbf{s}) + \mathbf{E}(\mathbf{v}), \tag{A.4}$$

$$\mathbf{E}(\mathbf{y}) = \mathbf{s}(\boldsymbol{\theta}), \tag{A.5}$$

$$\mathbf{C_y} = \boldsymbol{\Sigma} = \mathbf{E}\left((\mathbf{s}+\mathbf{v})(\mathbf{s}+\mathbf{v})^H\right) = \mathbf{E}(\mathbf{s}\mathbf{s}^H) + \sigma^2\mathbf{I}, \tag{A.6}$$

$$\boldsymbol{\Sigma} = \mathbf{s}\mathbf{s}^H + \sigma^2\mathbf{I}, \tag{A.7}$$

where $\boldsymbol{\Sigma}$ is of size $P \times P$. Therefore, the samples in $\mathbf{y}$ are assumed to be complex Gaussian distributed with $\mathbf{y} \sim \mathcal{CN}(\mathbf{s}(\boldsymbol{\theta}), \boldsymbol{\Sigma})$, for which the probability distribution is given by

$$f_{\mathbf{y}}(\mathbf{y}; \mathbf{m_y}, \boldsymbol{\Sigma}) = \frac{1}{\sqrt{\pi^N |\boldsymbol{\Sigma}|}} \exp\left(-(\mathbf{y}-\mathbf{m_y})^H \boldsymbol{\Sigma}^{-1} (\mathbf{y}-\mathbf{m_y})\right). \tag{A.8}$$

Taking the log-likelihood function and neglecting the first term because it is not dependent upon the parameters, it can be denoted as

$$l_{\mathbf{y}} = -(\mathbf{y}-\mathbf{m_y})^H \boldsymbol{\Sigma}^{-1} (\mathbf{y}-\mathbf{m_y}). \tag{A.9}$$

Differentiating this with respect to an arbitrary parameter yields

$$\frac{\partial l_{\mathbf{y}}}{\partial \boldsymbol{\theta}_i} = -\left[(\mathbf{y}-\mathbf{m_y})^H \boldsymbol{\Sigma}^{-1} \frac{\partial(-\mathbf{m_y})}{\partial \boldsymbol{\theta}_i} + \frac{\partial(-\mathbf{m_y})^H}{\partial \boldsymbol{\theta}_i} \boldsymbol{\Sigma}^{-1} (\mathbf{y}-\mathbf{m_y})\right], \tag{A.10}$$

with $\boldsymbol{\theta}_1 = \tau$ and $\boldsymbol{\theta}_2 = f_\mathsf{D}$. For this distribution, the CRLB of the parameters that needs to be estimated is found with the help of the Fisher matrix [45]. According to that, each element of the Fisher matrix which is of size 2×2 can be defined as

$$I(\boldsymbol{\theta})_{i,j} = \mathbf{E}\left[\frac{\partial l_{\mathbf{y}}}{\partial \boldsymbol{\theta}_i}\frac{\partial l_{\mathbf{y}}}{\partial \boldsymbol{\theta}_j}\right], \tag{A.11}$$

where $i = 1, 2$ and $j = 1, 2$ correspond to the parameter indices to which the log-likelihood function is differentiated. Substituting from (A.10) and noting that the first, second and third order moments are zero [46], this can be simplified as

$$\begin{aligned} I(\boldsymbol{\theta})_{i,j} = \mathbf{E}\left[(\mathbf{y}-\mathbf{m}_{\mathbf{y}})^H\boldsymbol{\Sigma}^{-1}\frac{\partial(\mathbf{m}_{\mathbf{y}})}{\partial\boldsymbol{\theta}_i}\frac{\partial(\mathbf{m}_{\mathbf{y}})^H}{\partial\boldsymbol{\theta}_j}\boldsymbol{\Sigma}^{-1}(\mathbf{y}-\mathbf{m}_{\mathbf{y}})\right] \\ + \mathbf{E}\left[\frac{\partial(\mathbf{m}_{\mathbf{y}})^H}{\partial\boldsymbol{\theta}_i}\boldsymbol{\Sigma}^{-1}(\mathbf{y}-\mathbf{m}_{\mathbf{y}})(\mathbf{y}-\mathbf{m}_{\mathbf{y}})^H\boldsymbol{\Sigma}^{-1}\frac{\partial(\mathbf{m}_{\mathbf{y}})}{\partial\boldsymbol{\theta}_j}\right] \\ = \frac{\partial(\mathbf{m}_{\mathbf{y}})^H}{\partial\boldsymbol{\theta}_j}\boldsymbol{\Sigma}^{-1}\mathbf{E}\left[(\mathbf{y}-\mathbf{m}_{\mathbf{y}})(\mathbf{y}-\mathbf{m}_{\mathbf{y}})^H\right]\boldsymbol{\Sigma}^{-1}\frac{\partial(\mathbf{m}_{\mathbf{y}})}{\partial\boldsymbol{\theta}_i} \\ + \frac{\partial(\mathbf{m}_{\mathbf{y}})^H}{\partial\boldsymbol{\theta}_i}\boldsymbol{\Sigma}^{-1}\mathbf{E}\left[(\mathbf{y}-\mathbf{m}_{\mathbf{y}})(\mathbf{y}-\mathbf{m}_{\mathbf{y}})^H\right]\boldsymbol{\Sigma}^{-1}\frac{\partial(\mathbf{m}_{\mathbf{y}})}{\partial\boldsymbol{\theta}_i}. \end{aligned} \tag{A.12}$$

Using the fact $E\left[(\mathbf{y}-\mathbf{m}_{\mathbf{y}})(\mathbf{y}-\mathbf{m}_{\mathbf{y}})^H\right] = \boldsymbol{\Sigma}$, this can be simplified as

$$I(\boldsymbol{\theta})_{i,j} = \frac{\partial(\mathbf{m}_{\mathbf{y}})^H}{\partial\boldsymbol{\theta}_j}\boldsymbol{\Sigma}^{-1}\frac{\partial(\mathbf{m}_{\mathbf{y}})}{\partial\boldsymbol{\theta}_i} + \frac{\partial(\mathbf{m}_{\mathbf{y}})^H}{\partial\boldsymbol{\theta}_i}\boldsymbol{\Sigma}^{-1}\frac{\partial(\mathbf{m}_{\mathbf{y}})}{\partial\boldsymbol{\theta}_i}. \tag{A.13}$$

Noting that the two terms are the conjugates of each other, final expression can be denoted as

$$I(\boldsymbol{\theta})_{i,j} = 2\Re\left[\frac{\partial\mathbf{m}_{\mathbf{y}}^H}{\partial\boldsymbol{\theta}_i}\boldsymbol{\Sigma}^{-1}\frac{\partial\mathbf{m}_{\mathbf{y}}}{\partial\boldsymbol{\theta}_j}\right]. \tag{A.14}$$

Substituting for $\mathbf{m}_{\mathbf{y}} = \mathbf{s}$ and $\boldsymbol{\Sigma} = \mathbf{s}\mathbf{s}^H + \sigma^2\mathbf{I}$ yields (4.52).